Universidad Miguel Hernández

Programa de Doctorado en

Tecnologías Industriales y de Telecomunicación

Decodificación y estimulación de la actividad cerebral sensorial y motora para potenciar el control de un exoesqueleto de miembro inferior

Tesis que presenta:

María de la Soledad Rodríguez Ugarte

Director de tesis:

José M. Azorín Poveda

Codirector de tesis:

Eduardo Iáñez Martínez

Elche, Alicante, España *Octubre, 2018*

UNIVERSITAS
Miguel
Hernández

La presente Tesis Doctoral está sustentada por un compendio de trabajos previamente publicados en revistas de impacto, indexadas según *JCR Science Edition*. El cuerpo de dicha tesis queda constituido por los siguientes artículos, cuyas referencias bibliográficas completas se indican a continuación:

- *Personalized offline and pseudo-online BCI models to detect pedaling intent*. [1]
  M. Rodríguez-Ugarte, E. Iáñez, M. Ortíz y J. M. Azorín.
  Frontiers in Neuroinformatics. Vol 11(45)
  ISSN: 1662-5196. Ed. FRONTIERS MEDIA SA.
  JCR-SCI Factor de impacto (2017): 3.074, Cuartil **Q1**.
  Fecha de publicación: 11 Julio 2017
  Web: https://www.frontiersin.org/articles/10.3389/fninf.2017.00045
  DOI: 10.3389/fninf.2017.00045

- *Effects of tDCS on Real-Time BCI Detection of Pedaling Motor Imagery*. [2]
  M. Rodríguez-Ugarte, E. Iáñez, M. Ortíz y J. M. Azorín.
  Sensors. Vol 18(4)
  ISSN: 1424-8220. Ed. MDPI AG.
  JCR-SCI Factor de impacto (2017): 2.475, Cuartil **Q2**.
  Fecha de publicación: 8 Abril 2018
  Web: http://www.mdpi.com/1424-8220/18/4/1136/htm
  DOI: 10.3390/s18041136

- *Improving real-time lower limb motor imagery detection using tDCS and an exoskeleton*. [3]
  M. Rodríguez-Ugarte, E. Iáñez, M. Ortíz y J. M. Azorín.
  Frontiers in Neuroscience. Vol 12(757)
  ISSN: 1662-453X. Ed. FRONTIERS MEDIA SA.
  JCR-SCI Factor de impacto (2017): 3.877, Cuartil **Q2**.
  Fecha de publicación: Aceptado 1 de Octubre 2018
  Web: https://www.frontiersin.org/articles/10.3389/fnins.2018.00757
  DOI: 10.3389/fnins.2018.00757

UNIVERSITAS
Miguel
Hernández

AUTORIZACIÓN DE PRESENTACIÓN DE TESIS DOCTORAL POR UN CONJUNTO DE PUBLICACIONES

Director: Dr. Ing. José M. Azorín Poveda

Codirector: Dr. Ing. Eduardo Iáñez Martínez

Título de la tesis: ***Decodificación y estimulación de la actividad cerebral sensorial y motora para potenciar el control de un exoesqueleto de miembro inferior.***

Autora: María de la Soledad Rodríguez Ugarte

Departamento de Ingeniería de Sistemas y Automática

Universidad Miguel Hernández de Elche

El director y codirector de la tesis reseñada AUTORIZAN SU PRESENTACIÓN EN LA MODALIDAD DE CONJUNTO DE PUBLICACIONES.

En Elche, a de de 2018.

Fdo: Dr. D. José M. Azorín Poveda Fdo: Dr. D. Eduardo Iáñez Martínez

UNIVERSITAS
Miguel
Hernández

UNIVERSITAS
Miguel Hernández

PROGRAMA DE DOCTORADO EN TECNOLOGÍAS INDUSTRIALES
Y DE TELECOMUNICACIÓN

Dr. D. Óscar Reinoso García, Coordinador del Programa de Doctorado en Tecnologías Industriales y de Telecomunicación de la Universidad Miguel Hernández de Elche.

Certifica

Que el trabajo realizado por Dña. María de la Soledad Rodríguez Ugarte titulado ***Decodificación y estimulación de la actividad cerebral sensorial y motora para potenciar el control de un exoesqueleto de miembro inferior*** ha sido dirigido por el Dr. D. José M. Azorín Poveda y codirigido por el Dr. D. Eduardo Iáñez Martínez y se encuentra en condiciones de ser leído y defendido como Tesis Doctoral ante el correspondiente tribunal en la Universidad Miguel Hernández de Elche.

Lo que firmo para los efectos oportunos en Elche, a de de 2018.

Fdo.: Dr. D. Óscar Reinoso García
Coordinador del Programa de Doctorado en Tecnologías Industriales y de Telecomunicación

DEPARTAMENTO DE INGENIERÍA DE SISTEMAS Y AUTOMÁTICA
Universidad Miguel Hernández de Elche. Ed. Innova. Avda. de la Universidad s/n, 03202 Elche
Telf: 96 665 8616

UNIVERSITAS
Miguel
Hernández

“Todo hombre puede ser, si se lo propone, escultor de su propio cerebro”

Santiago Ramón y Cajal

Agradecimientos

La verdad es que cuando empecé esta etapa de mi vida, creía que iba a tener mucho más tiempo. Sin embargo parece que fue ayer cuando llegué a Elche, y en un abrir y cerrar de ojos, me encuentro escribiendo el final de la tesis.

Lo primero de todo, quiero agradecer a mi director de tesis José M. Azorín por haberme dado la oportunidad de realizar este proyecto y por haber depositado su confianza en mí a lo largo de estos años. También dar las gracias al Ministerio de Economía y Competitividad por haber financiado el proyecto, que de otra manera no hubiera podido realizarlo.

¿Y cómo una ingeniera industrial ha terminado haciendo el doctorado en bioingeniería? pues fue gracias a Ana Vallés. Sin ti jamás hubiera descubierto este campo tan emocionante y gracias a tu forma apasionada de enseñar, caí rendida ante la bioingeniería. Por todo eso, te doy las gracias.

Quiero dar las gracias a mis compañeros y amigos del laboratorio: Enrique, Álvaro, Edu (también mi codirector, y qué gran codirector) y Andrés. Sin vosotros esto hubiera sido muy duro, y eso que poco a poco habéis ido abandonando el barco. Menos mal que de vez en cuando venía gente para hacer estancias y alegrar el laboratorio, particularmente Nayeli y Jorge. A ti Silvia te pongo aparte, por las risas y las cañas, los cotilleos y el apoyo moral que has supuesto para mí. No te lo he dicho nunca pero gracias por haber estado ahí. Cuando te conocí, me presentaste a Sergio, que me acogió en su grupo de almuerzo cuando todos los del laboratorio me habían abandonado, compi de gap y que se convirtió en amigo, gracias.

Quiero agradecer a todos mis amigos por su apoyo, por comprender que a veces no podía quedar y que tenía que estar centrada en la tesis o por no ir a Valencia y venir a Elche para tomarse algo conmigo, hablando por teléfono o Skype. Gracias a Vir, Patri y Mari por esas noches de japonés y nuestras charlas. Gracias

a Mireia y Esther, dos pilares fundamentales en mi salud mental y que no acabara desconectada del mundo :P. Gracias a Federico por su tiempo, paciencia y dedicación hasta el final en esta tesis, he aprendido muchísimo gracias a ti. Tampoco me puedo olvidar de mis amigos del IBV: Coti, Luis, Ana y Bruno. Gracias por esas quedadas, que aunque nos hagamos mayores, sigamos igual :P.

También quiero agradecer a Mari y a Bea, un par de leonesas que siempre que he ido a Madrid han hecho lo imposible por quedar conmigo y vernos, por no perder la amistad.

Tampoco me puedo olvidar de todo los «voluntarios» que he tenido, mil gracias por no asustaros cuando os perseguía para realizar las pruebas y participar en los experimentos. Gracias por haber sido parte de esta tesis.

Y cómo no agradecer a mi familia TODO lo que han hecho por mí. Sin ellos no hubiera llegado hasta aquí. Gracias a mis padres por haberme dado la educación tan magnífica que me han dado, por su apoyo, por los consejos tanto profesionales como personales. Gracias a mi hermano por haber estado siempre cuando le he necesitado, por atender la infinidad de llamadas, whatsapps y las largas conversaciones. Gracias a mi cuñi, que también ha sido un pilar importante en este periodo de mi vida; gracias por comprenderme, por escucharme, por las risas, por los masajes, los tintes, las tonterías...gracias! Y a mi tío José Miguel, que aunque no lo crea es muy importante en mi vida. Espero que estéis orgullosos de mi porque para mi sois mi ejemplo a seguir. Me hubiera gustado poder agradecérselo personalmente a mi abuela Lula, por ella acepté este proyecto, por ella me siento orgullosa de haber llegado hasta aquí. Y gracias a Dios por haberme puesto en el seno de esta familia.

Y por último pero no por ello menos importante, sino más, a mi novio Miguel por haber confiado siempre en mí desde el primer momento y por darme el empujón final que necesitaba para terminar esta tesis. Gracias por haber apostado por mí y querer compartir esta dura etapa conmigo.

A mi familia y, especialmente, a mi abuela Lula

Resumen

La presente tesis se centró en el estudio de interfaces cerebro-máquina (BMI: Brain-Machine Interfaces) basadas en señales electroencefalográficas (EEG) y en la estimulación transcraneal por corriente continua (tDCS: Transcranial Direct Current Stimulation) con el fin de controlar un exoesqueleto de miembro inferior en tiempo real. Uno de los objetivos principales fue desarrollar una BMI capaz de detectar en tiempo real la intención de movimiento o la distinción entre dos tareas cognitivas motoras. El segundo objetivo fue estudiar una configuración de tDCS capaz de mejorar el desempeño en las tareas cognitivas. Y el tercer objetivo fue controlar un exoesqueleto de miembro inferior utilizando la BMI y la configuración de tDCS diseñadas.

Inicialmente se evaluaron varios algoritmos y configuraciones de electrodos para que la BMI diseñada fuera capaz de detectar la intención del pedaleo mediante las señales EEG del usuario. Posteriormente se decidió cambiar de paradigma y diseño de la BMI para mejorar las detecciones cognitivas que hacía la BMI. Para ello, se diseñaron BMIs que distinguían entre la imaginación de dos tareas cognitivas motoras: la relajación y ya sea el pedaleo o la marcha.

Para los estudios de la tDCS, se probaron dos montajes diferentes para mejorar el desempeño de la detección de la imaginación de las tareas cognitivas. El primer montaje fue evaluado con el paradigma de identificar la relajación y la imaginación del pedaleo. Dicho montaje se focalizó en sobreexcitar el área de la corteza motora donde se encuentra la representación de las piernas en el cerebro. El segundo montaje se evaluó con el paradigma de detectar la relajación e imaginación de la marcha. Este montaje se centró en excitar tanto el cerebelo como la corteza motora donde se encuentra la representación de las piernas en el cerebro.

Finalmente, se realizó una prueba piloto con usuarios sanos que controlaban un exoesqueleto de miembro inferior en tiempo real con la BMI diseñada a través de la detección de dos tareas cognitivas de imaginación. Para esta prueba los participantes fueron estimulados con el segundo montaje de tDCS. Con este estudio

se comprobó que la BMI podía distinguir entre dos tareas de imaginación motora y que el montaje de tDCS mejoraba el desempeño de la detección.

Abstract

This thesis was focused on the study of brain machine interfaces (BMI) based on electroencephalographic signals (EEG) and transcraneal direct current stimulation (tDCS) with the aim of controlling a lower limb exoskeleton in real time. One of the main goals was to develop a BMI capable of detecting in real time the movement intent or the distinction between two cognitive motor tasks. The second goal was to study a tDCS configuration capable of improving the cognitive task performance. And the third goal was to control a lower limb exoeskeleton using the BMI and the tDCS configuration designed.

Initially several algorithms and electrode configurations were evaluated so that the BMI designed was capable of detecting pedaling intent by means of the user's EEG signals. Afterwards, the paradigm and design of the BMI were changed in order to improve the cognitive detections of the BMI. With this in mind, BMIs able to distinguish between the imagination of two cognitive motor tasks (relaxation and either pedaling or gait) were designed.

For the tDCS studies, two different montages were tested to improve the detection of cognitive motor imagery tasks. The first montage was evaluated with the paradigm of identifying relaxation and pedaling motor imagery. This montage focused on overexciting the motor cortex area where the legs are represented in the brain. The second montage analyzed the paradigm of detecting relaxation and gait motor imagery. This montage concentrated on exciting both the cerebellum and the motor cortex area where the legs are represented in the brain.

Finally, a pilot test with healthy subjects controlled a lower limb exoskeleton in real time with the BMI designed via the detection of two cognitive motor imagery tasks. In this experiment, participants were stimulated using the second tDCS montage. With this study, it was corroborated that the BMI could distinguish between two motor imagery tasks and that the tDCS montage improved the detection performance.

UNIVERSITAS
Miguel
Hernández

Índice general

Índice de figuras

Índice de tablas

UNIVERSITAS
Miguel
Hernández

Glosario

Acrónimo	Descripción en castellano	Descripción en inglés
ACC	Precisión	*Accuracy*
ACV	Accidente cerebro-vascular	*cerebrovascular accident*
AEP	Potencial Evocado Auditivo	*Auditory Evoked Potential*
AMLR	Potencial Auditivo de Latencia Media	*Auditory Middle Latency Response*
API	Interfaz de programación de aplicación	*Application Programming Interface*
AR	Auto Regresivo	*Auto-Regressive*
BCI	Interfaz Cerebro-Computador	*Brain-Computer Interface*
CAR	Referencia Media Común	*Common Average Reference*
CNV	Variación de Contingencia Negativa	*Contingent Negative Variation*
CSIC	Consejo Superior de Investigaciones Científicas	*Spanish National Research Council*
CSP	Patrones Espaciales Comunes	*Common Spatial Patterns*
ECoG	Electrocorticografía	*Electrocorticography*
EEG	Electroencefalografía	*Electroencephalography*
EMG	Electromiografía	*Electromyography*
EOG	Electrooculografía	*Electrooculography*
EPSP	Potencial Excitatorio postsiáptico	*Excitatory Postsynaptic Potential*
ERD	Desincronización Relacionada a Evento	*Event-Related Desynchronization*
ERP	Potencial Relacionado a Evento	*Event-Related Potential*
ERS	Sincronización Relacionada a Evento	*Event-Related Synchronization*
fMRI	Imagen por Resonancia Magnética Funcional	*Functional Magnetic Resonance Imaging*

Acrónimo	Descripción en castellano	Descripción en inglés
FP/min	Falsos positivos por Minutos	*False Positive per Minute*
FPR	Tasa de Falsos Positivos	*False Positive Rate*
IMU	Sensor de Movimiento Inercial	*Inertial Motor Unit*
IPSP	Potencial Inhibitorio postsiáptico	*Inhibitory Postsynaptic Potential*
MEG	Magnetoencefalografía	*Magnetoencefalography*
LFP	Potenciales de Campo Local	*Local Field Potential*
SMA	Área motora suplementaria	*Supplementary Motor Area*
SUA	Registro de Unidad Celular	*Single Unit Activity*
tDCS	Estimulación Transcraneal por Corriente Directa	*Transcranial Direct Current Stimulation*
TPR	Ratio de Verdaderos Positivos	*True Positive Rate*
PM	Corteza premotora	*Premotor cortex*

Capítulo 1

INTRODUCCIÓN

1.1. Motivación

De acuerdo al informe mundial de la discapacidad publicado por la Organización Mundial de la Salud (OMS), más de mil millones de la población mundial vive con algún tipo de disfunción de los cuales 200 millones sufren dificultades severas en su funcionamiento [4]. Una de las principales causas de este tipo de incapacidad son los accidentes cerebro-vasculares (ACVs) o ictus. Un ACV se produce por la interrupción del suministro de la sangre al cerebro y puede ser provocado por tener presión arterial alta, fibrilación auricular, colesterol alto en la sangre, edad avanzada, inactividad física o una dieta poco saludable [5].

En el mundo se producen 15 millones de ACV diariamente [6]. Particularmente en España, según la Sociedad Española de Neurología (SEN), se producen entre 110.000 y 120.000 ictus al año de los cuales el 50 % mueren o quedan con algún tipo de discapacidad [7]. Cuando ocurre un ACV, la comunicación existente entre el cerebro y el sistema nervioso central que conecta con los músculos para realizar una tarea motriz puede quedar dañada [8]. De hecho, tres de cada cuatro personas que sobreviven al ACV experimentan debilidad en los brazos o las piernas, lo que provoca disfunción motriz y esto conlleva a la pérdida de independencia en tareas cotidianas [7]. Sin embargo, el cerebro es un órgano plástico capaz de ge-

nerar nuevas conexiones neuronales tras una lesión o recuperar las previamente perdidas. Esta reorganización cerebral, comúnmente conocida como neuroplasticidad, se potencia con las terapias de rehabilitación y son más efectivas durante los primeros 6 meses de la recuperación [9, 10].

La principal motivación de este trabajo es mejorar el proceso de rehabilitación a aquellas personas que han sufrido un ACV que afecta a sus extremidades inferiores y que no han podido recuperarse por completo, por lo que continúan con algún tipo de disfunción motora en el miembro inferior.

1.2. Introducción al estado del arte

Los resultados de usar terapias convencionales como la fisioterapia para restablecer la funcionalidad en las extremidades inferiores afectadas por un ACV, no son particularmente alentadores [11]. Una nueva técnica de rehabilitación es el uso de exoesqueletos. Éstos son dispositivos que se acoplan a una extremidad y asisten el movimiento de dicha parte. Por otra parte, en los últimos años, se están desarrollando interfaces cerebro máquina o BMI por sus siglas en inglés (*Brain-Machine Interface*) [12]. Las BMIs orientadas a la neuro-rehabilitación crean un camino alternativo para controlar la extremidad en cuestión usando las señales cerebrales del usuario para controlar un dispositivo externo como puede ser un exoesqueleto. De esta manera, a través de las tareas cognitivas cerebrales, el paciente está involucrado en generar los comandos que hacen activar el sistema de control. Se cree que este acoplamiento de BMI y exoesqueletos puede mejorar la rehabilitación muscular y neurológica del paciente. Este tipo de mecanismos (BMI + exoesqueletos) afectan al sistema neurológico mediante la comunicación de abajo hacia arriba o *bottom up* por medio de neuronas aferentes que transportan los impulsos nerviosos desde los órganos sensoriales hasta el sistema nervioso central y éste al cerebro.

Además, se está investigando cómo influenciar la actividad cerebral para mejorar la función motora. Esto involucra comunicación neuronal de arriba hacia

abajo o *top down* por medio de neuronas eferentes que transportan la información desde el sistema nervioso central al músculo. Un ejemplo de incidir este tipo de actividad es mediante la estimulación transcraneal por corriente directa (tDCS por sus siglas en inglés, *Transcranial Direct Current Stimulation*). Esta técnica redescubierta hace 15 años intenta facilitar la reparación de conexiones neuronales, perdidas o debilitadas, o generar nuevas tras una lesión neuronal.

Hasta el momento, ambas técnicas, BMIs (con exoesqueletos) y tDCS, se han estudiado individualmente en el contexto de la rehabilitación de extremidades en pacientes con ACVs. La mayoría de los estudios involucran los miembros superiores de los pacientes, y existen pocos que se enfoquen exclusivamente en miembros inferiores [13, 14, 15]. Esto se debe en parte a una mayor dificultad de estimular la parte del cerebro que representa las piernas y a la complejidad mecánica (y por ende también del respectivo patrón neuronal) de la marcha humana. Adicionalmente, para que las BMIs sean efectivas en terapias de rehabilitación, se requiere que funcionen en tiempo real, lo cual presenta otra capa de complejidad pues pocos estudios se han enfocado en BMIs que verdaderamente funcionen en tiempo real. Finalmente, dado que se especula que las BMIs [16] y el tDCS [17] individualmente son beneficiosas para los pacientes con ACVs, es de esperarse que la combinación de ambas sea aún más beneficiosa en estos pacientes que quieren restablecer las conexiones entre la actividad cerebral y las funciones motoras de sus extremidades inferiores. Información mucho más detallada de todos estos aspectos se puede encontrar en el Capítulo 2 de este trabajo.

1.3. Objetivos de la tesis

La idea de esta tesis doctoral es desarrollar un sistema que en un futuro pueda ayudar en la rehabilitación del control motor, perdido o debilitado, de los miembros inferiores de personas que han sufrido un ACV afectando dichas extremidades. El objetivo principal es combinar BMIs (conectadas a exoesqueletos y que funcionen en tiempo real) y protocolos de tDCS que estén orientados a la rehabi-

litación de miembros inferiores. Más específicamente, los objetivos de esta investigación son:

- Diseñar y evaluar BMIs basadas en señales electroencefalográficas (EEG) capaces de distinguir entre diferentes procesos cognitivos involucrando las extremidades inferiores. En particular, poder distinguir entre un estado de relajación y ya sea la imaginación de alguna tarea motora, como la marcha humana o el pedaleo, o la intención de físicamente ejecutar ésta misma.
- Desarrollar BMIs capaces de detectar en tiempo real los diferentes procesos cognitivos estudiados previamente.
- Estudiar y evaluar diferentes montajes de tDCS para la potenciación de caminos neuronales que controlan las extremidades inferiores.
- Controlar en tiempo real un exoesqueleto de miembro inferior con la BMI previamente diseñada y aplicar un montaje de tDCS para poder mejorar su desempeño.

Esta tesis se ha desarrollado dentro del marco del proyecto Associate - Decodificación y estimulación de actividad cerebral sensorial y motora para permitir potenciación a largo plazo mediante estimulación Hebbiana y estimulación asociativa pareada durante la rehabilitación de la marcha (con referencia DPI2014-58431-C4-2-R), financiado por el Ministerio de Economía y Competitividad (Plan Estatal de I+D+I) y por la Unión Europea a través del Fondo Europeo de Desarrollo Regional - FEDER Una manera de hacer Europa.

1.4. Estructura de la tesis

A continuación se procede a explicar brevemente la estructura de la presente tesis dividida en cinco capítulos:

- Capítulo 1: Es este primer capítulo se ha definido la línea de investigación, se ha explicado la motivación, un breve resumen del estado del arte y los objetivos de la tesis.
- Capítulo 2: Los antecedentes que permiten entender mejor el marco de la tesis y tener un mayor conocimiento y comprensión de esta investigación.Se definen qué son los accidentes cerebrovasculares, sus causas, efectos y el proceso de rehabilitación que se observa a lo largo del tiempo. Además, se da una visión global acerca del cerebro humano y algunas de sus funciones. Finalmente se describen diferentes técnicas y tecnologías de rehabilitación para ser lo más autónomo posible y recuperar una vida normal tras sufrir un accidente cerebrovascular severo.
- Capítulo 3: Muestra un resumen global de los materiales y métodos empleados en la investigación, de los resultados y una discusión de los mismos.
- Capítulo 4: Presenta las conclusiones de la línea de investigación y trabajos futuros para que continuar con dicha línea.
- Capítulo 5: Muestra las separatas de los artículos publicados que soportan la presentación de esta tesis. Todos ellos son Open Access.

1.5. Resumen de materiales, métodos y discusión de los resultados

En este apartado se expone un resumen de los materiales y métodos utilizados en esta tesis. Asimismo, se muestran los resultados obtenidos y una discusión de los mismos.

1.5.1. Materiales

Durante el desarrollo de la investigación de esta tesis se han utilizado los siguientes materiales:

- Diferentes equipos de registro para adquirir señales electroencefalográficas (EEG): En particular se han utilizado los equipos comerciales Enobio32 y StarStimR32 de Neuroelectrics. El equipo StarStimR32 también suministra estimulación transcraneal por corriente directa (tDCS). Las características de dichos equipos se muestran en el capítulo 3.1.1 y 3.2.1.
- Sistema de captura de movimiento inercial (IMUs).
- Una pedalina utilizada en la aportación R1 (apartado 3.1.1)
- Un exoesqueleto de miembro inferior de la empresa Technaid. Este dispositivo fue utilizado durante la aportación R3 (apartado 3.2.1).

1.5.2. Métodos

Se han desarrollado diferentes métodos durante la realización de esta tesis. Se enumeran a continuación:

- Desarrollo de protocolos para detectar intención de movimiento e imaginación motora.
- Herramientas matemáticas empleadas: Transformada de Fourier, filtros espaciales y frecuenciales, densidad espectral de potencia y un método desarrollado por los autores nombrado *weighted discriminator* explicado en el apartado 3.1.1.
- Herramientas estadísticas: t-test y diferentes modelos de ANOVA.

1.5.3. Resultados y discusión

Durante el periodo de realización de esta tesis, se han obtenido diferentes resultados que permitieron avanzar en esta investigación. A continuación se expone un resumen de los resultados obtenidos y una discusión de los mismos.

- Se han desarrollado y diseñado interfaces cerebro-máquina (BMI) capaces de detectar la intención de movimiento y la imaginación de motora de las extremidades inferiores mediante el uso de las señales EEG de los usuarios.
- Se ha encontrado una configuración de electrodos tDCS capaz de mejorar el control de las BMI diseñadas.
- Se han combinado técnicas de tDCS junto con el control en tiempo real de un exoesqueleto por medio de BMIs que detectan la imaginación de movimiento en extremidades inferiores.

Todos estos resultados obtenidos son prometedores para aplicar estas tecnologías en personas que hayan sufrido un ACV y tengan deficiencia motora en el miembro inferior y puedan mejorar más rápidamente su proceso de rehabilitación .

UNIVERSITAS
Miguel
Hernández

Capítulo 2

ESTADO DEL ARTE

En este capítulo se hace una descripción sobre los términos relevantes para facilitar la comprensión de este trabajo. Se exponen las principales causas de accidente cerebrovascular y las principales tecnologías utilizadas para su recuperación. Además, se especifican diferentes técnicas de adquisición de seales corticales y la combinación de éstas para controlar un dispositivo externo en el campo de la rehabilitación.

2.1. Accidente cerebro vascular

El accidente cerebro vascular (ACV) es un evento neurológico caracterizado por la falta de circulación sanguínea a una parte del cerebro con una perdurabilidad de más de veinticuatro horas. Esto priva al cerebro de oxígeno y nutrientes causando daño en el tejido cerebral o incluso la muerte [18, 19].

2.1.1. Clasificación y causas

Existen diferentes formas por las cuales el cerebro puede dejar de recibir flujo sanguíneo. Según esto, el ACV puede dividirse principalmente en dos tipos

(Figura 2.1):

1. ACV isquémico: Se produce cuando un vaso sanguíneo que suministra sangre al cerebro queda bloqueado. Las causas más comunes de este tipo de ACV son:

    - Trombo: Es la formación de un coágulo sanguíneo dentro de una de las arterias que suministra sangre al cerebro [20].
    - Embolia: Es el desplazamiento, a través del torrente sanguíneo arterial, de desechos o partículas que se originan fuera del cerebro hacia las arterias cerebrales más angostas provocando su obstrucción [21].

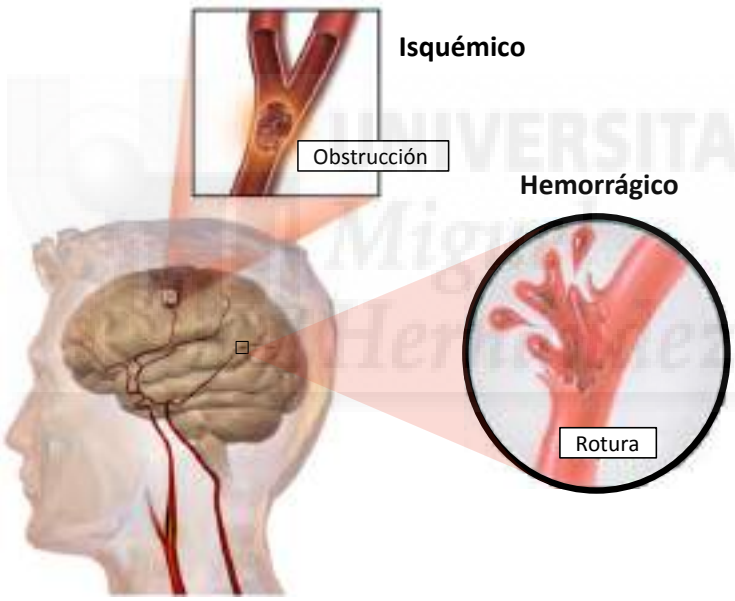

Figura 2.1: Principales tipos de accidente cerebrovascular: el ACV isquémico se produce por obstrucción de un vaso sanguíneo y el ACV hemorrágico es causado por la rotura de un vaso sanguíneo. Imagen adaptada de Creative Commons stroke por Blausen Medical Communications, Inc.

2. ACV hemorrágico: Se produce cuando un vaso sanguíneo se rompe produciendo un derrame de sangre dentro o alrededor del cerebro creando hinchazón y presión en la zona y, por consiguiente, dañando a las células y tejidos del cerebro [21]. Las principales clases de este tipo de ACV son:

    - Intracerebral: Se origina cuando un vaso sanguíneo del cerebro se rompe y se derrama sangre en el tejido cerebral circundante. Esto provoca

que las células del cerebro mueran y la parte afectada deje de funcionar [22].

- Subaracnoidea: Se produce cuando una arteria de la superficie del cerebro se rompe y el sangrado se produce entre la superficie del cerebro y el cráneo [23].

Algunas de las causas del ACV hemorrágico son:

- Hipertensión arterial: Es una patología en que la presión del flujo sanguíneo en la arteria es elevado. Esta presión se mide por medio de dos parámetros: tensión sistólica y tensión diastólica. Si la tensión sistólica es igual o superior a 140 mm Hg y/o la tensión diastólica es igual o superior a 90 mm Hg, la tensión arterial se considera alta o elevada [24].
- Aneurisma: Es la acumulación de sangre en forma de globo en las paredes de los vasos sanguíneos. Esta protuberancia puede llegar a desgarrarse provocando un derrame cerebral [25].
- Fístula arteriovenosa: Es una conexión anómala entre una arteria y una vena. En el sistema circulatorio de una persona sana, la sangre fluye de las arterias a los capilares y de aquí a las venas. Si se tiene una fístula arteriovenosa, la sangre pasa de las arterias a las venas directamente, pasando por alto algunos capilares. Estos capilares «olvidados» reciben un suministro de sangre inferior [26].

El ACV más común en la actualidad es el isquémico, suponiendo alrededor del 87 % de los accidentes cerebrovasculares [5].

2.1.2. Efectos

Los efectos que puede producir un ACV pueden ir desde la pérdida o cambios en las funciones autónomas, pérdida o dificultad en la comunicación, cansancio y fatiga, cambios emocionales o hasta incluso la muerte. Cuando una persona

pierde las funciones autónomas tras un ACV, afecta a diferentes áreas cerebrales. Entre ellas están la ínsula, amigdala y el hipotálamo lateral [27].

Por otra parte, se ha investigado que entre el 64 % y el 80 % de los pacientes de ACV con secuelas en la motricidad, vuelven a recuperarla a una velocidad de marcha menor de 0.8 m/s. Dicha velocidad no es suficiente para poder vivir una vida normal en la sociedad, ya que por ejemplo, no da tiempo a que puedan cruzar la calle dentro del tiempo establecido por el semáforo [28].

Según datos del estudio nacional de estadística, el ACV en España es una causa frecuente de morbilidad y muerte. En el 2014, el porcentaje de morbilidad se redujo en un 2,77 % respecto al 2012, sin embargo, continúa representando el 14,72 % de la población. Mientras que la tasa mortalidad causada por un ACV, a pesar de haber disminuido en un 11,32 %, sigue siendo del 27,19 % de la población (datos ajustados por edad) [29].

2.1.3. Rehabilitación

Para volver a recuperar una vida normal tras sufrir un ACV, a veces es necesario volver a adquirir y/o aprender las funciones perdidas y, por ello, es inevitable pasar por un proceso de rehabilitación el cual es complejo aunque heterogéneo en su naturaleza [30]. Las secuelas del ACV vienen determinadas por la localización donde se ha producido el ACV y el tamaño de la lesión. En los primeros seis meses después de sufrir un ACV, el cerebro tiene mayor capacidad plástica debido a que sufre una reorganización neuronal [31]. Por ello, es el periodo más intenso y donde hay que hacer más hincapié en las terapias que se han de realizar.

En la Figura 2.2 se puede ver el proceso de recuperación de las actividades y las funciones corporales respecto al tiempo desde que se sufre un ACV.

Durante los primeros días existe una recuperación neurológica espontánea. En él, los médicos evalúan la gravedad de la lesión, y si es oportuno, medican al paciente para que no surja en un futuro cercano otro caso de ACV. Dependiendo

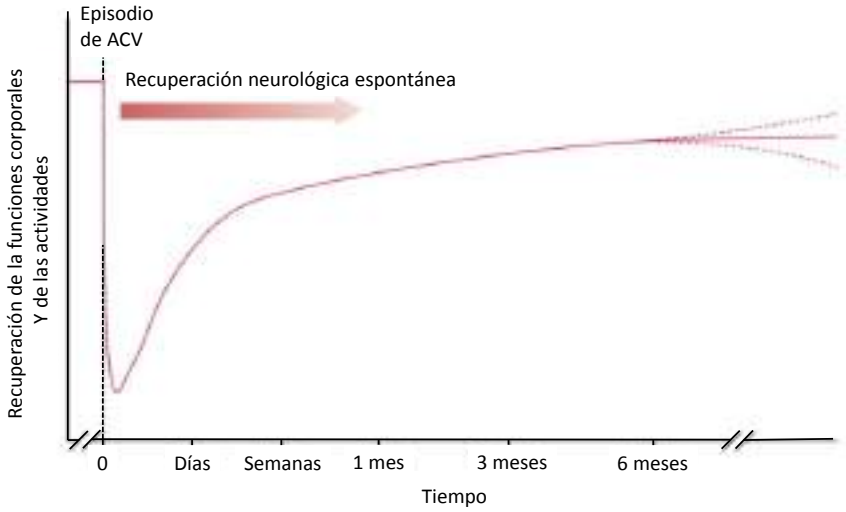

Figura 2.2: Evolución temporal del proceso de recuperación tras sufrir un ACV. Figura adaptada de Langhorne et. al. [30].

de la gravedad, el paciente tendrá que quedarse unos días en el hospital bajo cuidados o será enviado a casa. A partir de aquí, y si fuera necesario, el paciente recibirá unos cinco días por semana terapia de rehabilitación física y ocupacional hasta los 6 meses después de haber sufrido el ACV. Durante los primeros 3 meses se puede ver en la Figura 2.2 que los avances en la recuperación del paciente son más notables. Una vez pasado los seis meses, ver mejoras conlleva más tiempo y esfuerzo [32].

2.2. El cerebro humano

2.2.1. Estructura

Cada vez estamos más cerca de saber cómo funciona el cerebro humano y su estructura, sin embargo, éste sigue siendo desconocido. El cerebro humano está dividido en 4 lóbulos principales según su función [33]:

- Lóbulo Frontal: (Área azul de la Figura 2.3) Está situado en la parte anterior, por delante del surco central del cerebro, comúnmente conocido como surco de Rolando. Esta área está relacionada con las funciones motoras, el

lenguaje, el raciocinio, la resolución de problemas y las emociones.

- Lóbulo Parietal: (Área amarilla de la Figura 2.3) Se encuentra por detrás de la cisura de Rolando y por encima del surco lateral del cerebro, conocido como cisura de Silvio. Es el encargado de procesar la información sensorial procedente de las diferentes partes del cuerpo como por ejemplo la sensibilidad, el tacto, la percepción, la presión, la temperatura y el dolor.
- Lóbulo Occipital: (Área rosa de la Figura 2.3) Está ubicado en la zona posterior del cerebro. En este área del cerebro se encuentra la corteza visual, por lo que es donde se interpretan las imágenes que vemos.
- Lóbulo Temporal: (Área verde de la Figura 2.3) Está situado por debajo y detrás de la cisura de Silvio y localizado frente al lóbulo occipital. En esta área se encuentra la corteza primera de la audición, por lo que el procesamiento auditivo se realiza en esta zona. Además está implicado en tareas de reconocimiento facial y la memoria.

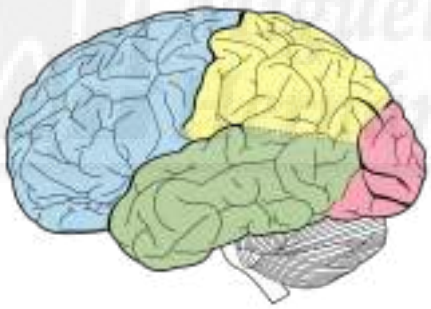

Figura 2.3: Los diferentes lóbulos del cerebro humano. Imagen de Gray H. [34]

En 1909, Korbinian Brodmann realizó una investigación más rigurosa sobre las áreas del cerebro y sus funciones. Dividió en 46 regiones la corteza cerebral según la estructura y organización de las células. Entre ellas se encuentra: la corteza motora primaria, el área motor suplementario, la corteza premotora, la corteza somatosensorial, la corteza visual primaria y asociativa, la corteza auditiva, el área de broca, etc.

Posteriormente, en 1951 Wilder Penfield obtuvo una representación distorsionada del cuerpo humano de la corteza motora primaria y la corteza somatosensorial conocidas como homúnculo motor y homúnculo sensorial respectivamente.

Esta representación está basada en los movimientos de las funciones motoras y sensoriales de cada parte del cuerpo. Así por ejemplo, fijándonos en el homúnculo motor (Figura 2.4), la mano tiene un mayor tamaño que el pie, esto significa que los movimientos generados por la mano requieren de un control voluntario más fino, y por ello tiene una representación cortical mucho mayor [35]. Sin embargo, en el homúnculo sensorial, las áreas más sensibles al tacto, presión o dolor del cuerpo son representadas más grandes.

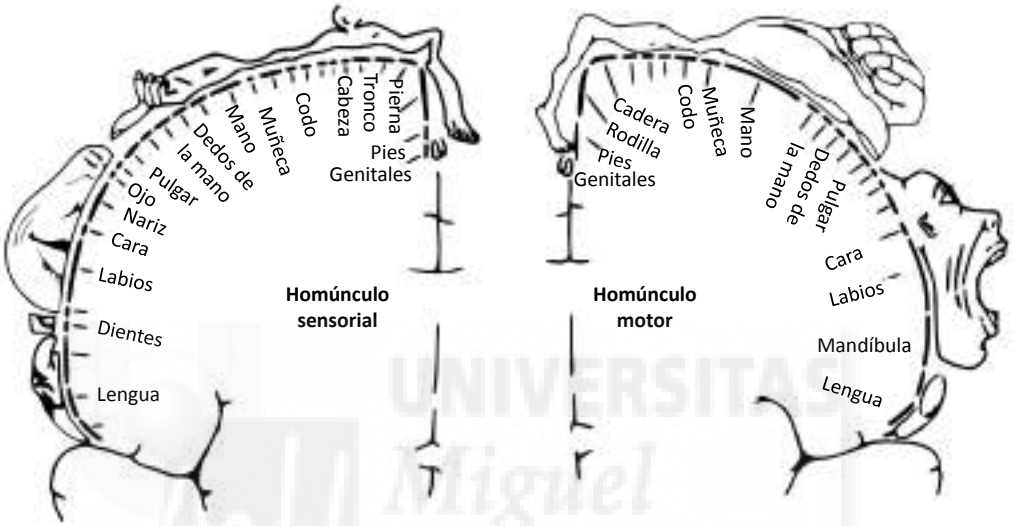

Figura 2.4: Homúnculo motor de Penfield. Imagen adaptada de Ayacop [36]

A continuación, se van a explicar brevemente las áreas de la corteza motora de mayor interés para esta tesis y su localización en la Figura 2.5.

La corteza motora primaria. También conocida como M1, esta área pertenece al lóbulo frontal y está situada en la parte dorsal de la circunvolución precentral y en la cisura de Rolando. La corteza motora primaria se puede considerar primaria porque tiene el umbral más bajo para la licitación del movimiento al aplicar una corriente eléctrica, y parece estar relacionada con los movimientos que conciernen principalmente a nuestros cuerpos. En la capa cinco de esta área, se encuentran las células Betz, que son las células más largas de toda la corteza cerebral y contribuyen al tracto corticoespinal. Esto quiere decir que estas neuronas dan lugar a proyecciones en las neuronas motoras inferiores de la médula espinal

y el tronco del encéfalo para informar de cuáles son los músculos concretos que deben contraerse o relajarse [37].

El área motora suplementaria. Es conocida como SMA por sus siglas en inglés. Esta área pertenece al lóbulo frontal y se encuentra en el hemisferio derecho justo en la parte anterior de M1. Regula el tono muscular en movimientos precisos y tiene una memoria motriz compleja para gestos y comportamientos. Si se sufre una lesión en esta área se podría perder la coordinación de las extremidades [38].

Figura 2.5: Áreas de la corteza motora. Imagen sacada de [39].

La corteza premotora. Es conocida como PM por sus siglas en inglés. Esta área pertenece al lóbulo frontal y se localiza en el hemisferio izquierdo justo en la parte anterior de M1. La función de esta área está aún por descubrir. Sin embargo, hay estudios que indican que esta área está asociada a la planificación de las acciones o reconocimiento de objetos [40, 41].

La corteza somatosensorial (S1). Esta área pertenece al lóbulo parietal, en el giro postcentral, y es la encargada de recibir estímulos sensoriales como el tacto, presión o dolor de las diferentes partes del cuerpo [33]. Como se ha dicho anteriormente, el homúnculo de Penfield somatosensorial reside en esta región.

El cerebelo. Además de estas áreas cerebrales, se ha investigado el cerebelo. Antiguamente se creía que el cerebelo sólo hacía la función de la coordinación de

movimientos. Sin embargo, en los últimos años se ha investigado que el cerebelo también está implicado en el aprendizaje de la realización de una tarea y en los procesos cognitivos [42].

La manera en que funciona el cerebelo a la hora de aprender una nueva tarea es mediante la combinación de órdenes ejecutivas sobre las intenciones de nuestros movimientos, con la retroalimentación sensorial sobre la forma en que nuestro cuerpo se está moviendo realmente. Esta integración de la señal ejecutiva y la retroalimentación sensorial es lo que da lugar a las correcciones del comportamiento y del rendimiento instante a instante, como por ejemplo el aprendizaje de interpretar una nueva pieza de piano [43].

2.2.2. Procesamiento de la información

Los movimientos realizados de un lado del cuerpo, por ejemplo el derecho, son gobernados por las células nerviosas del cerebro (también conocidas como neuronas motoras superiores) pertenecientes al lado contralateral de la médula espinal, en este caso el izquierdo. Esto implica que en algún punto las fibras cruzan la línea media. A esta vía se la conoce como vía corticoespinal lateral [44]. El punto donde se cruzan las fibras se llama decusación piramidal y se produce en el bulbo raquídeo.

En la Figura 2.6 se puede ver el flujo de información para realizar un movimiento con el lado derecho del cuerpo. Las neuronas corticoespinal del hemisferio izquierdo cruzan la línea media en el bulbo raquídeo para controlar el lado derecho del cuerpo. Además, las fibras corticopontinas mandan mensajes al núcleo pontino que se proyectan en la corteza cerebelosa. Las células Purkinje, que son las neuronas que se encuentran en el cerebelo, procesan la información y la envían al núcleo dentado. Para que las salidas del cerebelo impacten los circuitos motores superiores, debe haber un cruce de la línea media: una decusación. En el núcleo dentado crecen un axones que salen del cerebelo a través del pedúnculo cerebeloso superior. Algunos de estos axones ascienden y terminan en el núcleo

ventral lateral del tálamo. También hay otros axones que alcanzan el núcleo rojo. Finalmente, M1 y PM reciben la información del tálamo. De esta manera se cree que las señales de corrección de errores pueden modular la salida de la corteza motora [43].

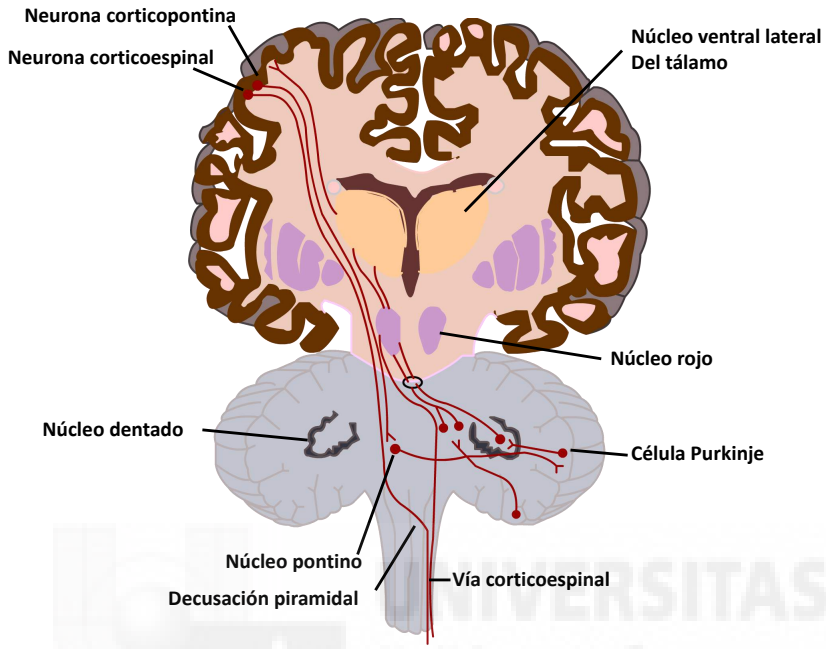

Figura 2.6: Flujo de información de las neuronas.

Observando bien la figura, uno puede darse que, por ejemplo, el lado derecho del cuerpo, es gobernado por el hemisferio contraleteral del cerebro y el hemisferio ipsilateral del cerebelo.

2.2.3. Plasticidad cerebral

Como ya se ha comentado, el cerebro es un órgano plástico. Jerzy Konorski fue el primer neurociencítifico en usar el término plasticidad neuronal en 1948 [45, 46]. La plasticidad cerebral, neuroplasticidad o reorganizacion neuronal son cambios estructurales del cerebro a lo largo de la vida.

Un estudio realizado por Marasco et. al. [47] investigó los cambios corticales en una rata sana. Mediante estimulación eléctrica determinó qué áreas estaban asociadas a qué funciones. Posteriormente, se le amputó una pata y pasado un tiempo se volvió a realizar el mapa cortical. El resultado fue que la región de-

dicada a mover esa pata se dividió y esas partes se juntaron a otras áreas para fortalecer dichas funciones, es decir, hubo neuroplasticidad.

Por otra parte, en los últimos años se ha estudiado con imagen de resonancia magnética funcional (fMRI) que personas que han sufrido un ACV producen cambios en los patrones de activación de las áreas cerebrales [48, 49].

Con todo lo comentado anteriormente, se podría decir que si se sufre un ACV y queda dañada una parte del cerebro que impide realizar ciertos movimientos, con el tiempo, entrenamiento y ayuda externa, se podría reactivar o utilizar una nueva zona del cerebro para aprender nuevas formas de ejecutar dichos movimientos.

2.3. Técnicas y tecnologías de rehabilitación

2.3.1. Terapias convencionales

Las terapias convencionales son el método más antiguo y común que tratan rehabilitar a una persona que ha sufrido un ACV. Las personas más involucradas en la recuperacón de la pérdida de movimilidad, afectación del lengaje u otras alteraciones causadas por el ACV son: enfermeros de rehabilitación, fisioterapeutas, terapeutas ocupacionales y patólogos del habla y del lenguaje [50].

Este tipo de terapias se basa en actividades de transferencia o colocación de objetos, movilidad de partes del cuerpo que tienen disfunción motora, como la marcha o el pedaleo, realización de ejercicios de la vida cotidiana y actividades sociales [51]. Sin embargo, este tipo de terapias muchas veces son insuficientes ya que las sesiones realizadas a la semana son escasas y pueden producir en el paciente la pérdida del interés y frustración ante la falta de progreso y la carencia de autonomía.

2.3.2. Interfaces cerebro-máquina

En los últimos años, la comunidad científica está investigando nuevos tratamientos y tecnologías de rehabilitación para que el paciente que haya sufrido disfunción motora pueda volver a recuperar su independencia [52]. Este tipo de terapias, utiliza elementos asistenciales, como órtesis o prótesis, los cuales favorecen y acompañan el control motor de la parte afectada. De esta manera, el paciente podrá realizar tareas que por si solo no puede, dotándole de una mayor confianza y autonomía. Sin embargo, como hemos comentado anteriormente, a veces la lesión es más grave y se produce bloqueo entre los caminos neuronales que comandan las órdenes del movimiento y el sistema nervioso que ejecuta la actividad de los músculos, por lo que las órtesis o prótesis no son suficientes.

Las interfaces cerebro-máquina (Brain-machine interface o BMI en inglés), mediante la decodificación de las señales eléctricas que produce el cerebro, pueden utilizarse parar generar comandos con el fin de controlar un dispositivo externo. Es decir, las BMI ofrecen un camino alternativo para gobernar un dispositivo sin realizar ningún tipo de movimiento muscular.

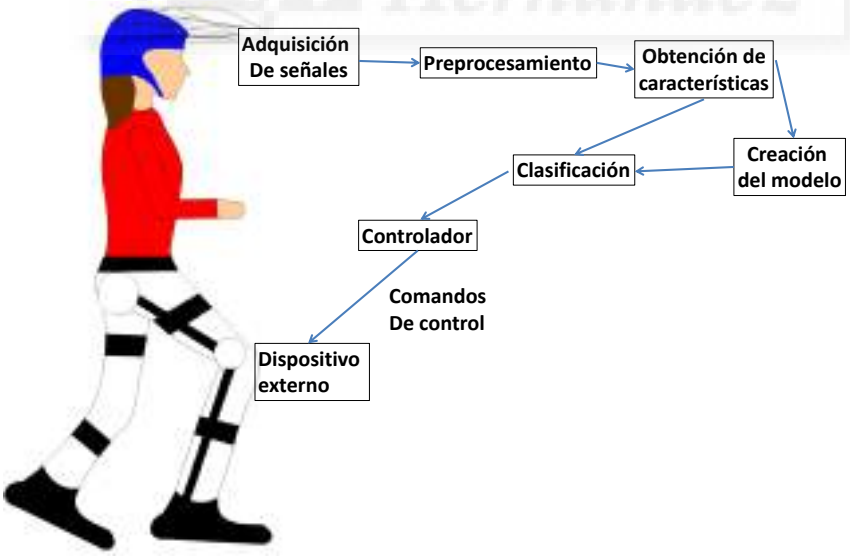

Figura 2.7: Esquema de una interfaz cerebro-máquina.

En primer lugar, para poder controlar un dispositivo externo, es necesario tener un modelo matemático capaz de identificar los diferentes comportamientos o patrones corticales. Esta fase se denomina fase de entrenamiento la cual

se permite analizar la información para relacionarla con la tarea asociada. Para ello, mediante el uso de equipos específicos, las señales cerebrales son registradas de manera no invasiva para el usuario mientras está realizando las tareas. Estas señales corresponden a los impulsos generados cuando se realiza una tarea cognitiva o de movimiento. Para poder identificar y extraer las características que definen los procesos corticales de interés, es necesario realizar una etapa de preprocesamiento en la cual las señales son filtradas para eliminar posibles fuentes de ruido. Una vez generado el modelo matemático, el sistema ya puede decodificar nueva información y clasificar a qué proceso cognitivo corresponde para así poder controlar un dispositivo externo. Esta fase se la conoce como testeo. El dispositivo externo a controlar puede ser desde una pelota en una pantalla [53] hasta mecanismos asistenciales como los exoesqueletos [54].

Este tipo de mecanismos ayuda en el proceso de rehabilitación de los pacientes porque están más involucrados en sus terapias y van generando y modulando nuevos caminos neuronales para superar la lesión [55, 56].

2.3.2.1. Técnicas de adquisición de señales

Existen diferentes técnicas de adquisición de los impulsos eléctricos que se produce entre las neuronas. Estos sistemas se dividen principalmente en dos grandes grupos: invasivos y no-invasivos.

Los procedimientos invasivos requieren de cirugía para implantar el electrodo en la superficie del cerebro o dentro de éste. La gran ventaja de este tipo de sistemas es que tienen una resolución espacial muy alta, por lo que se puede apreciar con mayor precisión y calidad la señal cerebral generada. Sin embargo, una vez implantado el electrodo, éste puede generar bioincompatibilidad o con el paso del tiempo moverse, perdiendo de esa manera la eficacia y siendo necesario volver a realizar una intervención para colocar otro el electrodo en el sitio correspondiente y realizar otra vez la etapa de entrenamiento con dicho electrodo. Este tipo de operaciones puede generar infecciones y daño tisular. Además, este tipo

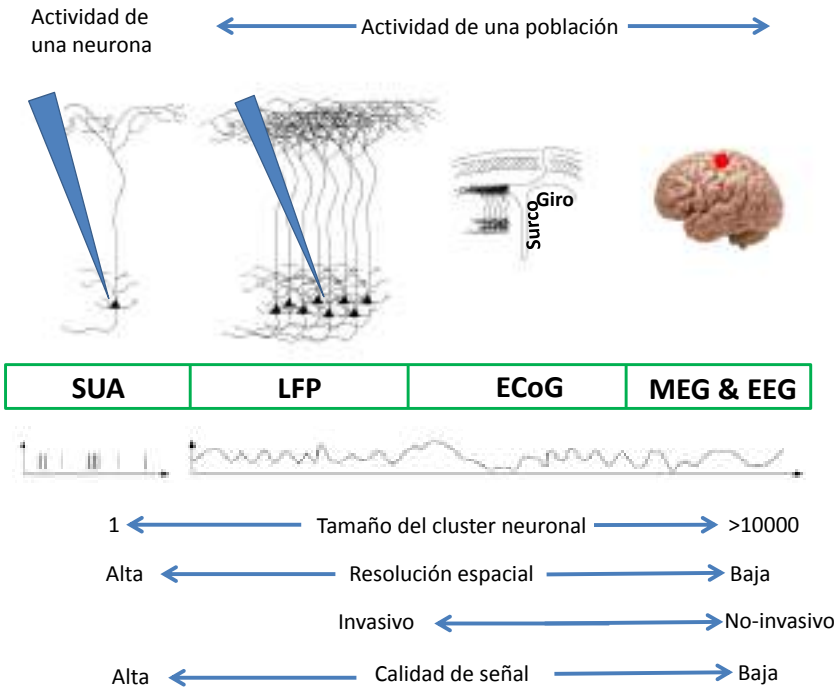

Figura 2.8: Técnicas de adquisición directa de las señales cerebrales. SUA: Registro de unidad-celular (single unit-activity en inglés). LFP: Potencial de campo local (local field potential en inglés), ECoG: Electrocorticografía, MEG: Magnetoencefalografía, EEG: Electroencefalografía.

de sistemas conlleva problemas éticos que a día de hoy están por resolver.

Los procedimientos no-invasivos no requieren de cirugía y los electrodos se colocan en la superficie del cuero cabelludo. Por esta razón, la resolución espacial es muy baja, perdiendo calidad de la señal. Sin embargo, el tiempo de colocación y su coste es mucho menor que los sistemas invasivos, además de evitarse los problemas éticos que los anteriores plantean.

La Figura 2.8 muestra un esquema de diferentes técnicas de adquisición directa de las señales cerebrales. En ella, se pueden ver las ventajas e inconvenientes de cada una de ellas. A continuación se van a describir brevemente el funcionamiento de cada técnica.

Registro de unidad-celular (SUA, por sus siglas en inglés). Esta técnica de registro adquiere la actividad eléctrica de una sola neurona. Para ello, el electrodo ha de ser implantado dentro del cerebro. Para poder realizar la medida, la punta del electrodo ha de estar en el medio extracelular de la neurona teniendo cuidado de no colocarlo en el núcleo de ella. La señal que se obtiene son pulsos

eléctricos que son generados cuando la neurona trata de comunicarse con otras neuronas. Uno de los principales problemas de esta técnica, a parte de la cirugía necesaria para implantar el electrodo, es lo costoso de grabar la actividad de una sola neurona; el electrodo se va moviendo conforme pasa el tiempo porque los tejidos reaccionan ante el electrodo y por ello el cerebro reacciona con un ligero movimiento.

Normalmente, este tipo de registro se hace en investigaciones con animales como ratas, gatos o primates no humanos con el objetivo de entender mejor el funcionamiento del cerebro límbico [57, 58, 59].

Potenciales de campo local (LFP, por sus siglas en inglés). Esta técnica no mide la acción potencial. Más específicamente miden los potenciales excitatorios (EPSP, por sus siglas en inglés) e inhibitorios (IPSP, por sus siglas en inglés) postsinápticos de una población de neuronas. Se produce EPSP cuando los iones positivos (i.e. Na) fluyen hacia dentro de la neurona produciendo una depolarización de la membrana. Esto resulta en más facililidad producir una acción potencial. IPSP sucede cuando los iones negativos (i.e. K+) fluyen hacia fuera generando hiperpolarización de la membrana, lo que resulta que sea más difícil producir una acción potencial. Para implementar esta técnica, se inserta en el cerebro una matriz de electrodos. Dicha matriz puede tener diferentes longitudes de electrodos para poder registrar la actividad de diferentes profundidades del cerebro. La Figura 2.9 muestra la implantación de un vector de electrodos LFP. Como el cerebro es un órgano flexible, es necesario insertar la matriz de electrodos con un golpe seco para que se clave al instante produciendo el mínimo daño.

Electrocorticografía (ECoG). Esta técnica también es invasiva, ya que se coloca una malla con electrodos que han de ir sobre la superficie del cerebro (Figura 2.10). Las principales contribuciones las realizan los potenciales sinápticos de las neuronas piramidales. Este procedimiento es menos invasivo que los dos anteriores, tiene mayor estabilidad y la adquisición de las señales es más fácil. Debido a la ubicación de la malla de electrodos, la resolución espacial es menor que las anteriores pero tiene una buena calidad de señal al estar cerca de las neuronas.

Figura 2.9: Implantación de un vector de electrodos para medir potenciales de campo local (LFP). Imagen sacada de [60]

Este sistema se usa para definir zonas epilépticas.

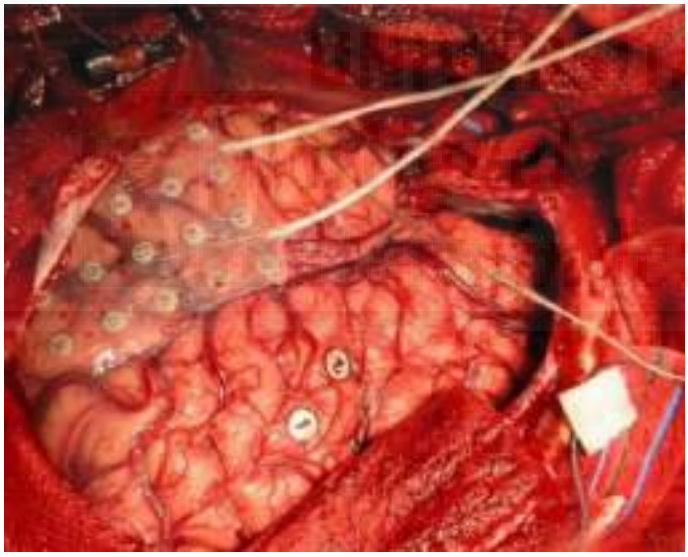

Figura 2.10: Electrocorticografía (ECoG). Imagen sacada de [61]

Magnetoencefalografía (MEG). Es una técnica no invasiva que registra la actividad cerebral mediante campos magnéticos a través de unos sensores llamados SQUID. Las medidas han de realizarse en total aislamiento y sobre las neuronas piramidales ya que en ellas se producen la mayor actividad cortical [62]. Las principales desventajas es que no es portable, tiene un coste elevado, baja resolución espacial y relación señal-ruido. Sus principales ventajas es que es fácil de grabar las señales, no implica riesgo médico y es no-invasivo. En la Figura 2.11 se puede apreciar las dimensiones del equipo para poder registrar la actividad cerebral

mediante esta técnica.

Figura 2.11: Magnetoencefalografía (MEG). Figura del National Institute of Mental Health, National Institutes of Health, Department of Health and Human Services [63].

Electroencefalografía (EEG). Esta técnica no-invasiva (Figura 2.12) es la más barata y portable que existe hoy en día. Por ello, es la más utilizada en la comunidad científica. Se basa en la exploración neurofisiológica cuyos principios residen en el registro de la actividad bioeléctrica cerebral por medio de unos electrodos que se colocan en la corteza cerebral. Los electrodos registran la diferencia de potencial causadas por los potenciales postsinápticos en la membrana celular de las neuronas corticales. Debido a las propiedades mitigantes del cráneo, la actividad cortical generada produce un voltaje registrable desde el cuero cabelludo [64].

De acuerdo al sistema internacional, existen dos modelos estandarizados de la distribución de los electrodos: el 10-10 y el 10-20. El 10 y el 20 se refieren a que las distancias reales entre electrodos adyacentes son del 10 % o del 20 % de la distancia inion a nasion o de derecha/izquierda del cráneo (Figura 2.13) [65]. Por otra parte, existen dos diferentes tipo de electrodos, los electrodos húmedos o de gel y los secos. Los electrodos húmedos han de ser utilizados con una solución salina que mejora las propiedades conductivas entre el cuero cabelludo y el electrodo. Los electrodos secos no requieren de ningún gel ya que entra en contacto directa-

Figura 2.12: Electroencefalografía (EEG).

mente con el cuero cabelludo. Sin embargo son menos robustos y más propensos al ruido que los electrodos de gel, por lo que la calidad de la señal es menor.

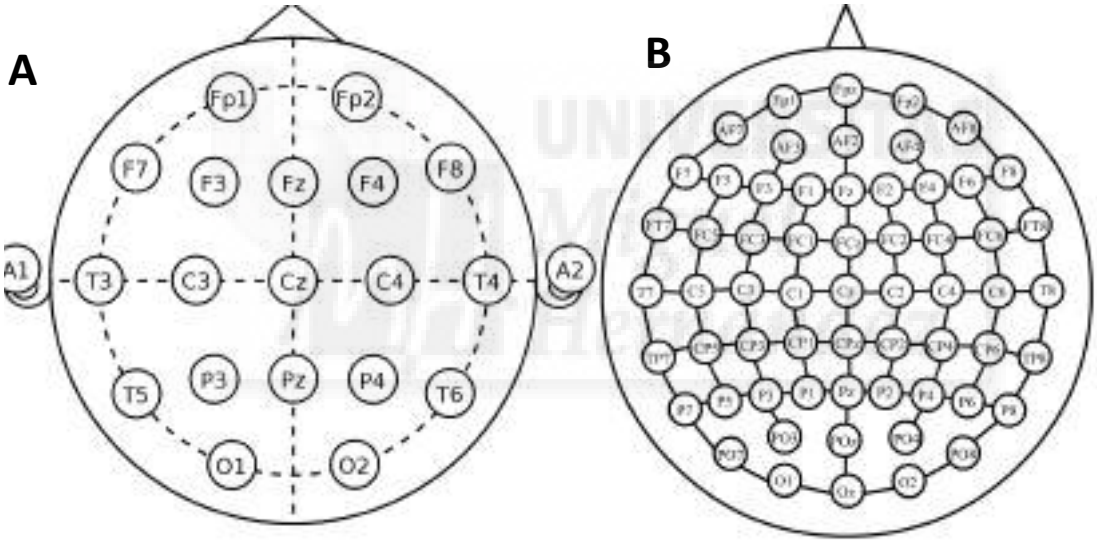

Figura 2.13: Sistema Internacional A) 10-20 y B) 10-10 de electrodos. Imagen adaptada de [66]

Las señales de EEG se describen en términos de ritmos corticales. Éstos se dividen en bandas definidas por rangos de frecuencia. Existen 5 bandas de frecuencia: delta (<4 Hz), theta (4-7 Hz), alfa (8-15 Hz), beta (16-31 Hz) y gamma (>32 Hz) [67]. Dependiendo del paradigma ejecutado durante el EEG, las bandas de frecuencia asociadas a la respuesta neurológica sufren más cambios que otras.

Existen diferentes compañías que se dedican a fabricar equipos de registro EEG. Los equipos que más se utilizan provienen de: g.Tec, Brain Products, Emotiv o Neuroelectrics.

g.Tec: Esta empresa se dedica a fabricar diferentes tipos de electrodos, amplificadores de señal y software. Particularmente, el equipo g.USBamp registra con resolución de 24 bits a una frecuencia de muestreo máxima de 38,4 kHz. Tiene incorporado un filtro Notch para eliminar el ruido debido a la corriente eléctrica, un pasa banda y admite tanto electrodos pasivos como activos. Además, permite comprobar la impedancia generada entre el electrodo y el cuero cabelludo. Sin embargo, este sistema no es inalámbrico (Figura 2.14.A). Se pueden seleccionar hasta 32 canales; en particular, el G.UMBamp registra 16 canales pero se puede combinar con varios equipos hasta conseguir el número de canales deseados, obteninedo las señales sincronizadas.

Brain Products: Uno de los equipos más conocidos de esta empresa es el actiCHamp. Este sistema se compone de dos módulos, un amplificador y la batería. Tiene una resolución de 24 bits y puede registrar hasta 100 kHz de frecuencia de muestreo con electrodos activos. Este sistema tampoco es inalámbrico (Figura 2.14.B). Sin embargo, el sistema MOVE, convierte al anterior en un sistema inalámbrico (Figura 2.14.C). Con este equipo se puede medir la impedancia generada entre el electrodo y el usuario. Se pueden seleccionar 32 canales, sin embargo, se pueden combinar equipos, consiguiendo hasta 160 canales .

Emotiv: Registra con una resolución de 14 bits a una frecuencia de muestreo de 2048 Hz. Tiene incorporado un filtro Notch para eliminar el ruido que genera la corriente eléctrica y un pasa banda. Los electrodos funcionan con solución salina y sólo dispone de 14 canales. Este sistema es inalámbrico (Figura 2.14.D). Comparando este sistema con los equipos anteriores, es muy barato pero la calidad de la señal es más baja.

Neuroelectrics: El equipo más conocido de esta empresa es el Enobio 32 el cual registra con resolución de 24 bits a 500 kHz de frecuencia de muestreo. Utiliza electrodos secos o húmedos ya sea usando solución salina o gel. Este sistema no mide impedancias pero tiene un parámetro que mide la calidad de la señal que se está registrando. Este sistema es inalámbrico y dispone de 32 canales (Figura 2.14.E). Por otro lado, recientemente han empezado a comercializar una nueva

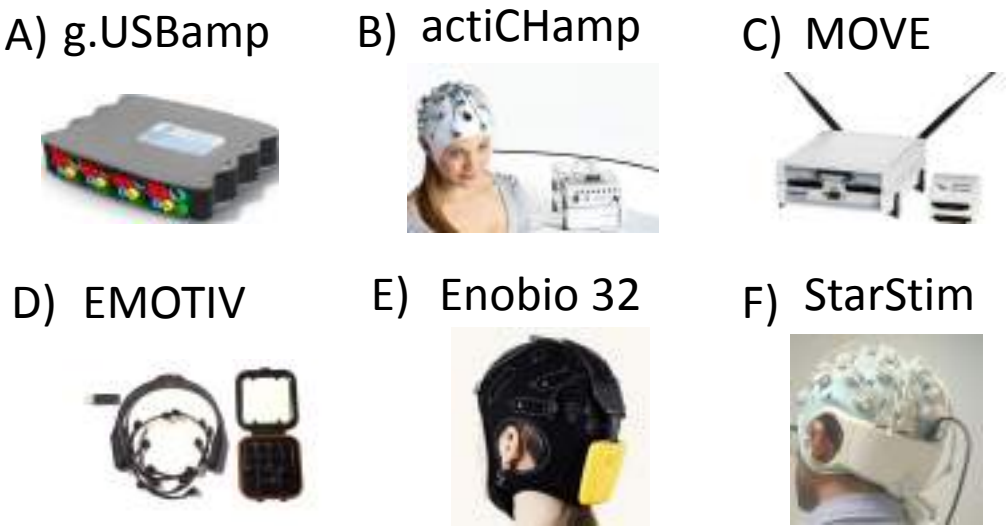

Figura 2.14: Equipos de adquisición de señales EEG. A) Equipo g.USBamp de g.Tec. Fuente: http://www.gtec.at/Products/Hardware-and-Accessories/g.USBamp-Specs-Features. B) Equipo actiCHamp de Brain Products. Fuente: http://www.brainvision.com/actichamp.html. C) Equipo MOVE de Brain products. Fuente: http://www.brainproducts.com/productdetails.php?id=40. D) Equipo Emotiv. Fuente:http://mint.fh-hagenberg.at/?p=3483. E) Enobio 32 de Neuroelectrics. Fuente: https://www.neuroelectrics.com/products/enobio/enobio-32/. F) StarStim de Neuroelectrics.

versión, el equipo StarStim, que además de incluir todas las prestaciones anteriores, puede funcionar por cable y puede estimular eléctricamente en los 32 canales (Figura 2.14.F).

En la presente tesis, se han registrado las señales eléctricas del cerebro mediante EEG con los equipos Enobio 32 y el StarStim. El funcionamiento de ambos sistemas se explicarán más en detalle en siguientes apartados.

2.3.2.2. Potenciales evocados

Un potencial evocado es una respuesta del sistema nervioso a la aparición de cierto estímulo externo. Su amplitud es baja, del rango de microvoltios. Por ello, un evento individual, es difícil de detectar, por lo que se requiere analizar la media de multitud de ellos. Estos eventos se pueden medir a distintos niveles: corteza cerebral, espina dorsal o nervios periféricos. Los potenciales evocados pueden utilizarse, entre otros, en el control de dispositivos externos o en el diagnóstico de patologías. Existen diferentes tipos de potenciales evocados:

- *Potenciales evocados visuales (en inglés Visual Evoked Potential, VEPs)*: Un potencial visual es una respuesta del cerebro a un estímulo externo de tipo visual, por ejemplo, flashes o luces. Esta respuesta visual se suele localizar sobre la corteza occipital del cerebro. Los VEPs se usan principalmente para medir la integridad funcional de las vías visuales desde la retina a través de los nervios ópticos hasta la corteza visual del cerebro; es decir, medir el tiempo de respuesta entre el estímulo y la respuesta cerebral [68]. Este tipo de potenciales son muy útiles en diagnóstico y monitorización. El ejemplo más común que utiliza este tipo de potencial, es el P300. El P300 es una deflexión positiva de voltaje que se produce 300 ms depués del estímulo visual. La persona está sentada enfrente de un ordenador que contiene una matriz con diferentes opciones. El usuario se ha de fijar en una de esas opciones mientras se van produciendo flashes en una fila y una columna. El punto de intersección de dichos flashes es la opción a resaltar. Cuando dichos flashes coincide con la elegida por el usuario, es cuando se produce la respuesta P300.

- *Potenciales evocados auditivos (en inglés Auditory Evoked Potentials, AEPs)*: Un potencial auditivo genera cambios en la actividad cortical a causa de un estímulo auditivo. Consisten en deflexiones positivas y negativas del potencial tras el estímulo. Existen tres tipos de respuesta en base a la latencia: alta (los primeros 10 ms), media (de 10 a 80 ms) y lenta (de 80 a más de 500 ms) [69]. Entre sus usos se encuentran estudios sobre el análisis de audición de niños recién nacidos, desorden auditivo o demencia [70, 71, 72]

- *Potenciales evocados somatosensiorales (en inglés somatosensory evoked potential, SSEPs)*: Un potencial somatosensorial es un estímulo generado por la excitación de los nervios periféricos. Este tipo de potenciales ha estudiado considerablemente la respuesta de transmisión de los nervios aferentes hasta la corteza motora en diferentes enfermedades estimulando el nervio mediano. Si por el contrario se desea evaluar anormalidades en la médula espinal, se suele utilizar la estimulación del nervio tibial [73]. El SSEP se ha usado, entre otros, en pacientes con escoliosis, monitorización de la aorta toracoabdominal y operaciones de cervicales [74, 75, 76].

2.3.2.3. Potenciales relacionados con eventos

Un potencial relacionado con eventos (en inglés event-related potential, ERP) es la respuesta electrofisiológica de un evento específico sensorial, cognitivo o motriz [77]. Este tipo de potenciales es muy habitual en sistemas de control voluntario de una BMI. Existen dos grandes grupos en función del tipo de tarea a realizar:

- Ritmos sensoriomotores (en inglés Sensorimotor Rhythms, SMR): son fluctuaciones de potencia respecto a una línea base en las banda de frecuencia alpha (8-13 Hz) y beta (14-30 Hz). Estos ritmos sensoriales se producen cuando se va a ejecutar una tarea motora (en inglés motor execution, ME) o se imagina dicha tarea (en inglés motor imagery, MI) ya que ambos activan caminos neuronales comunes [78]; y como se ha visto anteriormente, se generan en el hemisferio contralteral del mismo. Estos fenómenos se conocen como sincronización/desincronización de eventos relacionados (en inglés event-related synchronization and desynchronization, ERS/ERD). Por convención se estableció que las fluctuaciones negativas correspondían a ERD mientras que las positivas a ERS [79].
- Potenciales corticales lentos (Slow Cortical Potentials en inglés, SCPs): son cambios lentos de potencial en la membrana de las dendritas corticales a causa de la intención de la realización de un evento [80]. Se producen en la banda delta (<4 Hz) y se caracterizan por durar desde 300 ms hasta varios segundos [81]. Los sistemas BMI basados en este tipo de potenciales tienen un baja eficiencia y altos falsos positivos debido ha que hay que esperar al menos una duración completa del potencial para poder detectarlo.

2.3.3. Técnicas de neuromodulación

Las técnicas de neuromodulación más comunes hoy en día son: la estimulación profunda del cerebro (en inglés deep brian stimulation, DBS), la estimulación

magnética transcraneal (en inglés transcraneal magnetic stimulation, TMS) y estimulación transcraneal por corriente (en inglés transcraneal current stimulation, tCS).

2.3.3.1. Estimulación profunda del cerebro (DBS)

Esta técnica de neuromodulación consiste en la implantación de un dispositivo médico en el cerebro que manda impulsos eléctricos a partes específicas del cerebro a través de electrodos implantados. Está conformado por tres elementos: el electrodo, la extensión y el neuroestimulador. El neurostimulador está dentro de una carcasa de titanio y envía pulsos eléctricos al cerebro. Normalmente, este dispositivo está ubicado debajo de la clavícula. El electrodo es un cable aislado delgado y aislado que se conecta al neuroestimulador por medio de la extensión. El electrodo pasa por debajo de la piel desde la cabeza, pasando por el costado del cuello a la oreja hasta el neuroestimulador (Figura 2.15) [82]. Esta técnica trata enfermedades como el Parkinson, distonia, dolor crónico, depresiones, trastornos obsesivos compulsivos y el síndrome de Tourette [83].

Figura 2.15: Estimulación profunda del cerebro (DBS). Imagen adaptada de [84] licencia de Creative Commons Attribution 3.0 Unported.

2.3.3.2. Estimulación magnética transcraneal (TMS)

Está técnica no invasiva se basa en producir pulsos eléctricos a través de un campo magnético generados por una bobina (Figura 2.16). El principio físico que sigue esta técnica es la inducción electromagnética descrito por M. Faraday que dice: « La variación temporal del flujo del campo magnético que atraviesa la superficie limitada por una espira conductora, induce en esta espira una corriente eléctrica conocida como inducción magnética» [85]. El circuito básico de esta técnica está formado pro un condensador, un tiristor, una resistencia y una bobina(Figura 2.17). El funcionamiento de este circuito es el siguiente: el capacitor se carga generando el cierre del circuito. Debido a ese cierre, se produce flujo de corriente que llega a la bobina produciendo una señal senoidal. Después de un ciclo se apaga [86]. Los parámetros más importantes de esta técnica es la orientación de la bobina y la intensidad. Para saber dónde se ha de posicionar la bobina, hay que encontrar el punto caliente (en inglés hot spot) que es el punto de máxima respuesta antes el estímulo. Posteriormente, para saber qué intensidad se ha de aplicar, hay que determinar el umbral motor de reposo que es la corriente mínima necesaria para producir una respuesta [87]. Los principales usos de esta técnica es para tratar depresiones y migrañas [88, 89].

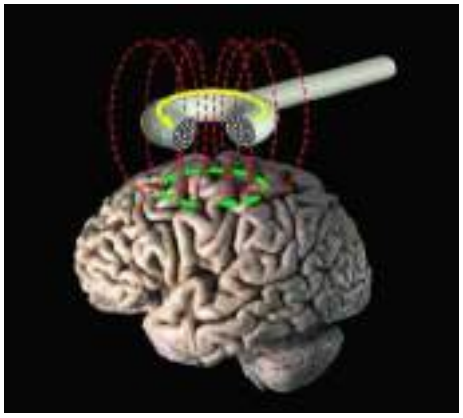

Figura 2.16: Estimulación magnética transcraneal (TMS). Figura del National Institue of Health [90]

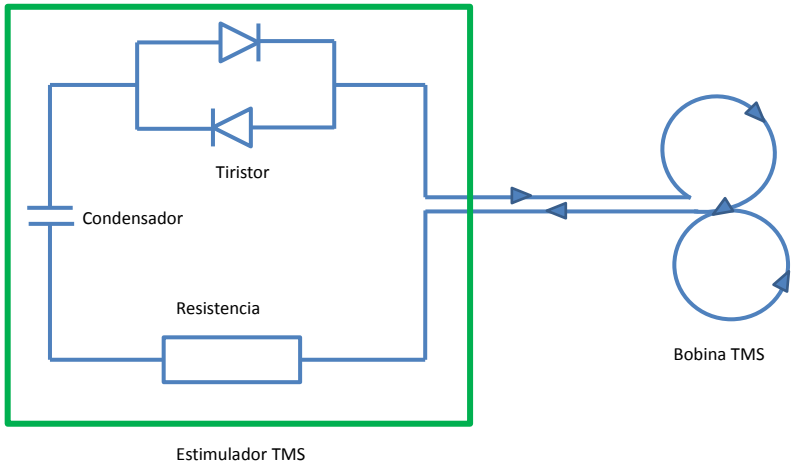

Figura 2.17: Circuito de funcionamiento de estimulación magnética transcraneal (TMS).

2.3.3.3. Estimulación transcraneal por corriente (tCS)

Es una técnica que tiene como finalidad modular el potencial de reposo de las neuronas y, por consiguiente, la excitabilidad cortical, a través de un mínimo de dos electrodos: ánodo y cátodo [91]. Hay tres tipos de tCS: por corriente directa (transcranial direct current stimulation en inglés, tDCS), por corriente alterna (transcranial alternating current stimulation en inglés, tACS) y ruido aleatorio (random noise stimulation en inglés, tRNS). Ninguna de las tres es invasiva y se basan en suministrar corrientes de baja intensidad al cerebro [92].

La presente tesis utiliza tDCS. Por ello, se va a explicar más en profundidad. Los efectos que tiene la tDCS aún no son claros pues dependen de varios factores como la intensidad aplicada, el tamaño de los electrodos y el tiempo de estimulación [93, 94]. Además, funciona de una manera de polaridad específica [95]. Es decir, la corriente por convenio, fluye del ánodo al cátodo y se ha investigado que las neuronas afectadas por el ánodo tienen más actividad mientras que por el contrario, las afectadas por el cátodo, se inhiben [96, 97]. Esto puede verse en la Figura 2.18. La parte de la izquierda muestra el ánodo, en donde el flujo de corriente va hacia la neurona. Esto produce depolarización en el soma que es lo que genera el aumento de la actividad neuronal. También se genera hiperpolarización de las dendritas pero esto no tiene mucha influencia. La parte de la derecha muestra el cátodo y se aprecia que el flujo de corriente va desde la neurona has-

ta el electrodo. De esta manera se produce el efecto contrario al anterior caso; el soma se depolariza generando disminución de la actividad neuronal.

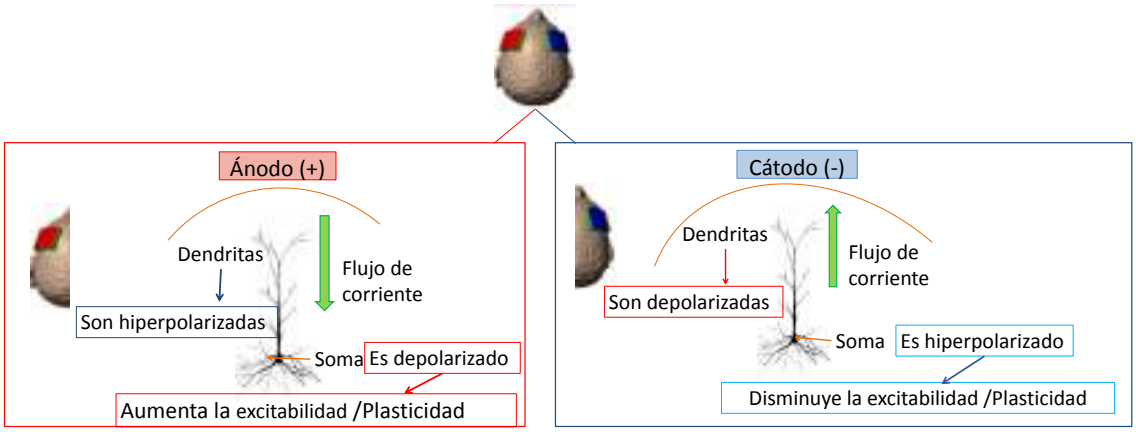

Figura 2.18: Efectos de los electrodos de la tDCS.

La mayoría de los estudios utilizan un tamaño de electrodos entre 25 y 35 cm^2. Este tamaño es considerablemente grande, y a la hora de conocer qué áreas han generado la respuesta deseada es más ambiguo [98, 99]. Hay que tener en cuenta que la densidad de corriente (medida en A/cm^2) es lo que determinará si se puede producir daño neuronal o no. Por lo que, si se reduce el tamaño de los electrodos, la intensidad se debe disminuir para que no exceda el límite de daño neurológico [100].

Otra particularidad de esta técnica, es que se puede suministrar falsa intensidad (sham en inglés) para eliminar el efecto placebo. Es decir, La corriente empieza a aumentar gradualmente hasta llegar al valor fijado y acto seguido empieza a disminuir también gradualmente durante unos pocos segundos. Posteriormente, se deja el tiempo acordado de estimulación a una intensidad nula y antes de terminar la sesión, se produce otra vez el aumento gradual de corriente seguido de su disminución. Esto genera una sensación al usuario de que ha sido estimulado.

2.3.4. Aplicaciones

Estas técnicas y tecnologías de rehabilitación son cada vez más comunes ya que tienen una ventaja añadida a las terapias convencionales. Las terapias convencionales tratan de rehabilitar el músculo. Sin embargo, la utilización de elementos asistenciales como exoesqueletos, mejora la motricidad de los pacientes y mejora su calidad de vida [101, 102]. Sin embargo, estos sistemas tienen limitaciones ya que los exoesqueletos mueven de forma pasiva la extremidad afectada. Es aquí donde la incorporación de una BMI, siempre y cuando funcionen en tiempo real, puede impulsar una mejora en el proceso de la rehabilitación. Esto es debido a que las BMI ayudan a crear caminos neuronales alternativos con la posibilidad de que pueda volver a mover voluntariamente la parte afectada [103].

La combinación de una BMI con exoesqueletos hace que sea una terapia más completa para el paciente ya que, está implicado tanto muscularmente como neurológicamente y por ello, está involucrado de una forma más activa en su rehabilitación [103, 104].

Los exoesqueletos son estructuras rígidas articulables que asisten el movimiento de una persona [105]. Éstos puede ser de miembro inferior o superior (Figura 2.19); y las articulaciones del exoesqueleto han de coincidir con las del usuario para que el movimiento sea natural. Por ejemplo, la colocación de un exoesqueleto de miembro inferior sería de la siguiente manera: la persona se ha de sentar y hacer coincidir tres puntos marcados del exoesqueleto con las articulaciones del trocante, rodilla y tobillo. Una vez ajustado, se ciñe al cuerpo de la persona.

Por otro lado, recientemente se está usando la tDCS para mejorar la afasia, la memoria y el control motor [107, 108, 109, 110]. Sin embargo, hay estudios contradictorios que indican que las estimulación en cierta área es beneficiosa cuando otros obtienen resultados opuestos [111, 112]. Por otra parte, este tipo de neuromulación, se ha investigado poco en la rehabilitación del miembro inferior, ya que la representación de las piernas en el cerebro se encuentra en lo profundo de

Figura 2.19: Exoesqueleto de miembro inferior H2. Diseño realizado por el CSIC y producido por la empresa Technaid. Imagen sacada de [106]

la fisura longitudinal y alcanzar dicho punto representa un problema añadido.

Además, en la presente tesis, se está investigando cómo las BMI pueden detectar la intención de movimiento [1, 113, 114]. A partir de las señales cerebrales del usuario, si se detecta el momento cuando el paciente intenta realizar un movimiento con alguna extremidad, éste podría activar el exoesqueleto pertinente que le ayude a hacerlo. Sin embargo, detectar la intención es una tarea ardua y aún queda mucho por investigar tanto a nivel de hardware como neurológicamente.

Capítulo 3

RESUMEN GLOBAL DE LAS APORTACIONES

En este capítulo se muestra un resumen global los materiales y métodos, resultados y una discusión de los mismos de las publicaciones que conforman esta investigación:

- R1 (aportación en revista 1): Personalized offline and pseudo-online BCI models to detect pedaling intent. Ver publicación 5.1.
- R2 (aportación en revista 2): Effects of tDCS on real-time BCI detection of pedaling motor imagery. Ver publicación 5.2.
- R3 (aportación en revista 3): Improving real-time lower limb motor imagery detection using tDCS and an exoskeleton. Ver publicación 5.

El objetivo principal de R1 se centró en detectar la intención del pedaleo. Posteriormente, en el resto de las aportaciones y debido a los resultados obtenidos anteriormente, se decidió detectar la imaginación motora del pedaleo y la marcha. En R2 se estudió la deteción de dos tareas cognitivas: la relajación y la imaginación del pedaleo. En R3 se extrapoló el paradigma anterior a detectar la relajación y la imaginación de la marcha, que es el fin que se busca para mejorar las terapias

de rehabilitació n. Además, para estas dos últimas aportaciones, se utilizó estimulación transcraneal por corriente directa (tDCS) para determinar si potenciaba la precisión con que el usuario controlaba la interfaz cerebro-máquina. En función de los resultados obtenidos en R2 y dado que se cambia de paradigma cognitivo (se cambió de detectar imaginación de pedaleo a marcha), se modificaron algunos parámetros del montaje de estimulación. Los participantes del estudio principal de R2 y R3 recibían realimentación visual. Además, en R3 se realizó un estudio piloto en que los participantes controlaban un exoesqueleto de miembro inferior.

3.1. Aportación R1

3.1.1. Materiales y Métodos

Como se ha mencionado anteriormente, el objetivo de esta aportación fue la detectión de la intención del pedaleo. Se utilizó el Enobio 32 de Neuroelectrics© para adquirir las señales electroencefalográficas (EEG) de los usuarios y un sistema de captura de movimiento mediante sensores de movimiento inercial (IMUs, de la empresa Technaid) para saber en qué momento el usuario comienza a pedalear y poder estudiar las señales EEG. La Figura 3.1 muestra la arquitectura del sistema.

El protocolo que tenían que realizar los participantes fue el siguiente: al usuario se le indicaba que primero había un periodo de relajación el cual tenía que despejar la mente lo máximo posible y tras un periodo de tiempo el investigador le indicaba que empezara a pedalear cuando quisiera siempre y cuando esperara un mínimo de 3 segundos y sin contar entre el aviso y el pedaleo. Sólo en algunas repeticiones el usuario no esperaba lo suficiente y éstas eran descartadas.

Para poder detectar la intención del pedaleo, se estudiaron los cambios en sincronización y desincronización de eventos relacionados (ERS/ERD por sus siglas en inglés) que se producen en las bandas de frecuencias mu (8-12 Hz) y beta (12-

Figura 3.1: Arquitectura del sistema. El sistema de EEG graba las señales encefalográficas del usuario y el sistema de captura de medidas inerciales (IMUs por sus siglas en inglés) adquiere los datos del sujeto mientras pedalea. El ordenador recibe de manera síncrona los datos de las IMUs y el sistema EEG.

30 Hz). Según la literatura [115] [116], la intención de movimiento podría llegar a detectarse desde dos segundos antes de la realización del movimiento (ERD) y hasta dos segundos después (ERS) del comienzo de dicho movimiento. Por ello, en ambos estudios se analizaron dos tipos de ventanas para detectar la intención del pedaleo: sólo los 2 segundos previos a la realización del pedaleo; y desde 2 segundos antes hasta 2 segundos después de la realización de dicho movimiento, lo que conforma 4 segundos (Figura 3.2).

Para el análisis de los datos, primero se separaron los tramos de relajación y los de intención; el resto se desechó. La ventana de intención estaba definida por el comienzo real del pedaleo y por el tamaño de ventana a procesar; la ventana de relajación se definió con anterioridad a la de intención y siempre entre ambos casos una separación de 0.5 segundos para evitar el solapamiento entre las ventanas (Figura 3.2). Dichos datos fueron estudiados en ventanas de 1 segundo

cada 0.2 segundos. Primero se realizó un preprocesamiento para mejorar la relación señal-ruido basado en: filtro Notch a 50 Hz para eliminar la influencia de la corriente eléctrica, filtro Butterworth paso alto de 4 orden con una frecuencia de corte de 0.2 segundos para eliminar la corriente contínua y un filtro de referencia promedio común (common average reference en inglés, CAR) para mejorar la resolución espacial [117].

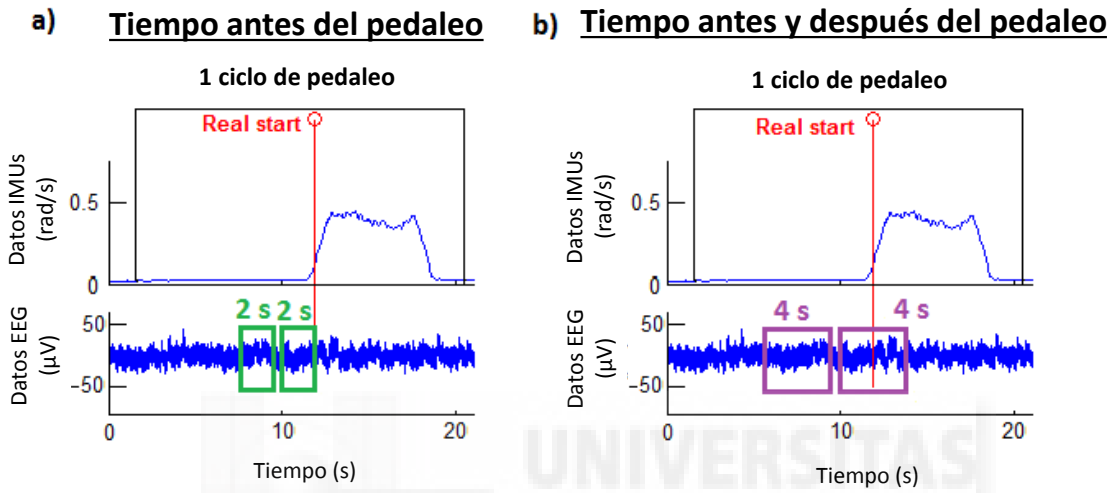

Figura 3.2: Tipos de procesamiento de ventana. El *Real start* se obtiene con la información proporcionada de las IMUs. A la izquierda (a), la ventana de intención se definió 2 segundos previos al la realización del movimiento. A la derecha (b), la ventana de intención se definió desde 2 segundos antes hasta 2 segundos después de la realización del movimiento.

Se estudiaron 8 configuraciones diferentes de electrodos (Figura 3.3) y 5 algoritmos de extracción de características distintos para los dos tipos de ventana de 2 y 4 segundos.

Los algoritmos empleados fueron los siguientes:

- Algoritmo A: Media de la potencia de la señal entre 18 y 28 Hz.
- Algoritmo B: Transformada de Fourier rápida por cada electrodo entre 0 y 50 Hz con resolución de 1 Hz. Posteriormente se calculaba la norma Euclidiana.
- Algoritmo C: La media de la potencia espectral para cada una de las bandas de frecuencia 1-4 Hz, 8-12 Hz, y 13-28 Hz.
- Algoritmo D: Densidad espectral de potencia media de cada electrodo en el

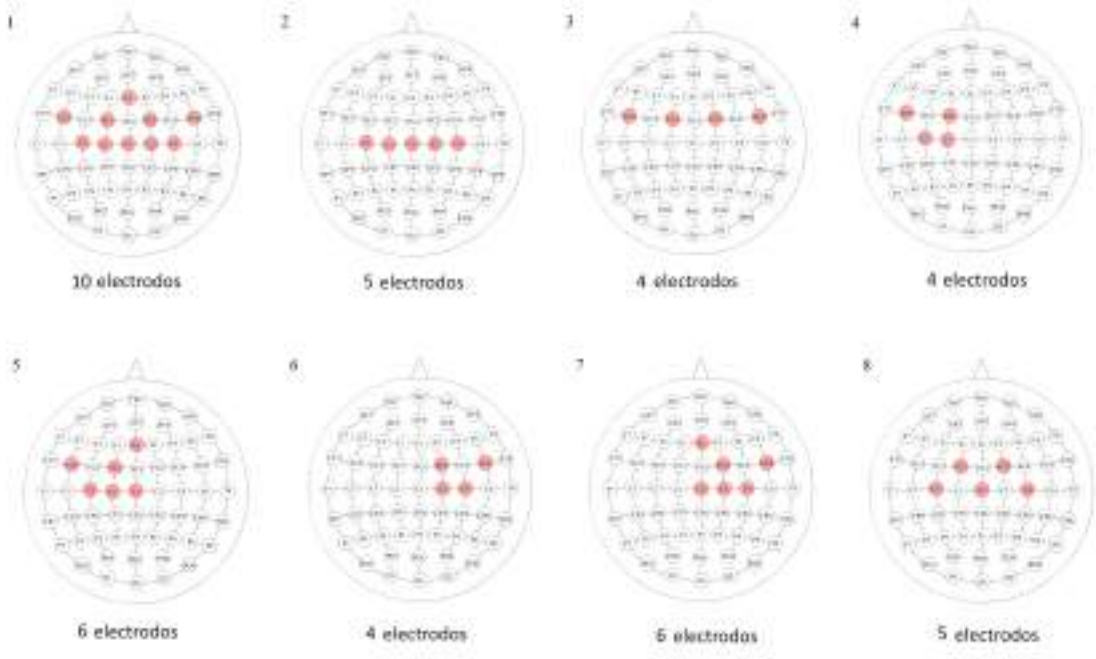

Figura 3.3: Configuraciones de electrodos basados en el Sistema Internacional 10-10. Para cada congfiguración de electrodos, los electrodos en rojo fueron los seleccionados. La configuración 1 se centraba en el área motor y premotor; la 2 se centraba en el área motor; la 3 se centraba en el área premotor; la 4 se centraba en el hemisferio izquierdo del área motor y premotor; la 5 se centraba en el hemisferio izquierdo del área motor, premotor y la línea media; la 6 se centraba en en el hemisferio derecho del área motor y premotor; la 7 se centraba en el hemisferio derecho del área motor, premotor y la línea media; y la 8 era una versión reducida de la primera configuración, centrada en el área motor y premotor.

rango de la frecuencia óptima ± 1 Hz de cada electrodo. Primero se buscaba la frecuencia óptima normalizada para cada electrodo que representaba la mayor diferencia de potencia entre la relajación y la intención de movimiento. Posteriormente se calculaba por cada electrodo la potencia a esa frecuencia óptima.

- Algoritmo E: Transformada de Fourier rápida por cada electrodo entre 0 y 50 Hz con resolución de 1 Hz. Luego se toma la respectiva suma para cada una de las tres bandas de frecuencia: mu (8-12 Hz), beta baja (12-24 Hz) y beta alta (24-30 Hz).

Para la clasificación se utilizó el algoritmo de máquinas de soporte vectorial (support vector machine en ingés, SVM) con kernel de función base radial (radial basis function en inglés).

Además, se estudiaron dos tipos de análisis: offline y pseudo-online. El análi-

sis offline se basa en realizar el experimento y posteriormente se obtienen los resultados; el análisis pseudo-online, hace una simulación de procesamiento en tiempo real. El experimento se realiza y a la hora de procesar los datos, se realiza como si se estuvieran recibiendo en tiempo real.

Para cada configuración de electrodos, algoritmo de extracción de características, ventana y tipo de procesamiento se calcularon tres parámteros de interés: la tasa de verdaderos positivos (TPR por sus siglas en inglés), el número de falsos positivos por minuto (FP/min) y la exactitud (Acc por su abreviación en inglés). Las definiciones de estos parámetros se pueden encontrar en la sección 2.4 de la separata de R1 en el Capítulo 6. Para poder evaluar la gran cantidad de datos, se creó el parámetro discriminador de pesos (weighted discriminator en inglés, WD) el cual ponderaba TPR, Acc y tasa de falsos positivos (FPR por sus siglas en inglés), asociándole distintos pesos a cada uno. El FPR se puede calcular del FP/min y teniendo en cuenta el tipo de procesamiento (offline o pseudo-online). La definición del WD, que varía entre -1 y 1, es la siguiente::

$$\mathrm{WD} = 0.4 \times \mathrm{TPR} + 0.6 \times \mathrm{Acc} - 1.0 \times \mathrm{FPR}\,. \tag{3.1}$$

Al FPR se le dio un peso grande negativo (-1.0), pues para controlar un sistema real (como un exoesqueleto) tener activaciones falsas no es en absoluto deseable. Por su parte, TPR y Acc tienen pesos positivos, pues son deseables, y Acc tiene un peso ligeramente superior porque se le quiere dar más importancia a este parámetro.

3.1.2. Resultados

En base a los resultados obtenidos en el análisis offline, se concluyó que la ventana de 2 segundos previos al movimiento no daban suficiente información para detectar la intención de movimiento. Por ello, en el análisis pseudo-online realizado, la ventana de 2 segundos quedó descartada y sólo se analizaron los

resultados usando ventanas de 4 segundos.

Utilizando los siguientes criterios en base al WD, fue posible definir de manera personalizada la configuración de electrodos (entre las 8) y algoritmos (entre los 5) que mejores resultados producían para cada uno de los usuarios:

1. Los dos mejores algoritmos se seleccionaron en base a los dos valores más elevados obtenidos de la media de los WD de las configuraciones de electrodos (C.E.) para cada algoritmo.

2. Entre los 16 valores de WD asociados a los dos algoritmos y las ocho configuraciones de electrodos, el valor máximo de WD se preseleccionó junto con todos los valores de WD dentro de $\pm$0,01 de ese máximo.

3. Por último, entre las combinaciones preseleccionadas, se eligió la que corresponde a la configuración del electrodo con el menor número de electrodos. Si hubo un empate en el número de electrodos, se seleccionó el que tenía el mayor WD. Si el empate continuaba, se elegía uno al azar.

De esta manera cada usuario tenía su propia BMI personalizada (en términos de la configuración de electrodos y algoritmo). Los resultados están en la Tabla 3.1.

Luego, se trató de determinar si la personalización de las BMIs para cada usuario verdaderamente valía el esfuerzo. Para ello se determinó el siguiente criterio para definir cuál era el algoritmo que mejores resultados producían en todos los usuarios:

1. Para cada sujeto y algoritmo, se calculó su WD promediada de las C.E. (los valores de WD se promediaron entre configuraciones de electrodos). Estos valores se promediaron entre los sujetos, de modo que un único WD promediado representaba cada algoritmo.

2. Se seleccionó el algoritmo asociado al promedio mayor.

Tabla 3.1: TPR, FP/min y Acc personalizando la configuración de BMI por cada usuario en una ventana de 4 segundos (Contribución R1).

S	Algorithm	C.E.	TPR (%)	FP/min	Acc (%)
1	D	4	83.3±15.1	10.3±6.33	25.1±11.7
2	B	8	76.7±23.4	0.08±0.20	96.7±8.16
3	D	2	86.7±20.7	6.83±3.29	32.1±9.33
4	C	2	76.7±15.1	3.74±2.20	81.8±15.9
5	E	4	60.0±17.9	3.73±1.82	39.9±14.7
		Average	**76.7**	**4.94**	**55.1**

El resultado de la generalización del algoritmo fue el D. Los resultados de cada usuario con este algoritmo y la personalización de la configuración de electrodos para cada usuario puede verse en la tabla 3.2.

Por último, se siguió el siguiente criterio para definir la configuración de electrodos que mejores resultados producían en todos los usuarios:

1. Dado el mejor algoritmo para todos los usuarios (D), los valores de WD se promediaron entre los sujetos para cada configuración de electrodo. Esto dio un WD promediado único para cada configuración de electrodo.

2. La configuración del electrodo asociada al mayor promedio fue seleccionada.

De esta manera, la BMI general para todos los usuarios fue el algoritmo D y la configuración de electrodos 4. Los respectivos resultados están en la Tabla 3.3. Al comparar los resultados de BMIs personalizadas con la BMI general se encontró que había diferencias estadísticamente significativas (p=0.0007), con los resultados de las BMIs personalizadas siendo más deseables. Sin embargo, los resultados donde se personalizó la configuración de electrodos con el algoritmo D fijado, no presentaban diferencias significativas en comparación con la BMI totalmente personalizada para cada usuario.

Tabla 3.2: TPR, FP/min y Acc para el análisis pseudo-online con el algoritmo D y la mejor configuración de electrodos para cada usuario (S) usando una ventana de procesamiento de 4 s.

S	C.E.	TPR (%)	FP/min	Acc (%)
1	4	83.3±15.1	10.3±6.33	25.1±11.7
2	4	66.7±16.3	0.26±0.45	90.0±16.7
3	2	86.7±20.7	6.83±3.29	32.1±9.33
4	6	86.7±16.3	3.76±2.10	47.0±9.38
5	1	56.7±23.4	3.83±1.07	35.5±9.63
Average		**76.0**	**5.00**	**46.0**

Tabla 3.3: TPR, FP/min y Acc para el análisis pseudo-online, extracción de características usando el algoritmo D y la configuración de electrodos 4 para cada sujeto (S) en una ventana de procesamiento de 4 s.

S	TPR (%)	FP/min	Acc (%)
1	83.3±15.1	10.3±6.33	25.1±11.7
2	66.7±16.3	0.27±0.45	90.0±16.7
3	96.7±8.16	10.1± 4.06	26.3±7.89
4	93.3±10.3	9.50±2.51	27.5±7.85
5	70.0±21.0	12.6±3.32	17.2±3.17
Average	**82.0**	**8.56**	**37.2**

3.1.3. Discusión

Se demostró que la personalización de BMIs a cada usuario (Tabla 3.1) ofrece mejores resultados comparados con un enfoque tradicional, donde se fija el algoritmo y la configuración de electrodos para todos los usuarios (Tabla 3.3 para el algoritmo D y la configuración de electrodos 4). Evidentemente, en dos de los parámetros de interés, FP/min (cuanto menos mejor) y Acc (entre más grande mejor), los resultados son superiores. Habiendo dicho eso, se encontró que sólo fijando el algoritmo (y personalizando la configuración de electrodos), los resultados eran estadísticamente comparables con los totalmente personalizados (de la Tabla 3.1). Esto implica que no es necesario personalizar toda la BMI, requiriendo menos tiempo para crear el modelo y continuar con la prueba.

En cuanto a otros trabajos en la literatura, se debe mencionar que la mayoría de los estudios se analizan offline [118, 119, 120, 114, 121, 122]. Los resultados parecen comparables en términos de TPR y Acc. Dicho esto, en muchos casos

las comparaciones son difíciles, ya que o bien los parámetros relevantes no se informan o deben ser post-procesados a partir de sus propios resultados. En un estudio donde también realizaron análisis pseudo-online [123], también presentaron resultados similares en todos los parámetros. Por lo tanto, los resultados en este trabajo parecen ser consistentes con aquellos en la literatura. Este estudio se enfocó en el pedaleo y no en la marcha. Sin embargo, el pedaleo parece ser un paso intermedio natural antes de realizar la rehabilitación de la marcha.

En cuanto a las limitaciones, una preocupación potencial en los resultados de este trabajo es el número relativamente alto de FP/min que es altamente indeseable cuando se trata de detectar el movimiento auto-iniciado. Por ello, en los siguientes estudios se realizan modificaciones en el protocolo y paradigma de este trabajo para buscar una mejora de los resultados.

3.2. Aportaciones R2 y R3

En estas aportaciones se analizaron configuraciones de tDCS capaces de mejorar la detección de imaginación del pedaleo (R2) y la marcha (R3) usando una BMI en tiempo real basada en las señales EEG de los usuarios. Adicionalmente, en R3 se hace un estudio piloto con personas sanas que activan un exoesqueleto de miembro inferior cuando imaginan que caminan para validar los resultados obtenidos en una situación real.

Primero, se explican los materiales y métodos de R2 y R3 explicando los puntos comunes y diferentes. Finalmente, se expondrán los resultados y se discutirán por separado.

3.2.1. Materiales y Métodos

El equipo utilizado en ambos casos tanto para adquirir las señales EEG (30 canales) como la aplicación de tDCS (2 y 3 canales) fue con el Starstim R32 de Neuroelectrics ©.

El protocolo, procesamiento y clasificación de ambas aportaciones es el mismo. Las diferencias entre R2 y R3 reside en la colocación de los electrodos de estimulación. En R2 está centrada en sobreexcitar M1 y la persona ha de imaginar que está pedaleando mientras está sentada; mientras que en R3 está centrada en excitar M1 y el cerebelo y además el usuario está de pie imaginando que caminaba (Figura 3.4.A y 3.4.B respectivamente).

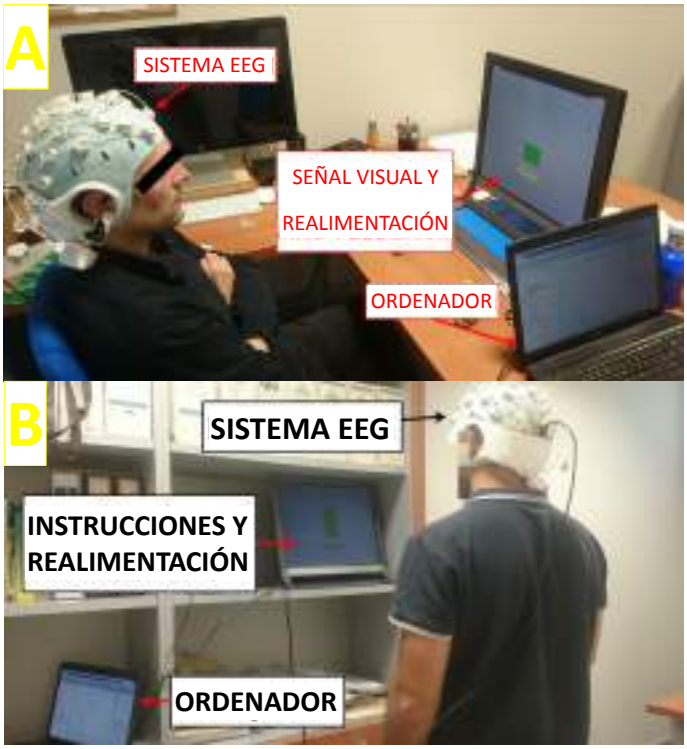

Figura 3.4: Diseño experimental. A) Los sujetos se sentaban enfrente de una pantalla que suministraba las instrucciones de las tareas a realizar mientras sus señales EEG estaban siendo grabadas. Las instrucciones dadas eran: Relajación, Imagina y + (transición). En le periodo de Imagina, el usuario imaginaba que estaba pedaleando. La pantalla daba realimentación sobre el desempeño de cada tarea. B) Los sujetos estaban de pie enfrente de una pantalla que daba las instrucciones de las tareas a realizar mientras sus señales EEG eran grabadas. Las instrucciones eran las mismas que en el caso anterior pero en este caso el usuario durante Imagina, tenía que imaginar que andaba. En ambos casos las tareas aparecían aleatoriamente pero nunca aparecía más de dos veces seguidas la misma tarea.

Montaje de estimulación en R2

En esta aportación se quería aumentar la excitabilidad en la corteza motora donde se encuentra la representación de las piernas. El principal reto de dicho montaje es que la estimulación alcance dicha área, ya que se encuentra en lo profundo de la fisura longitudinal. Previamente, se realizó una simulación con el software libre SimNIBS para asegurarnos que se estimulaban las áreas de interés (Figura 3.5). El montaje de estimulación constaba de dos electrodos: 1 ánodo y 1 cátodo. El ánodo se colocó en Cz por encontrarse sobre la representación de las piernas. El cátodo se ubicó en el hemisferio derecho del cerebelo. Esto fue debido a que previamente se ha estudiado que situar el cátodo sobre el cerebelo, produce excitación sobre M1. Por ello, se estaría sobre-excitando M1, tanto por el ánodo colocado en Cz como por el cátodo colocado en el cerebro-cerebelo derecho (Figura 3.6.A). La intensidad aplicada fue de 0.4 mA. En la figura 3.5 se puede apreciar la

excitación de la corteza motora donde se encuentra la representación de las piernas. Además, el área con mayor excitación está cerca del núcleo rojo y el tálamo. Dichas áreas pertenecen al camino de las salidas ascendentes del cerebelo hacia M1.

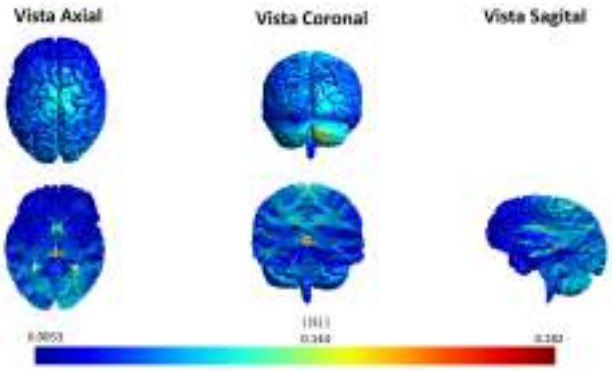

Figura 3.5: Vista axial, coronal y sagital de la simulación de tDCS. La escala representa el campo eléctrico (V/m) inducido por el ánodo ubicado sobre Cz y el cátodo sobre el cerebro-cerebelo derecho. La intensidad aplicada fue de 0.4 mA. El área más afectada (roja) está cerca del núcleo rojo. La imagen fue generada con el programa SimNIBS.

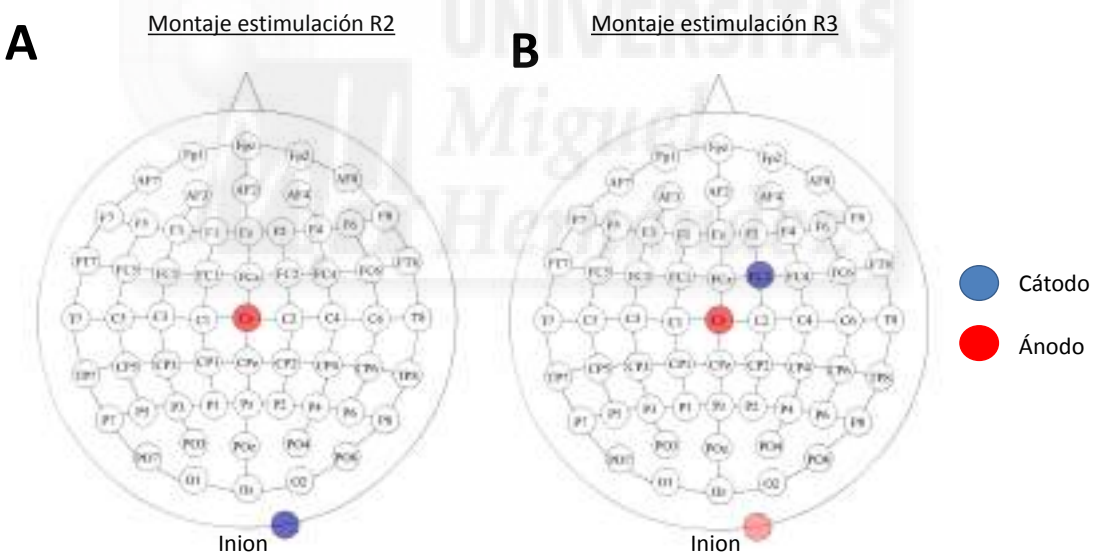

Figura 3.6: Montaje de los electrodos de estimulación de la aportación R2 (A) y R3 (B).

Montaje de estimulación en R3

En esta aportación se quería aumentar la excitabilidad de la corteza motora, donde se encuentra la representación de las piernas, y del cerebelo al mismo tiempo. Como en el estudio anterior, se realizó una simulación previa al experimento con el software libre SimNIBS para asegurarnos que se estimulaban las áreas de interés (Figura 3.7). El montaje de estimulación constaba de 3 electrodos: 2 ánodos y 1 cátodo. El ánodo A1 se colocó sobre el cerebelo, el ánodo A2 sobre Cz y el

cátodo sobre FC2 (Figura 3.6.B). La intensidad aplicada en A2 fue algo superior que en A1 (0.2 y 0.3 mA) para contrarrestar el efecto de la inhibición en la zona motora que produce el aumento de excitabilidad en el cerebelo. De esta forma, excitamos el cerebelo, la zona motora y además inhibimos el hemisferio derecho, dando preferencia al izquierdo. Esto fue decidido de esta manera porque a la hora de realizar pruebas con pacientes, se van a escoger aquellos en que hayan sufrido un ACV con afectación en la pierna derecha.

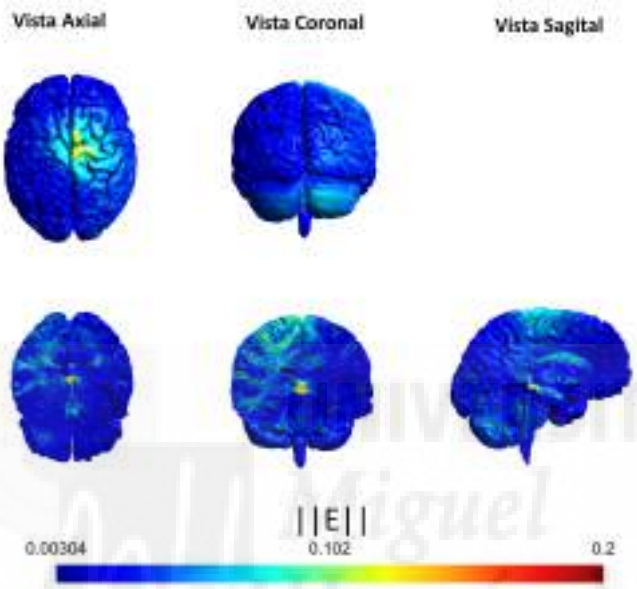

Figura 3.7: Vista axial, coronal y sagital de la simulación de tDCS. La escala representa el campo eléctrico (V/m) inducido por el ánodo ubicado sobre Cz y el cátodo sobre el cerebro-cerebelo derecho. La intensidad aplicada fue de 0.3 mA en la zona motora y 0.2 mA en el cerebelo. El área más afectada (roja) está cerca del núcleo rojo. La imagen fue generada con el programa SimNIBS.

Descripción del protocolo, procesamiento y clasificación

La Figura 3.8 muestra el diagrama de flujo experimental para ambas aportaciones. Los usuarios fueron separados aleatoriamente en sham, que es una estimulación falsa, y tDCS activo, aquellos que reciben estimulación verdadera. Luego, a simple ciego, cada usuario recibía, de acuerdo a su modalidad, 15 minutos de estimulación utilizando electrodos de 1 cm de radio. Después los usuarios realizaban la tarea de imaginación motora que consistía en 10 repeticiones de un ciclo de imaginación. Este ciclo de imaginación estaba compuesto por: 10 periodos de relajación y 10 periodos de imaginación; en R2 imaginaban que estaban pedaleando y en R3 que estaban caminando.

El procesamiento se aplica a ventanas de 1 segundo cada 0.2 segundos. A los

30 electrodos de cada ventana se les aplica un filtro Notch a 50 Hz para eliminar la corriente eléctrica, filtro paso alto a 0.05 Hz para eliminar la componente continua de la señal, filtro paso bajo a 45 Hz y filtro Laplaciano para eliminar la influencia del resto de los electrodos. Finalmente se seleccionan los 9 electrodos que se encuentran en la zona relacionada con la imaginación motora: CZ, CP1, CP2, C1, C2, C3, C4, FC1, FC2. Posteriormente, se obtiene el vector de características de los 9 electrodos seleccionados. El vector de características es la potencia a la frecuencia óptima normalizada por cada electrodo. Dicha frecuencia óptima normalizada es la frecuencia que representa la máxima diferencia entre los estados de relajación e imaginación de la actividad motora correspondiente.

Las primeras 4 repeticiones se usaron para entrenar un clasificador SVM usando un kernel de funciones de base radial (radial basis function en inglés). La frecuencia óptima normalizada se calcula durante este entrenamiento. Las 6 restantes se usaron para testear el clasificador en tiempo real midiendo la precisión global de cada día. Dicha precisión fue calculada como el número de aciertos (tanto de relajación como de imaginación) dividido por el numero total de ventanas analizadas.

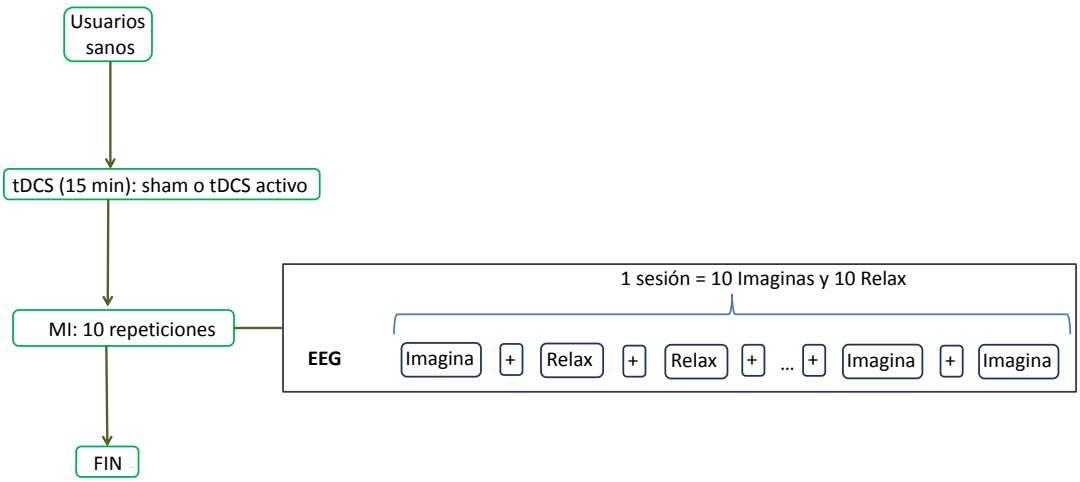

Figura 3.8: Diagrama de flujo experimental. Los participantes fueron aleatoriamente colocados en el grupo de sham y de tDCS activo. Durante 15 minutos recibían la correspondiente corriente de estimulación. Posteriormente realizaban 10 repeticiones de la tarea de imaginación motora basada dos tareas cognitivas: Relajación e Imaginación. Entre tareas había un periodo de transición representado por el símbolo +. Las tareas aparecían aleatoriamente pero nunca aparecía más de dos veces seguidas la misma tarea.

Prueba piloto

En R3 se hace un estudio piloto con personas sanas que activan en tiempo real un exoesqueleto de miembro inferior con sus seales EEG cuando imaginan que caminan. Esta prueba piloto se referencia como E2 para diferenciarla de la primera prueba hecha en R3, que a su vez se referencia como E1. El primer día, antes de empezar con el protocolo, los usuarios se familiarizaron con el exoesqueleto de miembro inferior. Hasta que los usuarios no estaban confiados de poder concentrarse en la imaginación motora mientras el exoesqueleto se movía, no se iniciaba la prueba.

El protocolo de dicha prueba fue modificado respecto al anterior para adecuarlo al control del exoesqueleto. Después de recibir los 15 minutos de estimulación (tDCS o sham), el usuario tuvo que realizar 80 repeticiones de la siguiente secuencia basada dos tareas cognitivas (Figura 3.9): Relajación e Imaginación. Se indicaba al usuario el comienzo del periodo de relajación donde tenían que concentrarse en su respiración. Posteriormente, una señal acústica indicaba el comienzo del periodo de imaginación de la marcha. Para finalizar, otra señal acústica indicaba el fin de la imaginación de la marcha y el comienzo de un segundo periodo de relajación. De las 80 repeticiones, la mitad fueron para crear el modelo. Durante el entrenamiento, el exoesqueleto se movió por sí solo, mientras que durante el periodo de test, el exoesqueleto era activado con las señales EEG del usuario. Durante los periodos de relajación, el exoesqueleto no estaba activado de acuerdo a las señales de EEG del usuario.

El procesamiento y la clasificación empleados fue el mismo que el explicado anteriormente.

3.2.2. Resultados R2

En este experimento participaron 14 usuarios, 7 pertenecían al grupo de sham y 7 al de tDCS activo. La Figura 3.10 muestra la evolución de cada día por cada grupo. Para evaluar si ha habido plasticidad, en la Tabla 3.4 muestra la significan-

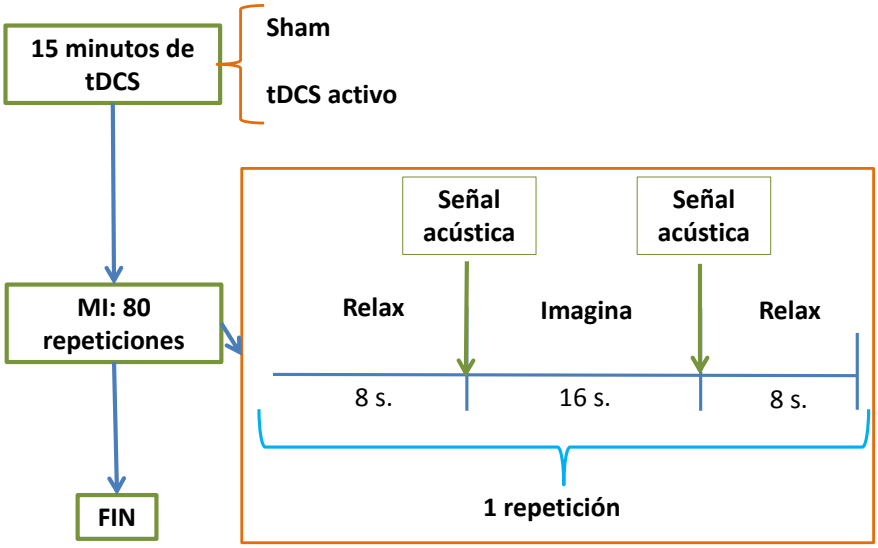

Figura 3.9: Diagrama de flujo experimental. Los participantes fueron aleatoriamente colocados en el grupo de sham y de tDCS activo. Durante 15 minutos recibían la correspondiente corriente de estimulación. Posteriormente realizaban 80 repeticiones de entrenamiento de la tarea de imaginación motora basada dos tareas cognitivas: Relajación e Imaginación. Durante la etapa de entrenamiento (40 primeras repeticiones), en los periodos de imaginación, el exoesqueleto se movía por sí mismo. En las 40 repeticiones posteriores, en el testeo de la BMI, los participantes activaban el exoesqueleto en los periodos de imaginación con sus señales EEG.

cia (valor de p) comparando cada día con el último y además se calculó el ERD en la banda mu de frecuencia del mejor usuario de cada grupo. La Figura 3.11 muestra la precisión obtenida y el ERD de dichos usuarios. En ella se puede apreciar que el aumento en la precisión corresponde con un aumento de la modulación del ERD.

Tabla 3.4: Comparación a pares de la precisión entre el grupo de tDCS y sham.

Día	1	2	3	4	5
Valor-*p*	0.04	0.29	1.00	0.74	0.60

3.2.3. Discusión R2

Aunque no se puede decir que existan diferencias entre el grupo de sham y el grupo de tDCS (60 % y 62.6 % de precisión alcanzada respectivamente), sí se puede afirmar que el grupo de tDCS alcanzó el mejor resultado el primer día, y mantuvo aproximadamente esos resultados por los siguientes 4 días. Mientras tanto, el grupo de sham tardó tres días en alcanzar dichos valores de precisión

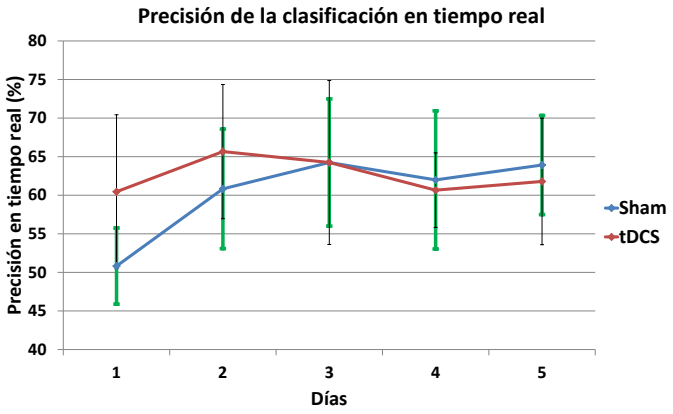

Figura 3.10: Precisión media en tiempo real de cada usuario por cada grupo y día.

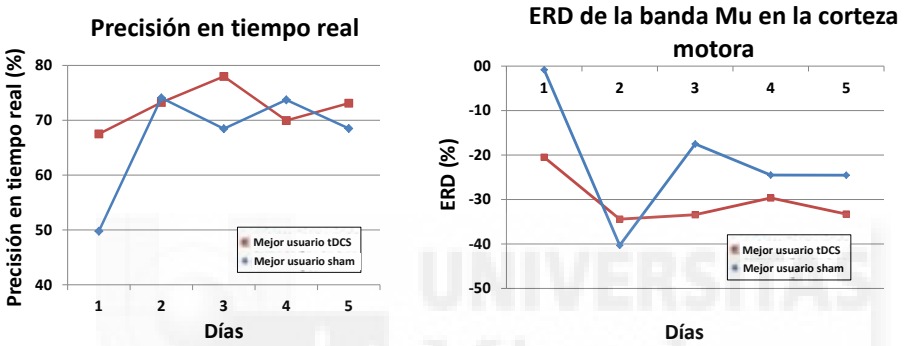

Figura 3.11: Precisión en tiempo real y ERD del mejor usuario de cada grupo.

(Figura 3.10). Por lo tanto parece que el tDCS tiene efecto inmediato en la activación de los caminos neuronales deseados, aunque eventualmente, y no de manera inmediata, el grupo sham parece lograr lo mismo (a pesar de que le tome más tiempo). Con el ánimo de observar diferencias significativas más fuertes entre los grupos, en el estudio R3 se cambió el número y colocación de los electrodos de estimulación, como ya se especificó previamente.

Para justificar la aparente baja precisión alcanzada en tiempo real de alrededor del 60 % (siendo el nivel de aleatoriedad del 50 %), se examinó detenidamente la literatura existente para hacer las comparaciones adecuadas. Los resultados que se reportan sobre BMIs en tiempo real está algo dispersa en la literatura actual [124], [125], [126], [127], [128], [129] [130], pero siempre que es posible comparar, nuestros resultados son equiparables con los de la literatura. Nuestros resultados son consistentes con los de Zich et al. [126] que tienen una precisión en tiempo real del 55-65 %, [124] con alrededor del 65 % de precisión (de las primeras 30

sesiones) y [125] con alrededor del 65 % de precisión entre otros.

3.2.4. Resultados R3

En el primer experimento (E1) participaron 12 usuarios, 6 pertenecieron al grupo de sham y 6 al de tDCS activo. La Figura 3.12 muestra la evolución de cada día por cada grupo.

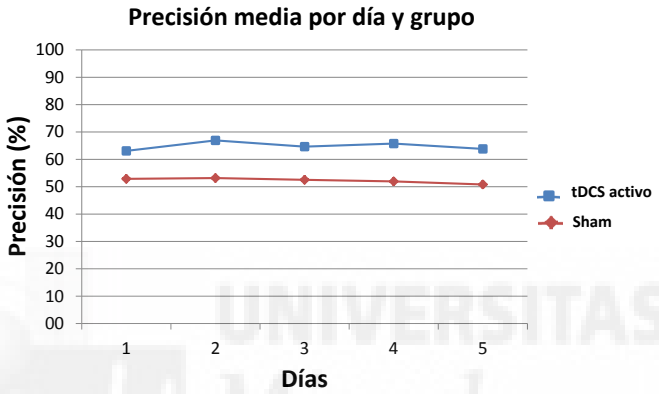

Figura 3.12: Precisión media en tiempo real de cada usuario por cada grupo y día.

En la prueba piloto (E2) participaron 4 usuarios, 2 pertenecieron al grupo de sham y 2 al de tDCS activo. La Figura 3.13 muestra la evolución de cada día por cada grupo.

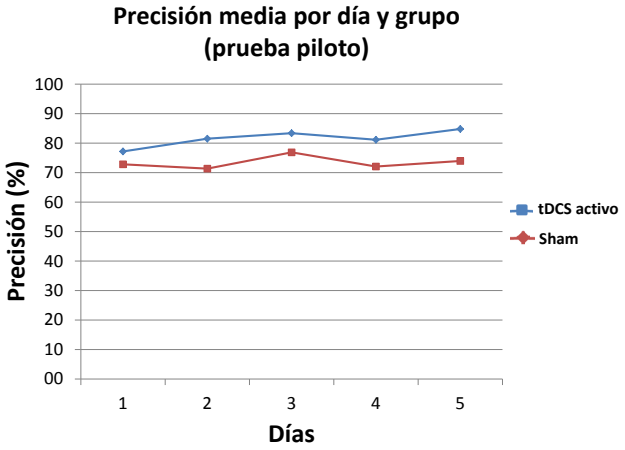

Figura 3.13: Precisión media en tiempo real de cada usuario por cada grupo y día.

Tanto para E1 como para E2, se realizó un histograma del porcentaje de frecuencias óptimas de los electrodos que se encuentran en las bandas de frecuencia relevantes (theta alta y mu, beta baja y media, y beta alta) para cada grupo (sham y tDCS activo). Para ambos experimentos se obtuvo que la banda de frecuencia más utilizada fue theta alta y mu (6-12 Hz).

Por otra parte, se realizó un mapa topográfico en la banda de frecuencia resultante anterior para ver los cambios de ERS (rojo) y ERD (azul) de E1 y E2 (Figura 3.14).

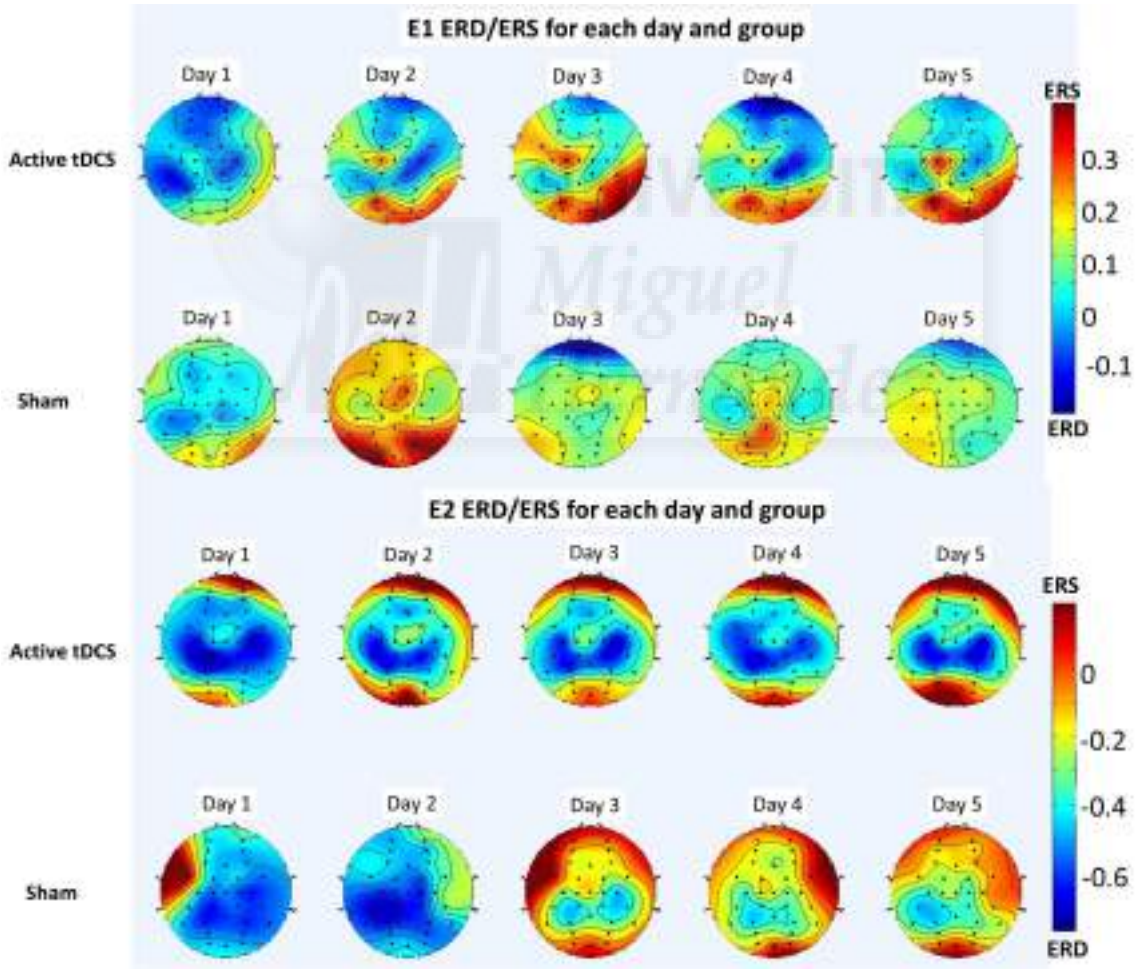

Figura 3.14: Mapa topográfico de ERS (rojo) y ERD (azul) para la banda de frecuencia 6-12 Hz promediada para todos los participantes en cada día y grupo del experimento. Los resultados de E1 se muestran arriba y los de E2 abajo.

3.2.5. Discusión R3

En esta aportación se ha evaluado un montaje nuevo de tDCS donde se estimulaba anodalmente tanto la corteza motora (Cz) como el cerebelo. Con esta configuración de electrodos se han encontrado diferencias significativas para el estudio principal (E1) entre el grupo de tDCS activo y el de sham. Además, los resultados preliminares de E2 también parecen soportar la hipótesis que la configuración novedosa de tDCS mejora la clasificación en tiempo real para una tarea de imaginación motora con control de exoesqueleto de miembro inferior. Primero, vale la pena dar una explicación neurológica de por qué este montaje de tDCS parece haber funcionado con éxito. El objetivo de la configuración de electrodos era mejorar las capacidades de aprendizaje del cerebro mientras se estimulaba la corteza motora, que es responsable del movimiento de las extremidades inferiores (y la imaginación). Con esto en mente, se colocó un ánodo sobre el cerebelo, ya que esto mejora las habilidades de aprendizaje del cerebro según varios estudios [131],[111],[132],[133]. Sin embargo, colocar este ánodo sobre el cerebelo también tiene otras consecuencias. Específicamente, produce la activación de las células de Purkinje que inhiben el núcleo dentado y provocan la desfacilitación de la corteza motora [134],[135],[136], que es lo contrario de lo que es deseado con respecto a la activación de la corteza motora. Por esta razón, para contrarrestar el efecto del primer ánodo y excitar la actividad neuronal de la corteza motora, se colocó un segundo ánodo directamente en Cz sobre la corteza motora, y con una corriente ligeramente más alta. De hecho, las corrientes utilizadas fueron 0.2 mA para el primer ánodo y 0.3 mA para el segundo ánodo.

El grupo activo de tDCS obtuvo de media un 12,6 % y un 8,2 % de mayor precisión que el grupo de sham para E1 y E2 respectivamente. Además, el grupo tDCS activo de E1 fue al menos un 10 % mejor que el grupo simulado en cada día (Figura 3.12), mientras que en E2, fue al menos un 4 % mejor en cada día (Figura 3.13).

Además, el análisis ERD / ERS de la Figura 3.14 muestra que, en general, tanto para E1 como para E2, parece haber más desincronización (ERD) en la banda

mu del grupo tDCS que en el grupo sham. Por otra parte, esta desincronización de la onda mu se produce principalmente en el área sensoriomotora, como se informa ampliamente en la literatura cuando hay ejecución motora o imaginación motora [137], [138]. Esta desincronización parece ser más evidente en el estudio preliminar E2 que en E1, pero en ambos casos se observa. Por lo tanto, el grupo tDCS activo para ambos experimentos parece mejorar la modulación de la banda mu y el control de BMI.

Comparando los resultados entre E1 y E2, el exoesqueleto mejoró la precisión y el control de la BMI obteniendo 16,7 % y 21,2 % más precisión para el grupo de tDCS y sham respecto a E1. Esto puede ser debido por diferencias en el protocolo experimental. Primero, por la distinta duración de los periodos de relajación e imaginación. Y más importante, los usuarios de E1 indicaron que la realimentación visual hacía más complicada la realización de la prueba, frustrándoles cuando la barra no incrementaba y generándoles ansiedad durante la prueba. Mientras que en E2 la realimentación del exoesqueleto era más natural ya que generaba movimiento del cuerpo, aunque no estaba inducida por los músculos del usuario. También es interesante comparar los resultados de E1 y E2 a través del análisis ERD / ERS. Se observa que la desincronización es más fuerte y más consistente en E2 que en E1. Esto parece ser consistente con algunos resultados en la literatura que involucran exoesqueletos de miembros superiores [139], que encontraron que el poder discriminativo del área sensoriomotora es mayor cuando se usa un exoesqueleto, proporcionando así un beneficio en términos de la BMI diseñada.

Esta aportación ha sido desafiante ya que implicaba la combinación de tDCS con una BMI en tiempo real conectado a un exoesqueleto. Los exoesqueletos normalmente están pre-programados o controlados por terceros dispositivos (joysticks, aplicaciones de teléfonos móviles, etc.), pero sólo hasta hace relativamente poco tiempo se comenzó a controlar a través de BMIs. El diseño de una BMI en tiempo real tampoco es trivial en sí mismo. Por lo tanto, el estudio de BMIs para controlar un exoesqueleto en tiempo real está apenas comenzando y tiene muchas posibles aplicaciones clínicas, especialmente en la rehabilitación de pacientes. Por ende, combinar este concepto con tDCS, que tiene como objetivo mejorar y acele-

rar la capacidad cognitiva, enriquece y aumenta esas aplicaciones aún más.

Para terminar, se van a comentar algunos aspectos respecto al funcionamiento en tiempo real del exoesqueleto en E2. Para tener una verdadera utilidad de usar una BMI con el exoesqueleto, el análisis de las detecciones falsas durante los períodos de relajación es importante, y reducirlo es un objetivo esencial. La tasa de tales detecciones se conoce como tasa de falsos positivos, o FPR (que es el complemento de la precisión cuando se restringe solo a los períodos de relajación). Al promediar ambos grupos en E2, el FPR fue del 11,7 % (equivalente a una precisión del 88,3 % durante la relajación), con un FPR del 11,3 % para el grupo tDCS y del 12,1 % para el grupo sham. Los valores para ambos grupos fueron muy similares, lo que muestra que el aumento general en la precisión resultante de la estimulación del grupo tDCS se debió a un aumento de la precisión durante los períodos de imaginación (de hecho, la precisión en esos períodos fue del 92,7 % para el grupo de tDCS y de 80,4 % para el grupo sham). En cualquier caso, en general, estos valores de FPR parecen razonables para este experimento preliminar, pero reducirlos aún más es un objetivo a futuro.

Capítulo 4

CONCLUSIONES Y TRABAJOS FUTUROS

Conclusiones

Cada año aumenta el número de personas que ha sufrido un accidente cerebrovascular (ACV) quedando con secuelas en su sistema motriz y, muchas veces, con pérdida de su autonomía. Ello ha provocado el impulso de la comunidad científica a investigar nuevas terapias de rehabilitación. Los primeros 6 meses tras este tipo de lesión son cruciales a la hora de experimentar una mejora notable y evitar sufrir consecuencias más agudas. Por esta razón, es importante disponer de herramientas que les involucren tanto a nivel muscular como cognitivo.

Para mejorar esta situación, esta tesis se ha centrado en la combinación de las interfaces cerebro-máquina (BMI por sus siglas en inglés) y la estimulación transcraneal por corriente directa (tDCS por sus siglas en inglés). Estas herramientas permiten tanto el desarrollo de mecanismos de asistencia como rehabilitación neurológica.

Las aportaciones más relevantes de esta tesis son las siguientes:

- Se han diseñado BMIs capaces de controlar un dispositivo externo en tiempo real usando las señales electroencefalográficas (EEG) del usuario.

- Se han diseñado BMIs capaces de detectar la intención de ejecutar el pedaleo.

- Usando las BMIs, se ha discernido entre la imaginación motora de las extremidades inferiores y la relajación. Esto se hizo tanto para pedaleo como para la marcha.

- Se ha encontrado una configuración de electrodos de tDCS capaz de mejorar el control de las interfaces cerebro-máquina diseñadas.

- Se han aplicado las BMIs basadas en señales EEG para controlar en tiempo real un exoesqueleto que se mueve en relación a la imaginación de marcha por parte de un usuario sano.

- Se han combinado técnicas de tDCS junto con el control en tiempo real de un exoesqueleto por medio de BMIs que detectan la imaginación de movimiento en extremidades inferiores.

- Se han obtenido resultados prometedores usando la combinación de la tDCS, BMI en tiempo real y exoesqueletos para aplicarlo a pacientes que hayan sufrido un ACV con secuelas en las piernas y mejorar su proceso de rehabilitación.

Trabajos Futuros

Aunque se han conseguido grandes avances con la realización de esta Tesis, aún queda mucho trabajo por realizar en este campo. Se deben seguir desarrollando diversos aspectos de las siguientes líneas de investigación para continuar mejorando el proceso de rehabilitación:

- Combinar la BMI en tiempo real, la estimulación tDCS y el uso de una pedalina para mejorar la movilidad de la pierna afectada tras un ACV. Antes

de que un paciente se ponga de pie e intente caminar, es recomendable fortalecer dicha vía neuronal. Para ello, la utilización de la imaginación motora en una BMI, al activar zonas neuronales comunes que la ejecución de dicho movimiento, puede reforzar dicha vía neuronal con entrenamiento. Además, el uso de la tDCS, al modular la excitabilidad cortical, puede favorecer la comunicación entre el cerebro y los movimientos de los músculos a través de la vía corticoespinal.

- Realizar experimentos en tiempo real con pacientes de ACV combinando la BMI, la tDCS y el exoesqueleto de miembro inferior. De esta manera se podrá comprobar si estos mecanismos mejoran el proceso de rehabilitación de los pacientes, su autonomía y calidad de vida.

- Incorporar la estimulación magnética transcraneal al protocolo experimental para evaluar si hay cambios plásticos neuronales. Esto permitirá obtener una medida más robusta de la plasticidad.

- Evaluar nuevas intensidades y montajes tDCS para estudiar su eficacia en la mejora del proceso de rehabilitación.

- Evaluar los artefactos generados por la BMI para dotar al sistema de mayor robustez durante las pruebas experimentales.

- Realizar un estudio comparativo de los beneficios de diferentes terapias de rehabilitación en pacientes de ACV.

UNIVERSITAS
Miguel
Hernández

Capítulo 5

PUBLICACIONES

5.1. Publicación revista R1

UNIVERSITAS
Miguel
Hernández

frontiers in Neuroinformatics

ORIGINAL RESEARCH
published: 11 July 2017
doi: 10.3389/fninf.2017.00045

Personalized Offline and Pseudo-Online BCI Models to Detect Pedaling Intent

*Marisol Rodríguez-Ugarte *, Eduardo Iáñez, Mario Ortíz and Jose M. Azorín*

Brain-Machine Interface Systems Lab, Systems Engineering and Automation Department, Miguel Hernández University of Elche, Elche, Spain

The aim of this work was to design a personalized BCI model to detect pedaling intention through EEG signals. The approach sought to select the best among many possible BCI models for each subject. The choice was between different processing windows, feature extraction algorithms and electrode configurations. Moreover, data was analyzed offline and pseudo-online (in a way suitable for real-time applications), with a preference for the latter case. A process for selecting the best BCI model was described in detail. Results for the pseudo-online processing with the best BCI model of each subject were on average 76.7% of true positive rate, 4.94 false positives per minute and 55.1% of accuracy. The personalized BCI model approach was also found to be significantly advantageous when compared to the typical approach of using a fixed feature extraction algorithm and electrode configuration. The resulting approach could be used to more robustly interface with lower limb exoskeletons in the context of the rehabilitation of stroke patients.

Keywords: pedaling intention, pseudo-online, offline, electrode configurations, feature extraction algorithms, personalized brain-computer interfaces

OPEN ACCESS

Edited by:
Jose Manuel Ferrandez, Universidad Politécnica de Cartagena, Spain

Reviewed by:
Monzurul Alam, Hong Kong Polytechnic University, Hong Kong
Miguel Almonacid, Universidad Politécnica de Cartagena, Spain

****Correspondence:***
Marisol Rodríguez-Ugarte
maria.rodriguezu@umh.es

Received: *03 April 2017*
Accepted: *26 June 2017*
Published: *11 July 2017*

Citation:
Rodríguez-Ugarte M, Iáñez E, Ortíz M and Azorín JM (2017) Personalized Offline and Pseudo-Online BCI Models to Detect Pedaling Intent. Front. Neuroinform. 11:45. doi: 10.3389/fninf.2017.00045

1. INTRODUCTION

The scientific community has increasingly become more conscious of the problems suffered by people with motor disabilities, including their rehabilitation process. The use of brain-computer interfaces (BCIs) as an alternative pathway for those people who cannot move their limbs properly has been extensively studied in the literature (Dobkin, 2007; Daly and Wolpaw, 2008). Offline processing of the electroencephalography (EEG) signals can often be accurate and useful as an a posteriori tool, while a continuous processing of the signals, called here a pseudo-online analysis, may produce results of lower quality, but is much more reliable for use in active therapies that directly involve the patient's central nervous system (Daly and Wolpaw, 2008; López-Larraz et al., 2014). Indeed, exoskeletons, which are devices assisting a patient's affected limb (Hortal et al., 2015), can be combined with BCIs to improve the rehabilitation process in terms of time and quality (Pennycott et al., 2012; Rodríguez-Ugarte et al., 2016).

The basis of BCIs is to extract neural oscillations (often in the form of EEG signals), commonly known as brain waves, and translate them into commands to control a device. These waves are categorized by the frequency bands associated with the performance of some activity, and by the predominant location where they are generated (Rao, 2013). Some frequency bands are: delta (0.1–4 Hz), associated to deep sleep (Amzica and Steriade, 1998); theta (4–7 Hz), related to drowsiness (Schacter, 1977); alpha (8–15 Hz); mu (8–12 Hz), detectable in the sensorimotor cortex (Steriade, 2005); beta (16–31 Hz), detectable over the parietal and frontal lobe (Rao, 2013); and gamma (21–100 Hz).

Accurately detecting movement intent ideally involves detecting the movement before it even initiates, but may encompass both the moments previous and the initial phases of movement. In any case, the idea is to detect the movement as early as possible from the brain waves, and typically, the earlier one wishes to detect movement initiation, the more challenging it becomes. Recent studies have found two phenomena to detect movement intent: the Bereitschaftspotential (BP) (Bhagat et al., 2014; Xu et al., 2014) and event-related desynchronization/synchronization (ERD/ERS) (Bai et al., 2007; Planelles et al., 2014). BP is a motor related cortical potential (MRCP) (Jahanshahi and Hallett, 2003). Its detection usually requires averaging across many trials due to its small amplitude and low frequency, meaning that its real-time detection is typically not viable. Meanwhile, ERD/ERS are frequency fluctuations detectable in the mu and beta bands. These phenomena start about 2 s before movement onset with a decrease of the band power (ERD), followed by its increment (ERS) at about 2 s after the movement onset (Toffanin et al., 2007; Nam et al., 2011). Overall, detection of movement intent using EEG signals has been studied in subjects when performing reaching tasks, walking, hand movement or hand motor imagery (Bai et al., 2007; Ibáñez et al., 2010; Bai et al., 2011; Lew et al., 2012; López-Larraz et al., 2014; Sburlea et al., 2015). However, many of these studies suffer from only being tested offline, or from experimental setups that produce unrealistic EEG signals when compared to real-life self-initiated movement (Pfurtscheller et al., 2006; Lehtonen et al., 2008).

Outcomes of the effectiveness of BCIs on detecting an activity are often highly subject-dependent (Ang and Guan, 2013; Rohm et al., 2013), and therefore processing the data in several different ways and choosing the most effective way for each subject can be very useful in improving the results. Key factors in data processing include window selection (whether only time before movement onset, or time before and after movement onset is considered), electrode configurations and feature extraction algorithms. The usual approach involves uniformly using a fixed subject-independent electrode configuration (with associated filters) and feature extraction algorithm. On the other hand, the approach in this work is distinctive in being flexible on the choice of these parameters, so that the BCI model is better adapted to each subject.

The purpose of this work was to design a personalized BCI capable of detecting the intention of self-initiated pedaling. This included consideration of a wide array of processing algorithms for both offline and pseudo-online. To compare the results, a metric was defined, and a procedure to choose the best algorithm for each particular subject was described. More precisely, two different processing windows, with eight different electrode configurations, and with five different extraction algorithms were studied. To determine the effectiveness and reliability of the BCI, the average and variance of three important parameters were reported: the true positive rate (TPR), the false positives per minute (FP/min) and the accuracy (Acc).

Detection of asynchronous pedaling intention was contemplated in the context of stroke patients looking to improve their walking ability. The results in this work are a stepping stone toward that final goal. Thus, there was more effort invested in the analysis of pseudo-online processing, due to its relevance in active therapies involving patients (e.g., via exoskeletons). Having said that, for now, only healthy subjects were considered. Pedaling, which is a complex motor task, was chosen over walking, because it may represent an important intermediate step in patient recovery before attempting gait. Additionally, it permits a more controlled experimental setting of the lower limbs, which for example avoids artifacts such as head movements.

2. MATERIALS AND METHODS

2.1. Subjects

Five healthy subjects between 24 and 35 years old (3 males and 2 females, 28.6 $\pm$ 4.2 years), all right footed, took part in this experiment. The subjects did not have any known neurological diseases and all of them gave written informed consent according to the Helsinki declaration. The Ethics Committee of the Office for Project Evaluations (Oficina Evaluadora de Proyectos: OEP) of the Miguel Hernández University of Elche (Spain) approved the study.

2.2. Test Description

The experiment consisted on pedaling and resting during periods of time in which EEG and motion signals were recorded. Subjects were sat at a comfortable distance from a pedal exerciser, as shown in **Figure 1**. Each subject performed one session, which was composed of 16 trials. Each trial consisted of 5 pedaling cycles, with each cycle defined as: 10 s of resting, followed by a cue from the experimenter indicating the subject to initiate pedaling at their own volition for about 5 s. Before starting the experiment, subjects were told to wait without counting a minimum of 3 s between the cue and the pedaling movement. This requirement was specified in order to avoid the influence of cue presentation in the EEG signals. If this period was not fulfilled, the trial was discarded. **Figure 2** shows a sketch of the protocol.

2.3. BCI Design

A BCI aiming to detect pedaling intent through EEG signals was designed by searching for ERD/ERS in the mu and beta bands. To achieve this, five different feature extraction algorithms were considered. In addition, each algorithm was applied using two different types of processing windows: those with only time before movement onset, and those with time before and after movement onset. Furthermore, each combination of window type and algorithm was tested with eight different electrode configurations. Then, all this data was utilized to select a personalized BCI for each subject. This will be explained in more detail throughout this section.

Data was divided in two types: training and test data. Both types follow the same process: signal acquisition, data selection,

Abbreviations: E.C., Electrode Configuration; MVA, Majority Vote Algorithm; Acc, Accuracy; WD, Weighted Discriminator.

FIGURE 1 | Experiment setup. Subjects sat at a comfortable distance to pedal in a pedal exerciser wearing two IMUs per leg and an EEG reader. Both systems were connected to a computer to process the signal. The participant in the picture gave written informed consent to publish the image.

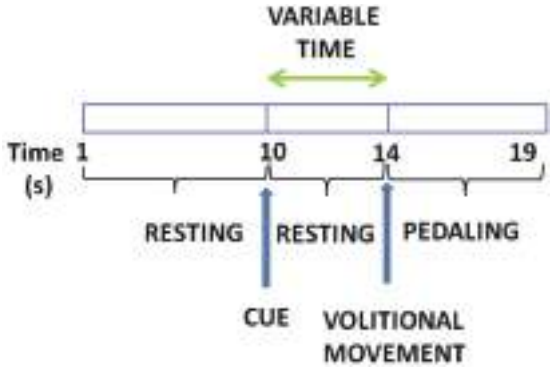

FIGURE 2 | Experiment protocol: Subjects remain for about 10 s still followed by a cue to start pedaling for about 5 s. Time between the cue and the pedaling start is at least 3 s.

preprocessing, channel selection, and feature extraction. The features and their corresponding class of training data were used to create the model. Then, that model was used to classify the features extracted from the test data. More details will follow later.

In terms of software, a MATLAB (MathWorks Inc., Massachusetts, United States) platform was developed to record, process and classify the EEG signals. Test data was processed using offline and pseudo-online analyses. The offline analysis consists of recording the EEG signals and then, without the acquisition hardware, loading and analyzing them. As will be observed later, classification and processing of data analyzed offline requires the knowledge of the full signal beforehand (e.g., use of cross validation and majority vote algorithms). On the other hand, the pseudo-online analysis bears some similarities with the offline analysis in the local processing of the data, but crucially differs in that the EEG signals are treated as if they were to be processed in real-time. Therefore, only the data before a given time is used for classification, and data selection requiring prior knowledge of the movement onset is impossible with this type of analysis. Hence, the pseudo-online analysis is more challenging to design and implement than the offline analysis, but has the advantage of having potential use in real-time activities, such as interfacing with exoskeletons. The word *pseudo* is used here to clarify that in this work the EEG data was not processed in real-time during the experiments themselves, but instead was collected and a posteriori was treated as such. This was done to test the different pseudo-online schemes, so that in the future a real-time processing of data is successfully achieved.

2.3.1. Signal Acquisition

The Enobio 32 EEG system (Neuroelectrics, Barcelona, Spain) was used to extract the signals from the brain. It is a wireless device with 32 electrodes based on the International 10-10 system (P7, P4, CZ, PZ, P3, P8, O1, O2, C2, F8, C4, F4, FP2, FZ, C3, F3, FP1, C1, F7, OZ, PO4, FC6, FC2, AF4, CP6, CP2, CP1, CP5, FC1, FC5, AF3, PO3) and with two reference electrodes (CMS and DRL). The reference electrodes were located on each subject's earlobe with the help of an earclip. Signals were acquired at a sampling frequency rate of 500 Hz. This system is shown in **Figure 1**.

Furthermore, to verify the reliability of the BCI system, its output was compared to the Tech MCS system's output (Technaid S.L., Spain). This wireless device is based on inertial measurement units (IMUs). Each IMU is composed by three micro sensors: a 3D gyroscope, a 3D magnetometer and a 3D accelerometer. Nineteen parameters are registered by each IMU, but only the gyroscope in X was utilized to detect when a real start of the pedaling movement was produced. Data was registered at a frequency of 20 Hz through a HUB connected to the USB port of the PC. Subjects wore two IMUs per leg: one located on the external part of the ankle and the other one located on the tibialis anterior, as can be appreciated in **Figure 1**. It should be noted that there are "cheaper" alternatives to measuring angular velocities which do not involve IMUs, but ultimately equipment availability was the deciding factor.

2.3.2. Data Selection

The angular velocities associated to the two IMUs in each leg were averaged, and the real start was defined when both leg averages exceeded a threshold. Meanwhile, 32 EEG signals where acquired and, part of this data was selected.

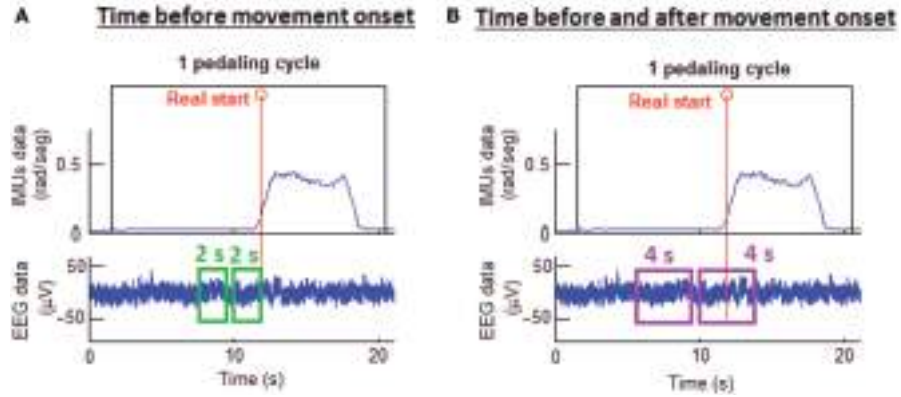

FIGURE 3 | Processing window types. On the left **(A)**, the start class window selection was 2 s before the movement onset. On the right **(B)**, the start class was 2 s before and 2 s after the movement onset.

As reported in Toffanin et al. (2007), the potential generated by movement intention appears 2 s before the movement onset and it lasts until around 2 s after the onset. Hence, two types of processing windows were studied: 2 and 4 s processing windows. In addition, data was separated in two classes: rest and start. These two classes were defined according to the real start and the processing window selected. For 4 s processing windows, the start class window was defined from 2 s before to 2 s after the real start was produced. For 2 s processing windows, the start class window was defined from 2 s before up to the real start. The rest class window was chosen to be the same duration as the corresponding start class window and was located before the start class window with a gap of 0.5 s between the two classes. **Figure 3** presents these two classes with the two different types of processing windows. The EEG training data was selected from these class windows.

For the offline analysis, the window placement also determined where EEG test data was selected from, while for the pseudo-online analysis the whole pedaling cycle data was used as EEG test data. Thus, for the pseudo-online analysis, the window placement merely served as a marker to determine if a given detection was located in the start class window or not.

2.3.3. Pre-processing

Preprocessing was carried out in order to improve the signal to noise ratio. Rest and start class windows were analyzed in 1 s epochs with a 200 ms shift. For each epoch a notch filter was applied to suppress the power line interference at 50 Hz. Then, a 4th order Butterworth high-pass filter with a cut-off frequency of 0.2 Hz was used to remove the direct current. Finally, a common average reference (CAR) filter was computed as in McFarland et al. (1997). This filter removed from each electrode the influence of the other ones by using the mean potential.

2.3.4. Channel Selection

Once the epoch was preprocessed, an electrode configuration was selected. Eight different electrode configurations (E.C.) were studied to determine which one presented better results for each subject. These are illustrated in **Figure 4**. The electrodes of each configuration were located on the somatosensory and motor cortex, which were the areas where most of the neural activity was expected.

2.3.5. Feature Extraction

For each epoch of interest, five different feature extraction algorithms were implemented in order to evaluate the optimal one for each subject:

- Algorithm A: The mean bandpower of the signal between 18 and 28 Hz was calculated for each electrode. Therefore, this method provided one feature per electrode.
- Algorithm B: Fast Fourier Transform (FFT) was applied to each electrode to evaluate the spectrum in the 0–50 Hz frequency range with 1 Hz resolution. The Euclidean norm of the resulting vector (of size 50) was then computed. Using this method, there was one feature per electrode.
- Algorithm C: This algorithm computed the mean of the power spectral density of the bands of 1–4 Hz, 8–12 Hz, and 13–28 Hz. Therefore, for each electrode there were three features.
- Algorithm D: For this method, the best frequency for each electrode, which corresponds to the potential with the highest variation between classes, was calculated. First, the power spectral density between 8 and 28 Hz with 0.5 Hz of resolution was applied. Then, rest and start class were separated and normalized. For each electrode, the frequency for which the maximum difference between classes occurred was selected and denominated as the optimal frequency. These optimal frequencies for each electrode were part of the model. Finally, the mean power spectral density of each electrode in the range of its optimal frequency $\pm$ 1 Hz was calculated. Using this method there was one feature per electrode.
- Algorithm E: FFT with a 1 Hz resolution was applied to each electrode. Then, the sum of three frequency ranges was determined for each electrode: mu (8–12 Hz), beta low

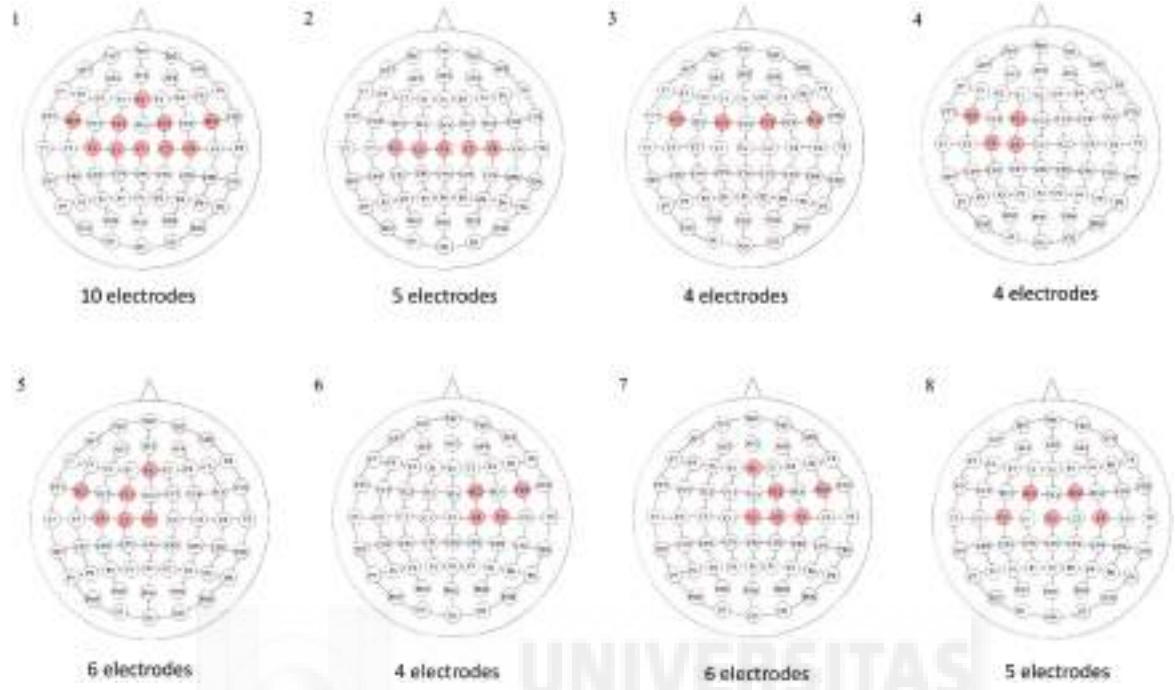

FIGURE 4 | Electrode configurations based on the International 10–10 system. For each electrode configuration, the red electrodes were the ones selected. Configuration 1 focused on the motor and premotor areas; 2 focused on the motor area; 3 focused on the premotor area; 4 focused on the left side of the motor and premotor areas; 5 focused on the left side of the motor, premotor and medial areas; 6 focused on the right side of the motor and premotor areas; 7 focused on the right side of the motor, premotor and medial areas; and 8 was a reduced version of the first configuration, which focused on the motor and premotor areas.

(12–24 Hz) and beta high (24–30 Hz). This method provided three features for each electrode.

2.3.6. Classification

A support vector machine (SVM) classifier was used to create the model and classify the data. This classifier is based in hyperplane separation by maximizing the margin between the nearest points of the different classes (Steinwart and Christmann, 2008). When combined with nonlinear kernels, the classifier is one of the most robust and often provides better outcomes than other classifiers like linear discriminant analysis (Hortal et al., 2016; Sburlea et al., 2016). In this work a radial basis function was utilized as a kernel for the SVM.

For the offline analysis a cross-validation was performed: fifteen trials were used to create the model and one to test it; the process was repeated 16 times until all the trials were tested; and the results were averaged among the 16 repetitions. Indeed, each of the 16 created models was applied to classify features of test data so that each epoch lying in the start or rest classes was associated with an epoch prediction of either 0 (indicating nothing is happening) or 1 (indicating a detection). Then, the epoch predictions were grouped appropriately into the corresponding class in which they belonged (resulting in groups of 16 for 4 s windows and groups of 6 for 2 s windows), and a majority vote algorithm (MVA) was used for each group to produce a single prediction (either 0 or 1) per group. If the output of the MVA was a tie, the output of the classifier for that group was 0. Then, that outcome was compared with the real value of the class (0 for the rest class and 1 for the start class). This process can be seen in **Figure 5A**.

For the pseudo-online analysis, the first 10 trials were used to create the model and the other 6 to test it. For each epoch, the classifier took a decision (an epoch prediction). Afterward, a voting queue algorithm was used. This algorithm determined that a pedaling initiation detection was produced after 5 consecutive detections. The detection was then checked to see if it lied in a start class window, in which case it was a true detection, and otherwise was labeled as a false positive. If many true detections occurred in a fixed start class window, only one true detection was counted. **Figure 5B** shows this classification analysis.

2.4. Post-processing

In order to quantify the results, different parameters were calculated:

- True positive rate (TPR): indicates the percentage of real pedaling intentions that were correctly classified as such,

$$\mathrm{TPR} = \frac{\text{Number of true detections}}{\text{Number of true events}}. \quad (1)$$

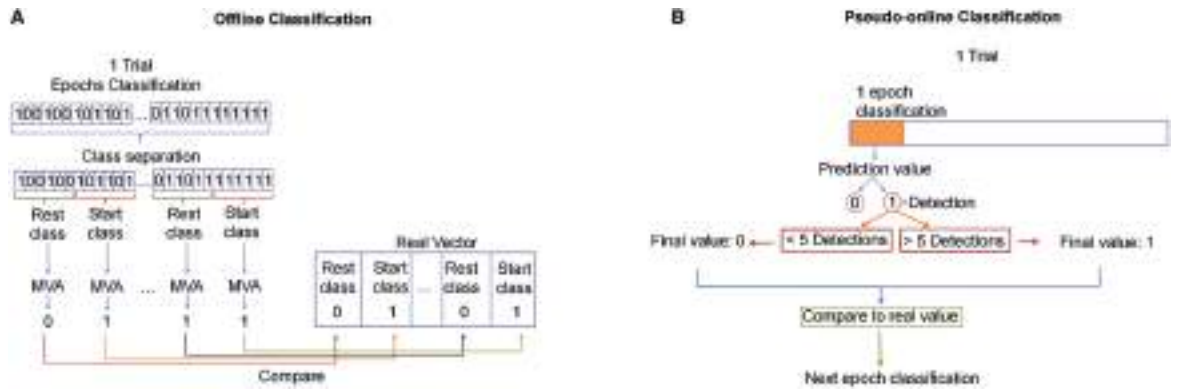

FIGURE 5 | (A) Offline analysis: All epochs are classified. Then, a MVA is applied for each class window. Finally it is compared with the real vector. **(B)** Pseudo-online analysis: Each epoch is analyzed. A pedaling intention detection is produced after 5 successive detections. This value is compared with the real one.

- False positives per minute (FP/min): represents how many times per minute the classifier detects a pedaling intent during resting,

$$\text{FP/min} = \frac{\text{Number of false detections}}{\text{Rest time in minutes}}. \quad (2)$$

- Accuracy (Acc): denotes how many pedaling intentions detected were actually real pedaling intentions,

$$\text{Acc} = \frac{\text{Number of true detections}}{\text{Number of total detections}}. \quad (3)$$

It is extremely convenient to have full knowledge of all three parameters. Indeed, if one of the parameters is not known, there are cases where one cannot determine with certainty whether the classifier is working properly or not. For instance, if Acc is 100%, FP/min is 0 and the TPR is missing, it could be because the classifier correctly detected just one pedaling intention out of five, meaning the BCI would not be working very well despite the known parameters having seemingly desirable values.

Moreover, as a unifying metric to differentiate results coming from distinct processing schemes, a new combined parameter was defined. It is called the weighted discriminator (WD) and is a linear combination of TPR, Acc, and the false positive rate (FPR), which is related to FP/min. The weights are chosen to reflect the preferences of the authors in the corresponding parameter. This unified parameter greatly facilitates statistical analysis and comparison between different electrode configurations and feature extraction algorithms. The weights chosen were -1.0 for FPR, which one would want to minimize as much as possible (the authors think false positives are highly undesirable in real-time applications of the BCI); 0.6 for Acc, which the authors want to give slight preference over TPR; and 0.4 for TPR, such that the range of WD goes from -1 (in the worst case scenario) to 1 (in the best case scenario). The equation for WD is then,

$$\text{WD} = 0.4 \times \text{TPR} + 0.6 \times \text{Acc} - 1.0 \times \text{FPR}. \quad (4)$$

Here, the false positive rate (FPR) is defined as

$$\text{FPR} = (\text{FP/min}) \times (\text{Duration of a single FP in mins}), \quad (5)$$

where that duration is precisely the window length (either 2 or 4 s) for the offline analysis and 1 s (equivalent to 5 consecutive detections, each represented by the shift of 200 ms) for the pseudo-online analysis.

3. RESULTS AND DISCUSSION

For each subject, the data was processed using both offline and pseudo-online analyses, with two different types of processing windows, five different extraction algorithms, and eight different electrode configurations, for a total of 160 possible combinations per subject. For each combination, the TPR, FP/min and Acc were calculated as in Equations (1–3), and from these, the values of FPR and WD were also computed as indicated in Equations (4) and (5).

3.1. Offline Analysis

Table 1 shows the values of WD per subject after using an offline analysis of the EEG data. As mentioned before, these were averages that resulted from the cross-validation among the 16 trials (see Section 2.3.6). Additionally, for each subject, type of processing window, and algorithm, the WD was averaged among the eight different electrode configurations (E.C.), and this is referred to here as the E.C.-averaged WD. These were reported in **Table 1** as well. Then, based on these E.C.-averaged WD values, the "best" two algorithms (for each subject and type of processing window) were chosen as those corresponding to the two highest averages. The selected algorithms were marked with two asterisks in **Table 1**.

The 4 s processing windows include time after which the movement has initiated (see **Figure 3**) and are comprised of 16 epochs, while the 2 s processing windows only include the 6 epochs preceding movement initiation. Thus, intuitively, it is much more demanding to detect the ERD/ERS phenomena when

TABLE 1 | WD value for all subjects using an offline analysis.

S	E. C.	Offline −2 s to 0 s					Offline −2 s to 2 s				
		A	B	C	D	E	A	B	C	D	E
1	1	0.11	0.09	0.47	0.08	0.40	0.28	0.16	0.60	0.51	0.27
	2	0.21	0.02	0.26	0.17	0.22	0.32	0.02	0.41	0.53	0.47
	3	0.07	0.26	0.40	0.24	0.26	0.17	0.27	0.61	0.50	0.39
	4	0.04	0.01	0.24	0.39	0.14	0.22	−0.05	0.61	0.68*	0.57
	5	0.05	0.19	0.30	0.23	0.39	0.10	0.07	0.50	0.33	0.35
	6	0.02	0.06	0.04	0.14	0.18	0.18	0.07	0.28	0.43	−0.01
	7	0.33	0.22	0.10	0.16	0.17	0.14	0.12	0.33	0.38	0.13
	8	0.12	0.16	0.31	0.21	0.16	0.24	−0.12	0.56	0.52	0.36
	Avg.	0.12	0.13	0.27**	0.20	0.24**	0.21	0.07	0.49**	0.48**	0.32
2	1	−0.13	0.12	−0.14	−0.07	0.29	0.36	0.68	0.62	0.74	0.72
	2	0.03	0.15	−0.07	0.04	0.41	0.07	0.59	0.39	0.70	0.70
	3	−0.21	0.11	−0.23	−0.04	0.16	0.27	0.71	0.57	0.69	0.67
	4	−0.02	0.12	0.09	−0.11	0.34	0.32	0.48	0.25	0.64	0.71
	5	−0.09	0.16	−0.07	0.09	0.21	0.28	0.68	0.64	0.76*	0.74
	6	−0.14	0.34	−0.11	−0.15	0.41	−0.16	0.56	0.58	0.74	0.75*
	7	−0.16	0.25	−0.27	−0.09	0.36	0.27	0.66	0.57	0.72	0.76*
	8	−0.17	0.41	−0.09	−0.12	0.35	0.29	0.68	0.56	0.75*	0.76*
	Avg.	−0.11	0.21**	−0.11	−0.06	0.32**	0.21	0.63	0.52	0.72**	0.73**
3	1	0.25	0.15	0.20	0.21	0.28	0.47	0.20	0.51	0.61*	0.41
	2	0.00	−0.01	0.17	−0.01	0.31	0.30	−0.12	0.51	0.57	0.40
	3	0.15	0.19	0.29	0.07	0.26	0.36	0.13	0.57	0.52	0.41
	4	0.17	0.37	0.19	0.21	0.23	0.30	0.11	0.57	0.55	0.50
	5	0.04	0.26	0.14	0.07	0.30	0.31	0.32	0.58	0.46	0.46
	6	0.02	0.10	0.20	0.19	0.15	0.28	0.07	0.58	0.59	0.27
	7	0.06	0.32	0.20	0.10	0.23	0.21	0.06	0.44	0.57	0.35
	8	−0.15	0.19	0.19	−0.05	0.12	0.29	0.11	0.53	0.57	0.44
	Avg.	0.07	0.20**	0.20	0.10	0.24**	0.32	0.11	0.54**	0.56**	0.41
4	1	0.14	0.02	0.47	0.26	0.22	0.35	0.22	0.60*	0.61*	0.50
	2	−0.03	0.12	0.26	0.32	0.08	−0.01	0.16	0.41	0.48	0.22
	3	0.10	−0.01	0.40	0.42	0.29	0.25	0.27	0.61*	0.59	0.53
	4	0.08	0.14	0.24	0.22	0.18	0.14	−0.12	0.61*	0.50	0.30
	5	0.13	0.16	0.30	0.34	0.20	0.16	0.21	0.50	0.53	0.38
	6	0.12	0.03	0.04	0.21	0.13	0.10	0.19	0.28	0.57	0.33
	7	0.12	0.24	0.10	0.34	0.16	0.21	0.12	0.33	0.57	0.49
	8	0.06	0.13	0.01	0.43	0.20	0.14	0.21	0.36	0.61*	0.40
	Avg.	0.09	0.10	0.23**	0.32**	0.18	0.17	0.16	0.46**	0.56**	0.39
5	1	0.17	0.18	0.25	0.27	0.10	0.59*	0.25	0.58	0.54	0.52
	2	0.11	0.02	0.07	0.15	0.08	0.53	0.15	0.32	0.56	0.40
	3	0.06	0.10	0.17	0.24	0.12	0.43	0.16	0.33	0.53	0.31
	4	−0.02	−0.08	0.01	−0.06	−0.02	0.48	0.23	0.10	0.24	0.31
	5	0.26	0.21	0.11	0.13	0.05	0.49	0.11	0.32	0.47	0.42
	6	0.24	0.03	0.26	0.27	0.09	0.42	0.28	0.45	0.50	0.46
	7	0.33	0.00	0.26	0.20	0.03	0.54	0.09	0.55	0.53	0.37
	8	0.15	-0.11	0.20	0.26	0.20	0.50	0.32	0.47	0.55	0.41
	Avg.	0.16	0.05	0.17**	0.18**	0.08	0.50**	0.20	0.39	0.49**	0.40

Results for the 2 s processing windows are shown on the left, while those of the 4 s processing windows are shown on the right. The best two feature extraction algorithms for each subject (S) are indicated with two asterisks. The best electrode configurations for those algorithms are also pointed out with one asterisk (those within 0.01 of the highest WD value among those two-asterisk-columns).

TABLE 2 | TPR, FP/min and Acc results for the best offline feature extraction algorithm and electrode configuration of each subject (S) with 4 s processing windows.

S	Algorithm	E.C.	TPR (%)	FP/min	Acc (%)
1	D	4	63.8 ± 24.5	1.69 ± 2.18	89.1 ± 13.7
2	E	6	50.0 ± 27.3	0.19 ± 0.75	93.8 ± 25.0
3	D	1	71.3 ± 29.2	2.25 ± 2.57	78.6 ± 26.9
4	C	3	67.5 ± 20.5	2.44 ± 2.50	83.7 ± 16.8
5	A	1	82.5 ± 21.8	3.56 ± 4.55	82.8 ± 20.8
		Average	67.0	2.03	85.6

using the 2 s windows than with the 4 s windows. Indeed, as expected, the WD values for the 2 s processing windows were considerably lower (the E.C.-averaged WD values did not go beyond 0.32) than those of the 4 s windows (where an E.C.-averaged WD value of 0.73 was observed).

Clearly, the results varied across subjects and it was evident that some electrode configurations and algorithms were better suited to certain individuals. With this in mind, the goal was to find the "best" combination of feature extraction algorithm and electrode configuration for each person. This selection was restricted to the 4 s processing windows given the stark difference in the quality of the results when compared to the 2 s windows. The "best" BCI for each subject was determined using the following procedure:

1. The best two algorithms were selected based on the two highest E.C.-averaged WD values. These were marked with double asterisks in **Table 1**.
2. Among the 16 WD values associated to the two algorithms and eight electrode configurations, the maximum WD value was preselected along with all those WD values within 0.01 of that maximum. These were marked with a single asterisk in **Table 1**.
3. Lastly, among the preselected combinations, the one corresponding to the electrode configuration with the lowest number of electrodes was chosen (see **Figure 4**). If there was a tie on the number of electrodes, the one with the highest WD was selected. If the tie continued, one was chosen at random.

The best personalized BCIs with an offline analysis and 4 s processing windows were tabulated in **Table 2**. The cross-validation averages and standard deviations of the TPR, FP/min and Acc were reported.

3.2. Pseudo-Online Analysis

A more detailed examination of the pseudo-online analysis is presented next. This is due to the long-term goal of using these BCIs in active therapies to aid recovering stroke patients, where an online processing of the signals is crucial. In real-time applications it would be ideal to use the 2 s windows over the 4 s windows, since they would produce more natural movement in a patient. Having said that, this choice is contingent upon the quality of the results. For the pseudo-online analysis, the test data was processed differently using the last 6 trials and then averaged (with the first 10 training trials being used to create the models). In fact, computing the WD values analogously to **Table 1** again showed much better results for 4 s processing windows than with 2 s windows. Thus, the results suggest that it is preferable to use the 4 s processing windows, even if slightly delayed movement is produced as a result of this choice. Indeed, from now on, only the 4 s processing windows will be investigated for the pseudo-online analysis.

3.2.1. Best Personalized BCIs

WD values were tabulated as in **Table 1**, but for compactness, only the WD results for the two best algorithms of each subject using 4 s processing windows were shown in **Table 3**. Note that the best two algorithms per subject were the same for the offline processing as with the pseudo-online processing, but this is a consequence of this particular data set. In general, the best two algorithms could be completely different for the two types of analyses.

Also, notice the apparent contradiction that WD results for some subjects seem to be higher with the pseudo-online analysis than with the offline analysis. This happened due to the way the false positives were detected, and thus in the way FP/min and FPR were computed with the two different analyses (see 5). Indeed, due to the nature of the offline analysis, only one FP can be detected per rest window. This means that if the FPs were abundant in pseudo-online (say, 6 per rest window), the FPR would be underestimated in the offline analysis, but if the FPs were scarcer (an average of less than 4 per 4 s rest window), the offline analysis would overestimate the FPR and produce lower WD offline values. This can be observed when computing the FPR from **Tables 2**, **4** and comparing. Thus, it is not wise to compare results between offline and pseudo-online analysis via WD. However, given a fixed type of analysis, it would be justifiable to compare between electrode configurations and feature extraction algorithms.

The best personalized BCIs were selected as described in Section 3.1. The TPR, FP/min and Acc for those personalized configurations are displayed in **Table 4**, where the standard deviations were computed from the 6 different test trials of each subject.

3.2.2. Are Personalized BCIs Worthwhile?

The purpose of this section is to show that the use of personalized BCIs is indeed preferable over a more traditional approach, were the electrode configuration and feature extraction algorithm are fixed and are used uniformly for all subjects. The goal is also to determine to what extent the personalization of the BCI among all subjects makes sense for this data set. To do this, a criteria to find the best feature extraction algorithm among all subjects (not *per* subject) is described. Then, for that fixed algorithm a procedure to choose the best (personalized) electrode configuration per subject is outlined. Next, the results are statistically compared with those of the "fully" personalized BCI described in the previous section (reported in **Table 4**). Finally, given the choice of the best algorithm, a method to choose the best electrode configuration among all subjects is described,

TABLE 3 | WD values for the best two feature extraction algorithms of each subject with pseudo-online analysis for the 4 s processing windows.

E. C.	Subject 1		Subject 2		Subject 3		Subject 4		Subject 5	
	C	D	B	E	C	D	C	D	A	E
1	0.24	−0.04	0.81	0.81	0.42*	0.37	0.74*	0.47	0.34	0.36
2	0.22	0.18	0.69	0.77	0.33	0.43*	0.74*	0.48	0.35	0.42*
3	0.30*	0.15	0.61	0.84	0.41	0.29	0.67	0.51	0.32	0.24
4	0.29	0.31*	0.53	0.85	0.38	0.38	0.67	0.38	0.23	0.42*
5	0.22	0.11	0.60	0.82	0.36	0.29	0.67	0.38	0.35	0.27
6	0.16	0.27	0.73	0.77	0.37	0.33	0.68	0.57	0.35	0.23
7	0.17	0.14	0.86	0.84	0.28	0.31	0.71	0.58	0.29	0.24
8	0.23	0.06	0.89*	0.76	0.35	0.35	0.70	0.57	0.28	0.32

The best electrode configurations are pointed out with one asterisk.

TABLE 4 | TPR, FP/min, and Acc results for the best pseudo-online feature extraction algorithm and electrode configuration of each subject (S) with 4 s processing windows.

S	Algorithm	E.C.	TPR (%)	FP/min	Acc (%)
1	D	4	83.3 ± 15.1	10.3 ± 6.33	25.1 ± 11.7
2	B	8	76.7 ± 23.4	0.08 ± 0.20	96.7 ± 8.16
3	D	2	86.7 ± 20.7	6.83 ± 3.29	32.1 ± 9.33
4	C	2	76.7 ± 15.1	3.74 ± 2.20	81.8 ± 15.9
5	E	4	60.0 ± 17.9	3.73 ± 1.82	39.9 ± 14.7
		Average	76.7	4.94	55.1

TABLE 5 | TPR, FP/min and Acc results for the pseudo-online feature extraction algorithm D and the best personalized electrode configuration of each subject (S) with 4 s processing windows.

S	E.C.	TPR (%)	FP/min	Acc (%)
1	4	83.3 ± 15.1	10.3 ± 6.33	25.1 ± 11.7
2	4	66.7 ± 16.3	0.26 ± 0.45	90.0 ± 16.7
3	2	86.7 ± 20.7	6.83 ± 3.29	32.1 ± 9.33
4	6	86.7 ± 16.3	3.76 ± 2.10	47.0 ± 9.38
5	1	56.7 ± 23.4	3.83 ± 1.07	35.5 ± 9.63
	Average	76.0	5.00	46.0

leading to a fixed algorithm and electrode configuration. Again, the results are statistically compared with those of the "fully" personalized BCI.

The procedure used to choose the best uniform feature extraction algorithm was as follows:

1. For each subject and algorithm its E.C.-averaged WD was computed (WD values were averaged among electrode configurations). These values were then averaged among the subjects, so that a single averaged WD represented each algorithm.
2. The algorithm associated to the highest such average was selected.

Taking these steps yielded that the best uniform algorithm was D, followed closely by algorithms C and E. Next, given this choice of best algorithm, the method to select the best electrode configuration per subject was:

1. Given the best uniform algorithm, there are eight WD values associated to the eight electrode configurations per subject. The maximum WD value was preselected along with all those WD values within 0.01 of that maximum.
2. Among the preselected WD values, the one corresponding to the electrode configuration with the lowest number of electrodes was chosen (see **Figure 4**). If there was a tie on the number of electrodes, the one with the highest WD was selected. If the tie continued, one was chosen at random.

For a pseudo-online analysis and 4 s processing windows, the BCIs associated with the best uniform algorithm and a personalized electrode configuration are presented in **Table 5**.

To get a better statistical sample to compare the results of **Tables 4**, **5**, the WD values of each of the 6 test trial sessions were computed for each subject. This yielded 30 WD values (from 5 subjects and 6 trial sessions) associated to the BCIs in **Table 4** and the same with **Table 5**. A Wilcoxon signed-rank test determined that the differences of these samples were not statistically significant ($p = 0.07$) at the standard 5% significance level. Thus, for this particular set of subjects it would make sense to use D as a fixed feature extraction algorithm. This can be helpful to reduce processing time when determining the best possible personalized BCI, since one must only seek between different electrode configurations, instead of different algorithms plus electrode configurations.

Lastly, the idea was to find the best "traditional" approach by finding the feature extraction algorithm and electrode configuration that best suited *all* subjects. The procedure to find the algorithm that best fitted all subjects was already described, while that of finding the optimal electrode configuration was as follows:

1. Given the best uniform algorithm, the WD values were averaged among the subjects for each electrode configuration. This gave a single averaged WD for each electrode configuration.

TABLE 6 | TPR, FP/min, and Acc results for the pseudo-online feature extraction algorithm D and electrode configuration 4 for each subject (S) with 4 s processing windows.

S	TPR (%)	FP/min	Acc (%)
1	83.3 ± 15.1	10.3 ± 6.33	25.1 ± 11.7
2	66.7 ± 16.3	0.27 ± 0.45	90.0 ± 16.7
3	96.7 ± 8.16	10.1 ± 4.06	26.3 ± 7.89
4	93.3 ± 10.3	9.50 ± 2.51	27.5 ± 7.85
5	70.0 ± 21.0	12.6 ± 3.32	17.2 ± 3.17
Average	82.0	8.56	37.2

2. The electrode configuration associated to the highest such average was selected.

Following this procedure yielded that the "traditional" approach that best suited all subjects was that associated to the fixed use of algorithm D and electrode configuration 4. The results associated to these parameters are shown in **Table 6**.

The results of **Tables 4**, **6** were compared using the Wilcoxon signed-rank test as described previously. In this case, there were statistically significant differences ($p = 0.0007$) of the two samples. A quick inspection of **Table 6** shows the results are much less preferable than those of **Table 4**. Thus, it is clear that a personalized BCI seems to be more suitable than a traditional approach. This shows the power of considering personalized BCIs, as they give greater versatility in providing the best results possible for a particular individual.

3.3. Further Discussion

To summarize, as one would expect, the 2 s processing windows with only time before movement onset produce results of lower quality (in terms of WD) than the 4 s processing windows which include time before and after the movement onset. For this reason, it seems preferable to use 4 s processing windows for most purposes, even if they may cause a slight delay when used in real-time applications. Furthermore, based on the WD values, a rigorous procedure to select the best feature extraction algorithm and electrode configuration for each subject was described. Generally speaking, the optimal combination involves high WD values along with the lowest number of electrodes possible. The "minimization" of the number of electrodes is in part to qualitatively pinpoint the areas of the brain that produce the best results, and in part because results can be processed faster (which may be useful in real-time processing of signals). Lastly, statistical analyses determined that the fully personalized BCIs produced better results than a traditional approach. Naturally, other choices of feature extraction algorithms and electrode configurations than those provided in this work are possible, and those are left to the criteria of new researchers. However, the overarching philosophy of personalizing the BCI to each subject is the key point.

Regarding other work in the literature, it should be mentioned that most studies are analyzed offline (Bai et al., 2007, 2011; Lew et al., 2012; Bulea et al., 2014; Jiang et al., 2015; Sburlea et al., 2015). The results seem comparable in terms of TPR and Acc. Having said that, in many cases comparisons are difficult, since either the relevant parameters are not reported or they must be post-processed from their own results. One study with a pseudo-online analysis Ibáñez et al. (2010) also presented similar results in all parameters. Thus, the results in this work seem to be consistent with those in the literature.

Pseudo-online personalized BCI models were preferred in comparison with offline models, due to their potential use with exoskeletons and other real-time applications. Specifically, the goal is to use this approach in therapies to improve the pedaling capabilities of recovering stroke patients who will be aided by an exoskeleton (or some other medium). Indeed, pedaling seems to be a natural intermediate step before fully rehabilitating gait. The results in this work are valid for the small sample of healthy subjects studied, but to make any assertions in terms of the quality of the results in larger population samples of healthy or recovering patients, more experiments are needed. Having said that, when compared with a traditional approach, the idea of personalizing the BCIs is also expected to yield better results in the population of stroke patients.

Regarding the limitations, a potential for concern in the results of this work is the relatively high number of FP/min which is highly undesirable when trying to detect self-initiated movement. Thus, there is still room for improvement in trying to reduce this variable. Finally, another future avenue of research with these personalized BCI models is the detection of pedaling or walking initiation via motor imagery, for which new protocols must be designed.

4. CONCLUSIONS

A personalized BCI model aimed at the prediction of the intention of self-initiated pedaling was successfully designed for each subject. This included choosing among different types of processing windows (2 possible), feature extraction algorithms (5 possible) and electrode configurations (8 possible). Moreover, this process was done both for offline analysis and pseudo-online analysis. More precisely, a metric developed by the authors, called the weighted discriminator (WD), was used to compare different BCIs. Indeed, a procedure based on the WD and used to select the best personalized BCI model of each individual was described in detail. This procedure resulted in a desirable choice of feature extraction algorithm and electrode configuration for each specific subject. In general, a processing window of longer duration and including time after movement onset was preferred over the other type of processing window. The results in pseudo-online for the best BCI models of each subject were in average 76.7% of TPR, 4.94 FP/min and 55.1% of Acc. More importantly, statistical analyses were used in a systematic fashion to show that personalized BCIs provide better results than a traditional approach, where a subject-independent feature extraction algorithm and electrode configuration are used for all subjects. Finally, in the context of the rehabilitation of stroke patients, this approach may be useful in active therapies to interface with a lower limb exoskeleton.

AUTHOR CONTRIBUTIONS

MR is responsible for the design, implementation, acquisition and data analysis. MR and EI took part in the interpretation of data. In addition, EI and MO supervised the work and contributed with the revision process. JA actively contributed as director of the work.

FUNDING

This research was carried out in the framework of the project Associate titled: Decoding and stimulation of motor and sensory brain activity to support long term potentiation through Hebbian and paired associative stimulation during rehabilitation of gait (DPI2014-58431-C4-2-R), which is funded by the Spanish Ministry of Economy and Competitiveness and by the European Union through the European Regional Development Fund (ERDF), "A way to build Europe."

ACKNOWLEDGMENTS

The authors thank Neuroelectrics® for lending the Enobio 32 EEG system used in the experiments. The authors are also grateful for the comments of the reviewers, which significantly improved the quality and readability of the article.

REFERENCES

Amzica, F., and Steriade, M. (1998). Electrophysiological correlates of sleep delta waves. *Electroencephalogr. Clin. Neurophysiol.* 107, 69–83. doi: 10.1016/S0013-4694(98)00051-0

Ang, K. K., and Guan, C. (2013). Brain-computer interface in stroke rehabilitation. *J. Comput. Sci. Eng.* 7, 139–146. doi: 10.5626/JCSE.2013.7.2.139

Bai, O., Lin, P., Vorbach, S., Li, J., Furlani, S., and Hallett, M. (2007). Exploration of computational methods for classification of movement intention during human voluntary movement from single trial EEG. *Clin. Neurophysiol.* 118, 2637–2655. doi: 10.1016/j.clinph.2007.08.025

Bai, O., Rathi, V., Lin, P., Huang, D., Battapady, H., Fei, D.-Y., et al. (2011). Prediction of human voluntary movement before it occurs. *Clin. Neurophysiol.* 122, 364–372. doi: 10.1016/j.clinph.2010.07.010

Bhagat, N. A., French, J., Venkatakrishnan, A., Yozbatiran, N., Francisco, G. E., O'Malley, M. K., et al. (2014). "Detecting movement intent from scalp EEG in a novel upper limb robotic rehabilitation system for stroke," in *2014 36th Annual International Conference of the IEEE Engineering in Medicine and Biology Society* (Chicago: IEEE), 4127–4130.

Bulea, T. C., Prasad, S., Kilicarslan, A., and Contreras-Vidal, J. L. (2014). Sitting and standing intention can be decoded from scalp EEG recorded prior to movement execution. *Front. Neurosci.* 8:376. doi: 10.3389/fnins.2014.00376

Daly, J. J., and Wolpaw, J. R. (2008). Brain–computer interfaces in neurological rehabilitation. *Lancet Neurol.* 7, 1032–1043. doi: 10.1016/S1474-4422(08)70223-0

Dobkin, B. H. (2007). Brain–computer interface technology as a tool to augment plasticity and outcomes for neurological rehabilitation. *J. Physiol.* 579, 637–642. doi: 10.1113/jphysiol.2006.123067

Hortal, E., Planelles, D., Iáñez, E., Costa, A., Úbeda, A., and Azorín, J. (2016). "Detection of gait initiation through a ERD-based brain-computer interface," in *Advances in Neurotechnology, Electronics and Informatics* (Rome: Springer), 141–150.

Hortal, E., Úbeda, A., Iáñez, E., Fernández, E., and Azorín, J. M. (2015). "Using EEG signals to detect the intention of walking initiation and stop," in *International Work-Conference on the Interplay Between Natural and Artificial Computation* (Elche: Springer), 278–287.

Ibáñez, J., Serrano, J., Del Castillo, M., and Barrios, L. (2010). "An asynchronous BMI system for online single-trial detection of movement intention," in *2010 Annual International Conference of the IEEE Engineering in Medicine and Biology* (Buenos Aires: IEEE), 4562–4565.

Jahanshahi, M., and Hallett, M. (2003). *The Bereitschaftspotential: Movement-related cortical potentials*. New York, NY: Springer Science & Business Media.

Jiang, N., Gizzi, L., Mrachacz-Kersting, N., Dremstrup, K., and Farina, D. (2015). A brain–computer interface for single-trial detection of gait initiation from movement related cortical potentials. *Clin. Neurophysiol.* 126, 154–159. doi: 10.1016/j.clinph.2014.05.003

Lehtonen, J., Jylanki, P., Kauhanen, L., and Sams, M. (2008). Online classification of single EEG trials during finger movements. *IEEE Trans. Biomed. Eng.* 55, 713–720. doi: 10.1109/TBME.2007.912653

Lew, E., Chavarriaga, R., Silvoni, S., and Millán, J. d. R. (2012). Detection of self-paced reaching movement intention from EEG signals. *Front. Neuroeng.* 5:13. doi: 10.3389/fneng.2012.00013

López-Larraz, E., Montesano, L., Gil-Agudo, Á., and Minguez, J. (2014). Continuous decoding of movement intention of upper limb self-initiated analytic movements from pre-movement EEG correlates. *J. Neuroeng. Rehabil.* 11:1. doi: 10.1186/1743-0003-11-153

McFarland, D. J., McCane, L. M., David, S. V., and Wolpaw, J. R. (1997). Spatial filter selection for EEG-based communication. *Electroencephalogr. Clin. Neurophysiol.* 103, 386–394. doi: 10.1016/S0013-4694(97)00022-2

Nam, C. S., Jeon, Y., Kim, Y.-J., Lee, I., and Park, K. (2011). Movement imagery-related lateralization of event-related (de) synchronization (ERD/ERS): motor-imagery duration effects. *Clin. Neurophysiol.* 122, 567–577. doi: 10.1016/j.clinph.2010.08.002

Pennycott, A., Wyss, D., Vallery, H., Klamroth-Marganska, V., and Riener, R. (2012). Towards more effective robotic gait training for stroke rehabilitation: a review. *J. Neuroeng. Rehabil.* 9:1. doi: 10.1186/1743-0003-9-65

Pfurtscheller, G., Brunner, C., Schlögl, A., and Da Silva, F. L. (2006). Mu rhythm (de) synchronization and EEG single-trial classification of different motor imagery tasks. *Neuroimage* 31, 153–159. doi: 10.1016/j.neuroimage.2005.12.003

Planelles, D., Hortal, E., Costa, Á., Úbeda, A., Iáñez, E., and Azorín, J. M. (2014). Evaluating classifiers to detect arm movement intention from EEG signals. *Sensors* 14, 18172–18186. doi: 10.3390/s141018172

Rao, R. P. (2013). *Brain-Computer Interfacing: An Introduction*. New York, NY: Cambridge University Press.

Rodríguez-Ugarte, M., Hortal, E., Costa, Á., Iáñez, E., Úbeda, A., and Azorín, J. M. (2016). Detection of intention of pedaling start cycle through EEG signals. *Conf. Proc. IEEE Eng. Med. Biol. Soc.* 2016, 1496–1499. doi: 10.1109/embc.2016.7590993

Rohm, M., Schneiders, M., Müller, C., Kreilinger, A., Kaiser, V., Müller-Putz, G. R., et al. (2013). Hybrid brain–computer interfaces and hybrid neuroprostheses for restoration of upper limb functions in individuals with high-level spinal cord injury. *Artif. Intell. Med.* 59, 133–142. doi: 10.1016/j.artmed.2013.07.004

Sburlea, A. I., Montesano, L., de la Cuerda, R. C., Diego, I. M. A., Miangolarra-Page, J. C., and Minguez, J. (2015). Detecting intention to walk in stroke patients from pre-movement EEG correlates. *J. Neuroeng. Rehabil.* 12:1. doi: 10.1186/s12984-015-0087-4

Sburlea, A. I., Montesano, L., and Minguez, J. (2016). Advantages of EEG phase patterns for the detection of gait intention in healthy and stroke subjects. *arXiv preprint arXiv:1605.04533*.

Schacter, D. L. (1977). EEG theta waves and psychological phenomena: a review and analysis. *Biol. Psychol.* 5, 47–82. doi: 10.1016/0301-0511(77)90028-X

Steinwart, I., and Christmann, A. (2008). *Support Vector Machines*. New York, NY: Springer Science & Business Media.

Steriade, M. (2005). *Cellular Substrates of Brain Rhythms*, vol. 5. Philadelphia, PA: Lippincott Williams and Wilkins.

Toffanin, P., Johnson, A., De Jong, R., and Martens, S. (2007). Rethinking neural efficiency: effects of controlling for strategy use. *Behav. Neurosci.* 121:854. doi: 10.1037/0735-7044.121.5.854

Xu, R., Jiang, N., Lin, C., Mrachacz-Kersting, N., Dremstrup, K., and Farina, D. (2014). Enhanced low-latency detection of motor intention from EEG for closed-loop brain-computer interface applications. *IEEE Trans. Biomed. Eng.* 61, 288–296. doi: 10.1109/TBME.2013.2294203

Conflict of Interest Statement: The authors declare that the research was conducted in the absence of any commercial or financial relationships that could be construed as a potential conflict of interest.

5.2. Publicación revista R2

sensors

MDPI

Article

Effects of tDCS on Real-Time BCI Detection of Pedaling Motor Imagery

Maria de la Soledad Rodriguez-Ugarte *, Eduardo Iáñez, Mario Ortiz-Garcia and José M. Azorín

Brain-Machine Interface Systems Lab, Miguel Hernández University of Elche, Avda. de la Universidad S/N Ed. Innova, Elche, 03202 Alicante, Spain; eianez@umh.es (E.I.); mortiz@umh.es (M.O.-G.); jm.azorin@umh.es (J.M.A.)

* Correspondence: maria.rodriguezu@umh.es; Tel.: +34-965-222-459

Received: 26 January 2018; Accepted: 5 April 2018; Published: 8 April 2018

Abstract: The purpose of this work is to strengthen the cortical excitability over the primary motor cortex (M1) and the cerebro-cerebellar pathway by means of a new transcranial direct current stimulation (tDCS) configuration to detect lower limb motor imagery (MI) in real time using two different cognitive neural states: relax and pedaling MI. The anode is located over the primary motor cortex in Cz, and the cathode over the right cerebro-cerebellum. The real-time brain–computer interface (BCI) designed is based on finding, for each electrode selected, the power at the particular frequency where the most difference between the two mental tasks is observed. Electroencephalographic (EEG) electrodes are placed over the brain's premotor area (PM), M1, supplementary motor area (SMA) and primary somatosensory cortex (S1). A single-blind study is carried out, where fourteen healthy subjects are separated into two groups: sham and active tDCS. Each subject is experimented on for five consecutive days. On all days, the results achieved by the active tDCS group were over 60% in real-time detection accuracy, with a five-day average of 62.6%. The sham group eventually reached those levels of accuracy, but it needed three days of training to do so.

Keywords: transcranial direct current stimulation (tDCS); brain–computer interface (BCI); real-time; pedaling motor imagery; cerebro-cerebellar pathway

1. Introduction

Transcranial direct current stimulation (tDCS) is a modern technique of non-invasive brain stimulation which has the purpose of temporally modulating cortical excitability [1,2]. Currently, its effects are not known with certainty, but they are believed to be dependent on several factors such as intensity applied [3], time of stimulation [4] and size of the electrodes used [5]. The majority of the studies focused their research on applying tDCS to the representation of the upper limbs in the brain to evaluate the performance of the subjects or to improve the quality of life of stroke patients who have had that area affected [6–8]. Only relatively few studies attempted to investigate how tDCS could affect the lower limbs [9,10]. This could be due to the challenge of reaching the area of the brain where the legs are represented, which is located deep in the longitudinal fissure corresponding to the primary motor cortex (M1).

From a cognitive perspective, brain activity during a lower limb complex motor task, such as gait or pedaling, involves the supplementary motor area (SMA), M1, the primary somatosensory cortex (S1) and the premotor area (PM) [11–14]. Moreover, lower limb motor imagery (MI) is also associated with these areas [15]. Hence, if a person imagines a complex motor task, the person will activate a similar neural pathway to that activated when the task is actually being performed. In addition, the cerebellum

is a key part during movement coordination, motor learning and cognition [16]. The underlying mechanism of the ascending outputs from the cerebellum relies on sending information to M1 through the dentate nucleus. Some of the axons in this area cross the midline of the brain to terminate in the ventral lateral complex of the thalamus, and then the motor thalamus sends inputs to the M1 and PM areas [17].

On the one hand, research findings have found that tDCS over the cerebellum produces cortical excitability changes in a polarity-specific manner [18]. While cathodal tDCS over the cerebellum decreases the inhibitory tone the cerebellum exerts over M1, anodal tDCS has the opposite effect [19,20]. From a physiological perspective, the principal neuron found in the cortex of the cerebellum is called the Purkinje cell. If the anode is located over the cerebellum, these neurons are excited producing inhibition in the dentate nucleus and resulting in disfacilitation of the motor cortex [21]. On the other hand, cortical excitability over M1 increases when the anode is located over M1 and the cathode over the contralateral hemisphere, or over the contralateral supraorbital region [22,23]. Nevertheless, no research has studied the cerebro-cerebellar pathway where simultaneously the anode is located over M1 and the cathode over the contralateral cerebellum. Doing this could increase the cortical excitability over M1 even more.

Brain–computer interfaces (BCIs) are devices that translate brain waves into commands to control an external device, such as exoskeletons. They can do this, for example, by reading electroencephalographic (EEG) signals from the brain, extracting useful features from those signals, and then using statistical methods to discern between relevant outputs. This technique can improve the rehabilitation process of a person that has suffered a cerebrovascular accident (CVA). The most challenging aspect of using BCIs is to detect neural cognitive processes in real time, so that, as soon as data are received, they are processed. However, researchers usually analyze data offline, where data are studied once the experiment has finished [24,25]. This can produce unrealistic results when compared to a more challenging online analysis, which is more relevant for real-time applications such as rehabilitation therapies involving exoskeletons.

Motor imagery has been detected using EEG-based BCIs in the past, but most studies focused on upper limbs or simple foot movements [26–29]. Much fewer studies concentrated on lower limb complex tasks such as gait or pedaling [30]. In most of these studies, BCIs have exploited in some way the fact that there is a suppression of the mu waves (8–12 Hz) and beta waves (13–30 Hz) around M1 when a motor task is being imagined [31,32]. The literature involving real-time processing and feedback of BCI signals associated to these types of movements is scarcer, and the methods of reporting results are disperse [26,30,33–37]. Nevertheless, there are many relevant applications of detecting lower limb movement in real time. Indeed, in the long run, it would be desirable to design an online BCI where patients with CVA are rehabilitated with the aid of a lower limb exoskeleton which they are able to control in real time. Additionally, if the effects of tDCS prove to be positive (by exciting M1 and facilitating detection), this could help in improving or simply accelerating the recovery of those patients even more.

Thus, the aim of this work is to strengthen the cortical excitability over M1 and the cerebro-cerebellar pathway by means of a new tDCS configuration to better detect lower limb motor imagery in real time using an online BCI that distinguishes between two different cognitive neural states: relax and pedaling MI. To do that, a single-blind study is carried out where people are randomly divided into two groups, sham and active tDCS, and experimented for five consecutive days. The sham group received a fake stimulation and the active tDCS group was given 0.4 mA. Our hypothesis is that the active tDCS group would achieve better detection accuracy results than the sham group.

2. Materials and Methods

2.1. Subjects

Fourteen healthy subjects between 23 and 38 years old (26.8 $\pm$ 4.9) took part in this experiment (most of them were MSc students). There were twelve male participants and two female participants.

All of them were right-footed. None of the subjects had any previous experience with BCIs or MI; they reported no neurological diseases; none of them were medicated; and they were not suffering the consequences of an intoxication during the time the experiments were carried out. Lastly, all participants gave written informed consent according to the Helsinki declaration. The Ethics Committee of the Office for Project Evaluations (Oficina Evaluadora de Proyectos: OEP) of the Miguel Hernández University of Elche (Spain) approved the study.

2.2. Experimental Protocol

This section explains the experimental protocol. Several studies which treat different problems such as phantom limb pain, Parkinson's disease or apraxia of speech after stroke, applied tDCS for five days and reported positive effects [38–40]. In addition, a study from [41] stated that the lasting effects of tDCS when it is applied for 15 min were up to 1.5 h. Therefore, taking into account these aspects, our stimulation protocol was established as five consecutive days (Monday to Friday) for 15 min to investigate if there was any improvement in developing pedaling MI.

The experiment consisted on recording the EEG signals (more details on Section 2.3) while the user was performing two mental tasks: relax and imagine. During the imagine task, subjects had to visualize a pedaling movement inside their heads. To remove the placebo effect, a single-blind study was designed in which subjects were randomly divided into two groups: sham or active tDCS. The participants sat in front of a screen which fed them with instructions. Each subject performed 1 session every day which consisted of tDCS supply and MI experiment. First, tDCS (sham or active) was administrated for 15 min (more details in Section 2.4). Then, each subject performed 10 trials of the MI experiment. Each trial included each task (relax and imagine) 10 times. The screen provided three types of instructions: *Relax*, *Imagine* and +. *Relax* and *Imagine* tasks lasted 5.8 s and the order appeared at random, but in such a way that no same task appeared more than two times consecutively. This was done to avoid the user to start an expected task beforehand. The symbol + was always shown between tasks and lasted 3 s. During *Relax* and *Imagine*, the subjects were told to avoid blinking, swallowing or any other kind of artifacts. They were told to postpone these until the + symbol appeared. Figure 1 shows the flow diagram of each session's experimental protocol, while Figure 2 shows the experimental setup.

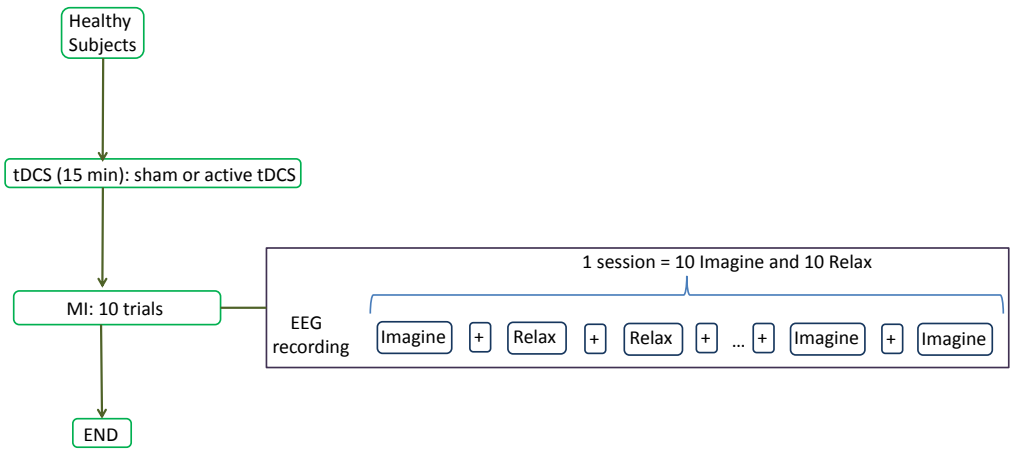

Figure 1. Flow diagram of the experiment for healthy subjects. The subjects were instructed by the screen to perform one of two possible mental tasks: *Relax* or *Imagine*. During *Relax*, subjects had to try not to think about anything, while, during *Imagine*, they had to imagine themselves pedaling. The *Relax* and *Imagine* tasks appeared at random and were always separated by an intermediate period (indicated by the screen with a + symbol). The setup also prevented two tasks of the same type to appear more than two times consecutively.

Figure 2. Experimental setup. Subjects sat looking at a screen which fed them with instructions while their EEG signals were recorded. Furthermore, the screen gave feedback about their performance in each task. The participant in the picture gave written informed consent to publish the image.

The first 4 trials were used to train a SVM classifier with which an online BCI was designed. This is explained in Section 2.5. For the remaining trials, the users received real-time positive feedback about their performance using the output from the BCI. That is, if during the relax task, the BCI detected that the subject had executed mental relaxation, then a green bar increased in size (otherwise it stayed the same size); and similarly with the pedaling MI task. The detection accuracy was calculated for each session, but this information was withheld from the subjects until the end of the last day to avoid influencing them.

2.3. EEG Acquisition

The StarStim R32 (Neuroelectrics, Barcelona, Spain) was used to acquire signals from the brain. The device was connected through a USB isolator to the computer. Based on the International 10-10 system, the EEG signals were acquired from 30 channels (P7, P4, CZ, PZ, P3, P8, O1, O2, C2, C4, F4, FP2, FZ, C3, F3, FP1, C1, OZ, PO4, FC6, FC2, AF4, CP6, CP2, CP1, CP5, FC1, FC5, AF3, and PO3) with two reference electrodes (CMS and DRL) at a frequency rate of 500 Hz. The system is shown in Figure 2.

2.4. Supply of tDCS

As mentioned before, the idea was to stimulate the cerebro-cerebellar pathway. To do this, a novel montage which aimed at strengthening the neural activity in M1 was proposed. It involved placing the anode over the primary motor cortex in Cz and the cathode over the right cerebro-cerebellum (two centimeters right and one centimeter down of the inion).

To corroborate that the cerebro-cerebellar pathway was being stimulated with such a choice of electrode placement, an electric field simulation of the brain was performed first. SimNIBS free platform [42] was used for the simulation, and Figure 3 shows the electric field generated by the anode over Cz (M1) and the cathode over the right cerebro-cerebellum. The parameters were set according to the materials utilized in the experiments. Both electrodes had a radius of 1 cm, 3 mm of thickness and 4 mm of space for the conductive gel. The tDCS intensity chosen was 0.4 mA, which produced 0.127 mA/cm^2 of current density. This current density was higher than in most studies (roughly 0.06 mA/cm^2) and it was selected because a previous study reported that a current density of 0.06 mA/cm^2 was not sufficient to reach the representation of the legs in the brain [43]. The current density also lies inside the range of neurological safety that avoids brain damage [44]. In Figure 3 it can be seen that the most affected area is close to the red nucleus and the thalamus. Both areas belong to the pathway of the ascending outputs from the cerebellum to M1 and PM [45], and therefore we expect this configuration to enhance the excitability in the area of interest.

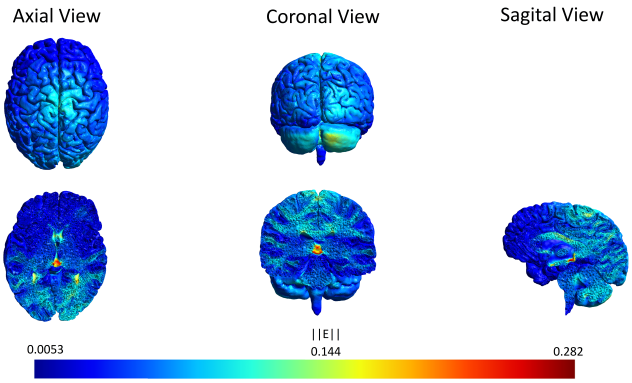

Figure 3. Axial, coronal and sagital view of the tDCS simulation. The scale represents the electric field (V/m) induced by the anode located over Cz and cathode over the right cerebro-cerebellum. The intensity applied was 0.4 mA. The most affected area (red) is close to the red nucleus. The image was generated with SimNIBS.

For the actual experiment, the StartStim R32 supplied anodal tDCS for 15 min at the beginning of each session (one session per day for five consecutive days) through two gel electrodes with a surface area of π cm^2 (1 cm radius). To create a placebo effect, the sham group received a 3 s ramp up until the intensity chosen, followed by 3 s ramp down; then, no stimulation was provided for almost 15 min until again there was a 3 s ramp up followed by a ramp down. Meanwhile, the active tDCS group received a 3 s ramp up until the intensity chosen, followed by constant stimulation throughout 15 min, and finally a 3 s ramp down.

2.5. Brain–Computer Interface (BCI)

As mentioned before, EEG signals were obtained as the subjects performed their relax and pedaling MI tasks. The first two seconds of each task were not considered to avoid influence of the visual cue and assure the total concentration of the subject in the respective task. Signals were processed in 1 s epochs with a 200 ms shift. For each epoch, a 4th order Butterworth high-pass filter with a cut-off frequency of 0.05 Hz was applied to remove the direct current. Then, a Notch filter was used to eliminate the power line interference at 50 Hz. Afterward, a 4th order Butterworth low-pass filter with cut-off frequency of 45 Hz was utilized. Subsequently, based on previous work (e.g., [46,47]), a Laplacian spacial filter was employed as in [48]. This filter eliminates the influence of the other electrodes by means of weighting by their distance. Of these filtered EEG signals, only those coming from nine carefully selected electrodes were considered: Cz, CP1, CP2, C1, C2, C3, C4, FC1 and FC2. These were chosen because the task involved imagination of the lower limbs, so their proximity to the M1, S1, SMA and PM regions of the brain was a deciding factor.

As mentioned above, the first four trials were used to train a support vector machine (SVM) classifier. This classifier is based on hyperplane tasks separation by maximizing the margin between the nearest points of the different tasks [49], with the outcomes obtained using non linear kernels being generally more robust than those of other classifiers [50]. In this work, a radial basis function was used as kernel for the SVM. For every given electrode, the power at each frequency between 6 and 30 Hz (resolution of 1 Hz via Burg's method) was calculated for each epoch. Then, the powers were separated according to the task (relax or pedaling imagery), normalized and averaged across all task-related epochs of the first four trials. Then, for each electrode, the frequency for which the maximum (normalized) power difference between tasks occurred was chosen and designated as the electrode's optimal frequency. Lastly, for each epoch, the feature associated to each electrode was the power at the electrode's optimal frequency, for a total of nine features per epoch. These features were then used to train the SVM classifier.

Therefore, the online BCI designed consisted of filtering the EEG signals of each epoch as described above, finding the nine features (the powers at each electrode's optimal frequency), and classifying the features with the (already trained) SVM. Thus, for each epoch, the BCI predicted whether it corresponded to a relaxed or pedaling state, and it was able to do this in real time (making a prediction every 0.2 s). The remaining six trials were utilized to determine the performance of the user in the day's session by measuring the real-time detection accuracy of the online BCI. The real-time detection accuracy was defined as the percentage of total correct classifications divided by the total number of classifications. As mentioned before, real-time positive feedback was given to the user, so that, if the BCI detected a relaxed state while the screen requested *Relax* (a correct classification), a green bar increased in size (otherwise it did not move), and similarly with the pedaling MI task.

3. Results

3.1. Statistical Analysis

IBM SPSS Statistics 22.0 for Windows (SPSS Inc., Chicago, IL, USA) was used for statistical analysis. First, we wanted to examine the differences in performance between groups (sham and active tDCS). Moreover, we wanted to study, within subjects of each group, the evolution of their performance throughout the five days of the experiment, which we refer to here as plasticity. Therefore, there were two independent variables: group and days; and only one dependent variable: real-time detection accuracy. Thus, a mixed factorial ANOVA was applied, but only after a Mauchly's test of sphericity was completed to verify the equality of variances of the differences within subjects [51]. In addition, pairwise comparisons between groups for each day, and within subjects of each group between days were computed. For every analysis, a p-value less than 0.05 was considered statistically significant.

Table 1 shows the results of applying Mauchly's test of sphericity. As it can be seen, variances were significantly different ($p < 0.05$), so data violated the sphericity assumption. Consequently, the correction with the biggest power was applied. In this case, it corresponded to Hyunh–Feldt ($\hat{\epsilon} = 0.987$). After applying this correction, a mixed factorial ANOVA was calculated.

Table 1. Mauchly's test of sphericity. Within subjects effect.

				Epsilon		
	Mauchly's W	**df**	***p*-Value**	**Greenhouse-Geisser**	**Hyunh-Feldt**	**Lower-Bound**
days	0.09	9	0.003	0.688	0.987	0.25

3.1.1. Effects of tDCS in MI

Table 2 shows the five-day mean real-time detection accuracies for each subject along with the overall average of the sham and active tDCS groups. In addition, from the mixed factorial ANOVA we obtained that the effects of tDCS in MI were not significant: $F(1, 12) = 0.37$, $p > 0.05$, $r = 0.03$. Moreover, Table 3 shows the comparisons, with Bonferroni adjustment applied for multiple comparisons, between both groups for each day. It can be appreciated that for the first day there was a significant difference ($p < 0.05$) in the real-time detection accuracies (see also Figure 4).

Table 2. Mean real-time detection accuracy.

Subject	Sham	tDCS
1	61.7	66.6
2	66.9	51.8
3	59.6	55.7
4	64.1	55.9
5	51.5	66.9
6	55.2	68.7
7	63.5	72.4
Mean	60.4 ± 5.4	62.6 ± 7.9

Table 3. Pairwise accuracy comparison between tDCS and sham group.

Day	1	2	3	4	5
***p*-Value**	0.04	0.29	1.00	0.74	0.60

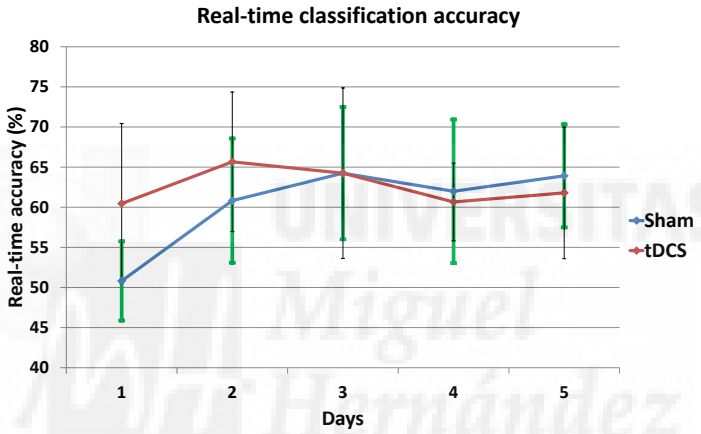

Figure 4. Mean real-time accuracy for all subjects of each group at each day.

3.1.2. MI Plasticity

Figure 4 represents the mean real-time accuracy for each group at each day of the experiment. From the mixed factorial ANOVA, it can be concluded that there was a significant interaction effect between the days and the group of stimulation: $F(3.95, 47.35) = 3.56$, $p < 0.01$, $r = 0.23$. Furthermore, Table 4 shows, for each group, the p-values comparing day five and the other days. There was only a significant difference between Day 5 and Day 1 within subjects of the sham group ($p < 0.01$).

Table 4. Comparison between Day 5 and the rest of the days for each group.

Group	Day	Day	*p*-Value
sham	5	1	0.002
		2	1.00
		3	1.00
		4	1.00
tDCS	5	1	1.00
		2	0.78
		3	0.85
		4	1.00

3.2. Optimal Frequencies

The optimal frequencies associated to the BCI model at each electrode on each day are also very useful information. They show where the greatest (normalized) changes in power were occurring, and therefore give a rough idea of the frequency bands that are most important in association with the lower limb motor imagery that is being studied. To present the results of all subjects together, a histogram was made showing, for each day and group, the number of optimal frequencies lying in three important frequency bands: 6–12 Hz (high theta and mu waves), 13–20 Hz (low and mid-range beta waves) and 21–30 Hz (high beta waves). For each group and day, there were a total of 63 optimal frequencies since there were nine electrodes selected for each of the seven subjects in each group. The results are presented in Table 5. The frequency band associated to mu waves seems to be the most preferred.

Table 5. Optimal frequencies histogram for each day and group.

Group	Frequency Range	Day 1	Day 2	Day 3	Day 4	Day 5
sham	(6–12) Hz	27	42	52	36	39
	(13–20) Hz	14	8	10	18	5
	(21–30) Hz	22	13	1	9	19
tDCS	(6–12) Hz	42	48	53	49	47
	(13–20) Hz	11	10	5	11	6
	(21–30) Hz	10	5	5	3	10

3.3. Real-Time Accuracy and ERD of the Best Subjects

As previously mentioned, lower limb motor imagery is thought to be associated to the attenuation of mu and beta waves in M1 [31,32]. This phenomenon is referred to as event-related desynchronization (ERD). To see the changes in ERD, the best subjects of each group were selected based on their five-day real-time detection accuracy (Table 2): Subject 2 of the sham group and Subject 7 of the active tDCS group. Given the results in the previous section and that those electrodes over M1 are thought to be mostly involved, the focus was on the mu waves (8–12 Hz) occurring in the Cz, C1, C2, C3 and C4 electrodes. For an electrode E, and for a fixed frequency f, the ERD was defined as

$$\mathrm{ERD}_E(f) = \left(\frac{P(f) - R(f)}{R(f)}\right) \times 100\,, \tag{1}$$

where $P(f)$ is the average of the power at the frequency f over all pedaling-epochs, and $R(f)$ is the same but averaged over all relaxing-epochs. Then, the mu band motor cortex ERD for a given day was simply the average of all $\mathrm{ERD}_E(f)$ over $f = 8, 9, 10, 11, 12$ and $E =$ Cz,C1,C2,C3,C4. These results, along with the real-time accuracies of the two best subjects, are shown in Figure 5.

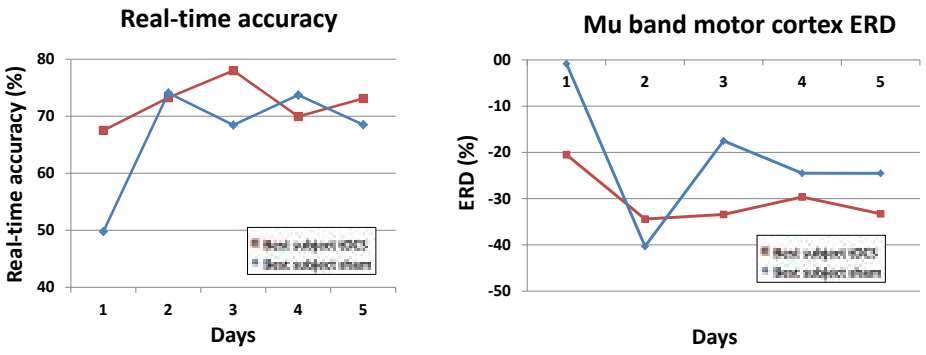

Figure 5. Real-time accuracy and ERD of the best subjects in each group.

4. Discussion

It can be seen in Table 2, as well as concluded from the mixed factorial ANOVA test, that in general there is no significant difference between the active tDCS and sham groups. Indeed, the active tDCS group achieved 62.6% of real-time detection accuracy and the sham group 60.4%. Nevertheless, the mixed factorial ANOVA results also indicated that there was a significant interaction effect between the days and the groups. This is because the sham and tDCS groups differ significantly in the first day, with the tDCS group having 9.6% better real-time accuracy, and also because within the sham group there is a significant variation when comparing the first and last day of the experiment.

Thus, the results show that the positive effects in performance due to tDCS are only relevant in the first few days, possibly only the first day, as the sham group then adapts and achieves the same performance. This is consistent with a study performed by Fernandez et al. [10] where it was observed that adaptation reached a lower limit the first day due to the simplicity of the task, leading to non-significant differences in the days that followed. However, it contradicts a study by Soekadar et al. [20] on upper limbs which suggested that only after three days did changes due to tDCS started to be differentiated from sham. This could be due to several reasons, including the different location of the tDCS electrodes and their surface area, as well as the different nature of the experiment and the way the data were processed. Longer experiment durations (over five days) could also help to discern the root cause of these slight differences. Meanwhile, the results agree in part with those of Wei et al. [8], which only had a one-day experiment showing slight improvement due to tDCS stimulation. Our results also show such slight improvement in favor of the tDCS group on the first day. Naturally, our real-time accuracy results differed from the offline accuracies shown in the study by Wei et al. [8], since they were able to improve on their classifier offline.

From another point of view, the subjects without stimulation showed evidence of brain plasticity, with an overall improvement of 13% in real-time accuracy from the first to the last day. Hence, their brains seem to have adapted very quickly to the task, meaning that if the intention is to eventually develop a therapy that elapses over several days, perhaps it is not necessary to apply tDCS at all. Having said that, tDCS did show evidence of speeding up improvement in the sense that it seems to have had an instantaneous effect in activating the desired neural pathway. Therefore, the results suggest that the active tDCS immediately induces the maximum performance that a subject could reach and it maintains it each day. Meanwhile, the sham group seems to require two to three days of training to reach the same level as the active tDCS group (see Figure 4). Nevertheless, it should be pointed out that these results involved only healthy subjects. When dealing with patients, we expect to see greater differences between the groups due to the greater potential of improvements in the case of rehabilitating patients.

These conclusions are also corroborated with results in Section 3.2. Indeed, looking at the histogram in Section 5 shows that the optimal frequencies lied the most often in the band containing the mu waves: 6–12 Hz. For the tDCS group on every single day at least 66% of the optimal frequencies lied in this band, while for the sham group from the second day onwards at least 57% of the optimal frequencies were in that band. However, on the first day, only 42% of the optimal frequencies of the sham group where in the preferred frequency band. This seems to indicate that the behavior was more disperse among the frequency bands, and could be a contributing factor explaining why the performance of the sham group in the first day was at chance level, while the tDCS group was already performing better on that day. Namely, it is possible that tDCS favored changes in the mu waves, whereas it took at least one day of training for the sham group to focus the motor imagery on that frequency band.

The results from Section 3.3 also confirm the conclusions, albeit at the level of the best subjects in each group. The best subject in the tDCS group started out with real-time accuracies of nearly 70% and remained above 70% from the second day onwards. On the other hand, the best subject in the sham group started at chance level (50%) and from the second day onwards significantly improved and remained at around 70% accuracy. The mu band motor cortex ERD (8–12 Hz in Cz, C1, C2, C3 and

C4) was also interesting. First, as expected, there was presence of ERD each day and for both subjects (negative values because the suppression means that the power while pedaling is lower than when relaxing). On the first day, the sham subject only showed a very subtle ERD, while the tDCS subject had a much more pronounced ERD of around −20%. Then, from the second day onwards, there was an even larger enhancement of the ERD levels of both groups, which remained at an average of about −30%. This shows some level of adaptation of the subjects to the task after the first day.

To address the seemingly low real-time accuracies of around 60% (chance level is 50%), we looked thoroughly at the existing literature to make the appropriate comparisons. It should be noted that the real-time accuracies reported in this study are taking into consideration every single prediction during the experiment (every single epoch is classified). Unfortunately, the current literature on real-time BCIs is somewhat disperse in the way the results are reported [26,30,33–37], but whenever it is possible to compare, our results coincide rather well with those of the literature. Our results are consistent with those of Zich et al. [33] which have a real-time accuracy of 55–65%, [26] with around 65% accuracy (of first 30 sessions), and [30] with around 65% accuracy. Meanwhile, Guger et al. [34] reported the results of the best time point of the best session of each of their three subjects (98%, 93% and 87%), but a careful analysis of their data shows the average real-time classification accuracy is about 80%, 65% and 65% for their three subjects respectively. Prasad et al. [35] averaged the maximum classification accuracies of each task and report them to be 60–75%. All of these studies involve upper limb or simple foot movements with the exception of the study by Liu et al. [30], which involved gait. Therefore, our results actually do not stray far from those found in the literature. Additionally, as pointed out by Prasad et al. [35], these results are reasonable given the fact that all the subjects are novices to BCIs and MI, so their performance is lower than that of experienced users. To improve on the accuracy levels, it might be necessary to change the nature of the motor imagery, since [26] reported significantly better results when doing so. Lastly, in other studies, it was simply not possible to make a fair comparison of the online results [8,36,37].

If the intention is to justify the use of active tDCS over the course of several days or more, then stronger evidence of its effects is needed. In this sense, it could be sensible to change the stimulation montage to one that could possibly lead to more marked differences among the groups. Some possible modifications of the experimental setup would be the number of stimulation anodes and cathodes and their placement, as well as increasing the intensity used whilst keeping safety in mind. From a physiological perspective, we first proposed that the excitation of Purkinje cells in the cerebellum might have the side effect of disfacilitating the motor cortex. However, there is also evidence that their activation can lead to improved motor learning [52]. In fact, anodal stimulation over the cerebellum can speed up learning [19,53,54]. Therefore, we propose an alternative for future use, where two anodes with differing intensities are utilized: one over M1 with relatively high intensity, and another over the cerebro-cerebellum with lower intensity (to prevent any major inhibitory behavior over M1 while still leading to improved motor learning). Meanwhile, a single cathode can be placed in an alternative location (such as FC1 or FC2).

Lastly, it should be said that the online BCI is perfectly apt for use in real-time applications, such as active therapies involving exoskeletons. In the future, we intend to use active tDCS and the online BCI to treat patients that have suffered a CVA accident. The idea is to improve their rehabilitation by engaging them in therapy where they have to control a lower limb exoskeleton in real time.

5. Conclusions

In this work, a new tDCS configuration intended to boost the cerebro-cerebellar pathway to improve the detection of lower limb MI via the use of a real-time BCI is tested. One anode is located over M1 and one cathode over the right cerebro-cerebellum. A single-blind experiment with duration of five days is completed using healthy subjects who are randomly separated into two groups: sham and active tDCS. The mental tasks they have to perform are: relax and pedaling MI. The online BCI designed is based on finding the power at an optimal frequency at each of nine carefully selected electrodes in the

proximity of M1, S1, PM and SMA. From the very first day, the real-time detection accuracy achieved by the active tDCS group is over 60% and remains around 62.6% on average. However, the sham group needs three days of training to reach that same level of accuracy. This, along with other supporting evidence, indicates possibly that the tDCS has an immediate effect in activating the desired neural pathway, and shows the potential advantages in accelerating recovery of patients undergoing therapy. However, overall, the long-term effects of tDCS seems to have been moderate at best. With this in mind, the stimulation montage could possibly be further improved to increase the effects of tDCS and hopefully justify its use. Lastly, the online BCI designed, with or without tDCS, is a desirable stepping stone in designing therapies that allow recovering patients' real-time control of lower limb exoskeletons, which is a future endeavor of interest.

Acknowledgments: This research was carried out in the framework of the project Associate titled: Decoding and stimulation of motor and sensory brain activity to support long term potentiation through Hebbian and paired associative stimulation during rehabilitation of gait (DPI2014-58431-C4-2-R), which is funded by the Spanish Ministry of Economy and Competitiveness and by the European Union through the European Regional Development Fund (ERDF), "A way to build Europe". M. Rodríguez-Ugarte wishes to thank Federico Fuentes for useful discussions and the careful revision of the manuscript. Lastly, the authors wish to thank the reviewers for the helpful comments that significantly improved the quality of the manuscript.

Author Contributions: M.d.l.S.R.-U. is responsible for the design, implementation, acquisition and data analysis. In addition, E.I. and M.O.-G. supervised the work and contributed with the revision process. J.M.A. actively contributed as director of the work.

Conflicts of Interest: The authors declare no conflict of interest.

Abbreviations

The following abbreviations are used in this manuscript:

CVA	Cerebrovascular accident
MI	Motor imagery
tDCS	Transcranial direct current stimulation
BCI	Brain–computer interface
M1	Primary motor cortex
S1	Primary somatosensory cortex
SMA	Supplementary motor area
PM	Premotor
EEG	Electroencephalographic
SVM	Support vector machine
ERD	Event-related desynchronization

References

1. Kumru, H.; Murillo, N.; Benito-Penalva, J.; Tormos, J.M.; Vidal, J. Transcranial direct current stimulation is not effective in the motor strength and gait recovery following motor incomplete spinal cord injury during Lokomat® gait training. *Neurosci. Lett.* **2016**, *620*, 143–147.
2. Flöel, A. tDCS-enhanced motor and cognitive function in neurological diseases. *Neuroimage* **2014**, *85*, 934–947.
3. Chieffo, R.; Ciocca, M.; Leocani, L.; Miranda, P.; Rothwell, J. 113. Short-term effect of different tdcs intensities on motor cortex excitability. *Clin. Neurophysiol.* **2015**, *126*, e26.
4. Batsikadze, G.; Moliadze, V.; Paulus, W.; Kuo, M.F.; Nitsche, M. Partially non-linear stimulation intensity-dependent effects of direct current stimulation on motor cortex excitability in humans. *J. Physiol.* **2013**, *591*, 1987–2000.
5. Bai, S.; Dokos, S.; Ho, K.A.; Loo, C. A computational modelling study of transcranial direct current stimulation montages used in depression. *Neuroimage* **2014**, *87*, 332–344.
6. Lee, S.J.; Chun, M.H. Combination transcranial direct current stimulation and virtual reality therapy for upper extremity training in patients with subacute stroke. *Arch. Phys. Med. Rehabil.* **2014**, *95*, 431–438.

7. Achilles, E.; Weiss-Blankenhorn, P.; Moos, K.; Hesse, M.; Sparing, R.; Fink, G. P649: Transcranial direct current stimulation (tDCS) of left parietal cortex facilitates gesture processing in healthy subjects. *Clin. Neurophysiol.* **2014**, *125*, S226–S227.
8. Wei, P.; He, W.; Zhou, Y.; Wang, L. Performance of motor imagery brain-computer interface based on anodal transcranial direct current stimulation modulation. *IEEE Trans. Neural Syst. Rehabil. Eng.* **2013**, *21*, 404–415.
9. Shah, B.; Nguyen, T.T.; Madhavan, S. Polarity independent effects of cerebellar tDCS on short term ankle visuomotor learning. *Brain Stimul.* **2013**, *6*, 966–968.
10. Fernandez, L.; Albein-Urios, N.; Kirkovski, M.; McGinley, J.L.; Murphy, A.T.; Hyde, C.; Stokes, M.A.; Rinehart, N.J.; Enticott, P.G. Cathodal transcranial direct current stimulation (tDCS) to the right cerebellar hemisphere affects motor adaptation during gait. *Cerebellum* **2017**, *16*, 168–177.
11. Cevallos, C.; Zarka, D.; Hoellinger, T.; Leroy, A.; Dan, B.; Cheron, G. Oscillations in the human brain during walking execution, imagination and observation. *Neuropsychologia* **2015**, *79*, 223–232.
12. Sahyoun, C.; Floyer-Lea, A.; Johansen-Berg, H.; Matthews, P. Towards an understanding of gait control: Brain activation during the anticipation, preparation and execution of foot movements. *Neuroimage* **2004**, *21*, 568–575.
13. Fukuyama, H.; Ouchi, Y.; Matsuzaki, S.; Nagahama, Y.; Yamauchi, H.; Ogawa, M.; Kimura, J.; Shibasaki, H. Brain functional activity during gait in normal subjects: A SPECT study. *Neurosci. Lett.* **1997**, *228*, 183–186.
14. Solodkin, A.; Hlustik, P.; Chen, E.E.; Small, S.L. Fine modulation in network activation during motor execution and motor imagery. *Cerebral Cortex* **2004**, *14*, 1246–1255.
15. Parsons, L.M.; Fox, P.T.; Downs, J.H.; Glass, T.; Hirsch, T.B.; Martin, C.C.; Jerabek, P.A.; Lancaster, J.L. Use of implicit motor imagery for visual shape discrimination as revealed by PET. *Nature* **1995**, *375*, 54–58.
16. D'Angelo, E.; Casali, S. Seeking a unified framework for cerebellar function and dysfunction: from circuit operations to cognition. *Front. Neural Circ.* **2012**, *6*, doi:10.3389/fncir.2012.00116.
17. Penhune, V.B.; Steele, C.J. Parallel contributions of cerebellar, striatal and M1 mechanisms to motor sequence learning. *Behav. Brain Res.* **2012**, *226*, 579–591.
18. Galea, J.M.; Jayaram, G.; Ajagbe, L.; Celnik, P. Modulation of cerebellar excitability by polarity-specific noninvasive direct current stimulation. *J. Neurosci.* **2009**, *29*, 9115–9122.
19. Block, H.J.; Celnik, P. Can cerebellar transcranial direct current stimulation become a valuable neurorehabilitation intervention? *Expert Rev. Neurother.* **2012**, *12*, 1275–1277.
20. Soekadar, S.R.; Witkowski, M.; Birbaumer, N.; Cohen, L.G. Enhancing Hebbian learning to control brain oscillatory activity. *Cerebral Cortex* **2014**, *25*, 2409–2415.
21. Cengiz, B.; Boran, H.E. The role of the cerebellum in motor imagery. *Neurosci. Lett.* **2016**, *617*, 156–159.
22. Wagner, T.; Fregni, F.; Fecteau, S.; Grodzinsky, A.; Zahn, M.; Pascual-Leone, A. Transcranial direct current stimulation: A computer-based human model study. *Neuroimage* **2007**, *35*, 1113–1124.
23. Sehm, B.; Kipping, J.; Schäfer, A.; Villringer, A.; Ragert, P. A comparison between uni-and bilateral tDCS effects on functional connectivity of the human motor cortex. *Front. Hum. Neurosci.* **2013**, *7*, doi:10.3389/fnhum.2013.00183.
24. Pfurtscheller, G.; Brunner, C.; Schlögl, A.; Da Silva, F.L. Mu rhythm (de) synchronization and EEG single-trial classification of different motor imagery tasks. *NeuroImage* **2006**, *31*, 153–159.
25. Lew, E.; Chavarriaga, R.; Silvoni, S.; Millán, J.d.R. Detection of self-paced reaching movement intention from EEG signals. *Front. Neuroeng.* **2012**, *5*, doi:10.3389/fneng.2012.00013.
26. Pfurtscheller, G.; Neuper, C. Motor imagery and direct brain-computer communication. *Proc. IEEE* **2001**, *89*, 1123–1134.
27. Cincotti, F.; Mattia, D.; Aloise, F.; Bufalari, S.; Schalk, G.; Oriolo, G.; Cherubini, A.; Marciani, M.G.; Babiloni, F. Non-invasive brain–computer interface system: Towards its application as assistive technology. *Brain Res. Bull.* **2008**, *75*, 796–803.
28. Müller-Putz, G.R.; Kaiser, V.; Solis-Escalante, T.; Pfurtscheller, G. Fast set-up asynchronous brain-switch based on detection of foot motor imagery in 1-channel EEG. *Med. Biol. Eng. Comput.* **2010**, *48*, 229–233.
29. Ang, K.K.; Guan, C.; Chua, K.S.G.; Ang, B.T.; Kuah, C.W.K.; Wang, C.; Phua, K.S.; Chin, Z.Y.; Zhang, H. A large clinical study on the ability of stroke patients to use an EEG-based motor imagery brain-computer interface. *Clin. EEG Neurosci.* **2011**, *42*, 253–258.

30. Liu, D.; Chen, W.; Lee, K.; Pei, Z.; Millán, J.d.R. An EEG-based brain-computer interface for gait training. In Proceedings of the 2017 29th Chinese Control And Decision Conference (CCDC), Chongqing, China, 28–30 May 2017; pp. 6755–6760.
31. Pfurtscheller, G.; Neuper, C. Motor imagery activates primary sensorimotor area in humans. *Neurosci. Lett.* **1997**, *239*, 65–68.
32. Naros, G.; Naros, I.; Grimm, F.; Ziemann, U.; Gharabaghi, A. Reinforcement learning of self-regulated sensorimotor β-oscillations improves motor performance. *Neuroimage* **2016**, *134*, 142–152.
33. Zich, C.; Debener, S.; Kranczioch, C.; Bleichner, M.G.; Gutberlet, I.; De Vos, M. Real-time EEG feedback during simultaneous EEG–fMRI identifies the cortical signature of motor imagery. *Neuroimage* **2015**, *114*, 438–447.
34. Guger, C.; Ramoser, H.; Pfurtscheller, G. Real-time EEG analysis with subject-specific spatial patterns for a brain-computer interface (BCI). *IEEE Trans. Rehabil. Eng.* **2000**, *8*, 447–456.
35. Prasad, G.; Herman, P.; Coyle, D.; McDonough, S.; Crosbie, J. Applying a brain-computer interface to support motor imagery practice in people with stroke for upper limb recovery: A feasibility study. *J. Neuroeng. Rehabil.* **2010**, *7*, 60.
36. Yu, T.; Xiao, J.; Wang, F.; Zhang, R.; Gu, Z.; Cichocki, A.; Li, Y. Enhanced motor imagery training using a hybrid BCI with feedback. *IEEE Trans. Biomed. Eng.* **2015**, *62*, 1706–1717.
37. Horki, P.; Solis-Escalante, T.; Neuper, C.; Müller-Putz, G. Combined motor imagery and SSVEP based BCI control of a 2 DoF artificial upper limb. *Med. Biol. Eng. Comput.* **2011**, *49*, 567–577.
38. Bolognini, N.; Spandri, V.; Ferraro, F.; Salmaggi, A.; Molinari, A.C.; Fregni, F.; Maravita, A. Immediate and sustained effects of 5-day transcranial direct current stimulation of the motor cortex in phantom limb pain. *J. Pain* **2015**, *16*, 657–665.
39. Ferrucci, R.; Mameli, F.; Ruggiero, F.; Priori, A. Transcranial direct current stimulation as treatment for Parkinson's disease and other movement disorders. *Basal Ganglia* **2016**, *6*, 53–61.
40. Marangolo, P.; Marinelli, C.; Bonifazi, S.; Fiori, V.; Ceravolo, M.; Provinciali, L.; Tomaiuolo, F. Electrical stimulation over the left inferior frontal gyrus (IFG) determines long-term effects in the recovery of speech apraxia in three chronic aphasics. *Behav. Brain Res.* **2011**, *225*, 498–504.
41. Nitsche, M.A.; Paulus, W. Sustained excitability elevations induced by transcranial DC motor cortex stimulation in humans. *Neurology* **2001**, *57*, 1899–1901.
42. Thielscher, A.; Antunes, A.; Saturnino, G.B. Field modeling for transcranial magnetic stimulation: A useful tool to understand the physiological effects of TMS? In Proceedings of the 2015 37th Annual International Conference of the IEEE Engineering in Medicine and Biology Society (EMBC), Milan, Italy, 25–29 August 2015; pp. 222–225.
43. Angulo-Sherman, I.N.; Rodríguez-Ugarte, M.; Sciacca, N.; Iáñez, E.; Azorín, J.M. Effect of tDCS stimulation of motor cortex and cerebellum on EEG classification of motor imagery and sensorimotor band power. *J. Neuroeng. Rehabil.* **2017**, *14*, 31.
44. Antal, A.; Alekseichuk, I.; Bikson, M.; Brockmöller, J.; Brunoni, A.; Chen, R.; Cohen, L.; Dowthwaite, G.; Ellrich, J.; Flöel, A.; et al. Low intensity transcranial electric stimulation: Safety, ethical, legal regulatory and application guidelines. *Clin. Neurophysiol.* **2017**, *128*, 1774–1809.
45. Llinas, R.; Negrello, M.N. Cerebellum. *Scholarpedia* **2015**, *10*, 4606.
46. Rodríguez-Ugarte, M.; Costa, Á.; Iáñez, E.; Úbeda, A.; Azorín, J. Pseudo-online detection of intention of pedaling start cycle through EEG signals. In *Converging Clinical and Engineering Research on Neurorehabilitation II*; Springer: New York, NY, USA, 2017; pp. 1103–1107.
47. Hortal, E.; Úbeda, A.; Iáñez, E.; Azorín, J.M.; Fernández, E. EEG-Based Detection of Starting and Stopping During Gait Cycle. *Int. J. Neural Syst.* **2016**, *26*, 1650029.
48. McFarland, D.J.; McCane, L.M.; David, S.V.; Wolpaw, J.R. Spatial filter selection for EEG-based communication. *Electroencephalogr. Clin. Neurophysiol.* **1997**, *103*, 386–394.
49. Steinwart, I.; Christmann, A. *Support Vector Machines*; Springer Science & Business Media: New York, NY, USA, 2008.
50. Hamedi, M.; Salleh, S.H.; Noor, A.M.; Mohammad-Rezazadeh, I. Neural network-based three-class motor imagery classification using time-domain features for BCI applications. In Proceedings of the Region 10 Symposium, Kuala Lumpur, Malaysia, 14–16 April 2014; pp. 204–207.
51. Field, A. *Discovering Statistics Using IBM SPSS Statistics*; Sage: Thousand Oaks, CA, USA, 2013.

52. Nguyen-Vu, T.B.; Kimpo, R.R.; Rinaldi, J.M.; Kohli, A.; Zeng, H.; Deisseroth, K.; Raymond, J.L. Cerebellar Purkinje cell activity drives motor learning. *Nat. Neurosci.* **2013**, *16*, 1734–1736.
53. Priori, A.; Ciocca, M.; Parazzini, M.; Vergari, M.; Ferrucci, R. Transcranial cerebellar direct current stimulation and transcutaneous spinal cord direct current stimulation as innovative tools for neuroscientists. *J. Physiol.* **2014**, *592*, 3345–3369.
54. Grimaldi, G.; Manto, M. Anodal transcranial direct current stimulation (tDCS) decreases the amplitudes of long-latency stretch reflexes in cerebellar ataxia. *Ann. Biomed. Eng.* **2013**, *41*, 2437–2447.

5.3. Publicación revista R3

UNIVERSITAS
Miguel
Hernández

Improving real-time lower limb motor imagery detection using tDCS and an exoskeleton

M. Rodríguez-Ugarte* [1], **E. Iáñez** [1], **M. Ortiz** [1] **and J. M. Azorín** [1]

[1] *Brain-Machine Interface Systems Lab, Systems Engineering and Automation Department, Miguel Hernández University of Elche, Elche, Spain*

Correspondence*:
Avda. de la Universidad S/N Ed. Innova, Universidad Miguel Hernández de Elche, Elche, Alicante 03202, Spain
maria.rodriguezu@umh.es

ABSTRACT

The aim of this work was to test if a novel transcranial direct current stimulation (tDCS) montage boosts the accuracy of lower limb motor imagery (MI) detection by using a real-time brain-machine interface (BMI) based on electroencephalographic (EEG) signals. The tDCS montage designed was composed of two anodes and one cathode: one anode over the right cerebrocerebellum, the other over the motor cortex in Cz, and the cathode over FC2 (using the International 10-10 system). The BMI was designed to detect two MI states: relax and gait MI; and was based on finding the power at the frequency which attained the maximum power difference between the two mental states at each selected EEG electrode. Two different single-blind experiments were conducted, E1 and a pilot test E2. E1 was based on visual cues and feedback and E2 was based on auditory cues and a lower limb exoskeleton as feedback. Twelve subjects participated in E1, while four did so in E2. For both experiments, subjects were separated into two equally-sized groups: sham and active tDCS. The active tDCS group achieved 12.6% and 8.2% higher detection accuracy than the sham group in E1 and E2 respectively, reaching 65% and 81.6% mean detection accuracy in each experiment. The limited results suggest that the exoskeleton (E2) enhanced the detection of the MI tasks with respect to the visual feedback (E1), increasing the accuracy obtained in 16.7% and 21.2% for the active tDCS and sham groups respectively. Thus, the small pilot study E2 indicates that using an exoskeleton in real-time has the potential of improving the rehabilitation process of cerebrovascular accident (CVA) patients, but larger studies are needed in order to further confirm this claim.

Keywords: transcranial direct current stimulation (tDCS), real-time, brain-machine interface (BMI), lower limb, exoskeleton, motor imagery (MI)

1 INTRODUCTION

Transcranial direct current stimulation (tDCS) is a non-invasive brain stimulation technique based on weak direct electrical current transferred between electrodes (from anode to cathode) over the scalp in order to modulate the neural membrane resting potential (Lefaucheur et al., 2017; Rodrıguez-Ugarte et al., 2016; Nelson et al., 2014). It modifies cortical excitability in a polarity-specific manner (Coffman et al., 2014). This means that neural excitability is generated under the area of the anode because the current flow goes into the brain, whereas in the underlying cortex where the cathode is, inhibition of neural activity is produced because the current flow goes out from the brain (Wiethoff et al., 2014; Filmer et al., 2014). Furthermore, the use of this technique implies adjusting four parameters: current density, stimulation duration, electrode size and electrode position. The vast majority of the studies focus their tDCS experiments on improving the performance of the upper limbs, the speech, or the balance; where

the areas stimulated are either the motor cortex, the frontal area or the cerebellum (Hortal et al., 2015; Monti et al., 2013; Foerster et al., 2017). In these studies, the range of current density used is typically between 0.04 and 0.06 mA/cm^2 with a duration of 15 or 20 minutes (Marquez et al., 2013) and electrode sizes of about 35 cm^2. However, there are just few studies that center their goals in meliorating lower limb performance and therefore, much remains to be investigated. In addition, stimulation with such big electrode surface areas gives only a vague idea of the areas of the brain that are important in producing the results.

Brain machine interfaces (BMIs) are a non-invasive technique that records and decodes electroencephalographic (EEG) signals to control an external device (Barrios et al., 2017). Two of the most common EEG-based BMIs are motor imagery (MI) and motor execution (ME). MI is defined as a mentally repetitive action without any overt motor movement (Park et al., 2013). Various functional magnetic resonance imaging (fMRI) studies have demonstrated that MI and ME activate common neural networks including the primary motor cortex (M1), supplementary motor area (SMA), premotor area (PM) and cerebellum (Sharma and Baron, 2013; Zapparoli et al., 2013; Hétu et al., 2013; Allali et al., 2013). Furthermore, MI is characterized by the decrease of power in the bands θ high (6-7 Hz), μ (8-12 Hz) and β (13-35 Hz) (Reynolds et al., 2015).

The purpose of this work is to test if a novel tDCS montage boosts the accuracy of lower limb MI detection using a real-time BMI. The tDCS montage is composed by three small electrodes that focus on the lower limbs: two anodes and one cathode. One anode is located over the right cerebrocerebellum, the other one over M1 in Cz, and the cathode over FC2 (using the International 10-10 system). Many studies have researched the stimulation just over the motor cortex or the cerebellum (Sehm et al., 2013; Clancy et al., 2014; Boehringer et al., 2013; Ferrucci and Priori, 2014), but never the two areas at the same time, like in this study. The effects of the stimulation over the cerebellum are still unclear, but recent studies showed an improvement of the task performed when the anode was over the cerebellum (Bradnam et al., 2015; Hardwick and Celnik, 2014a). However, the anode over the cerebellum is also believed to cause neural inhibition over the motor cortex (Grimaldi et al., 2016; Galea et al., 2009). This is why a second anode was added over Cz. This anode supplied a slightly higher current than the one over the cerebellum to counteract this effect and to excite neural activity in M1.

Two single-blind studies, E1 and E2, were conducted where subjects were randomly separated into two groups: sham and active tDCS. The sham group received a fake stimulation while the active tDCS group was given 0.3 mA over Cz and 0.2 mA over the right cerebrocerebellum. A BMI based on power difference in θ, μ and β bands was designed to detect two MI tasks: relax and gait MI. Both experiments had a duration of five consecutive days (for each subject). The first one, E1, was based on visual cues and feedback. The second one, E2, was a smaller pilot test which was based on auditory cues, where subjects wore a lower limb exoskeleton as feedback. It should be noted that the combination of a real-time BMI with a lower limb exoskeleton and tDCS is quite challenging and has the strong potential of improving (via tDCS) the quality of many clinical applications that involve the real-time control of these machines. Indeed, the intention of this second setup is the later use on real-time rehabilitation therapies of cerebrovascular accident (CVA) patients with lesions on the right leg. The main output to measure the effectiveness of the experiments was the MI detection accuracy, but given the experiments' duration, the development of brain plasticity over the course of the five days was also analyzed. Our hypothesis was that the active tDCS group would obtain better detection accuracy results than the sham group.

2 MATERIALS AND METHODS

This work studies a novel tDCS montage with two different experimental setups regarding cues and feedback. The first one, called in this paper E1, gives visual cues and visual feedback, while the second, named E2, gives auditory cues with the feedback coming from the movement/non-movement of an exoskeleton. E2 is a smaller pilot test to check if the feedback of the exoskeleton provides an improvement of the results, so that it can possibly be used later in the rehabilitation of CVA patients.

2.1 Subjects

Twelve healthy subjects with a mean age of 26.9 $\pm$ 5.8 years old (age range 20-39) volunteered to perform E1 and four volunteers with a mean age of 25.8 $\pm$ 0.7 years old (age range 22-34) participated in E2. All of them received information prior to the experiment and gave written informed consent according to the Helsinki declaration. None of the subjects had a history of neurological and/or psychiatric diseases or was receiving medication during the experiment that could alter the central nervous system. The Ethics Committee of the Office for Project Evaluations (Oficina Evaluadora de Proyectos: OEP) of the Miguel Hernández University of Elche (Spain) approved the study.

2.2 Experimental Design

The aim of both single-blind experiments was to detect two different cognitive states: relax and gait MI, using a real-time BMI based on EEG signals. For both experiments, initially subjects were randomly separated into sham or active tDCS groups of the same size (six participants in each group of E1 and two participants in each group of E2). For five consecutive days (Monday to Friday), each participant was subjected to one experimental session, which initiated with a period of stimulation. The sham group received 15 minutes of fake stimulation, while the active tDCS group received 15 minutes of real stimulation (more details in Section 2.3).

2.2.1 E1 Experiment

Participants performed one session each day for five consecutive days. One session was composed of the initial stimulation, followed by 10 MI trials. For each trial, subjects stood in front of a screen that provided instructions while their EEG signals were being recorded (Figure 1). Three types of instructions were supplied: *Relax*, *Imagine* and + (transition). During *Relax* periods, subjects had to clear their minds as much as possible; during *Imagine* periods, they had to imagine a gait movement. *Relax* and *Imagine* tasks appeared at random, but to avoid mind tiredness or getting bored, two tasks of the same type never appeared more than twice in a row. The transition periods, or + periods, separated different tasks of *Relax* or *Imagine*. *Relax* and *Imagine* lasted between 6 and 7.4 seconds, while the + (transition) periods lasted 3 seconds. Subjects were instructed to avoid blinking, swallowing, performing head movements or any other kind of artifact during the *Relax* and *Imagine* periods, postponing these actions to the + (transition) periods. Each trial consisted of 10 Relax and 10 Imagine periods. Figure 2 represents the temporal sequence of this experiment.

2.2.2 E2 Experiment

On the very first day, before any stimulation protocols, subjects were familiarized with the lower limb exoskeleton. They were mounted in the exoskeleton, and the exoskeleton was activated. Through verbal cues, the subjects were instructed to imagine gait until they felt comfortable that they were not trying to execute the motor task, but rather were imagining it. This pre-training phase was intended to remove any strong noise associated to the subjects trying to solely execute the movement later in the experiment.

Participants performed one session each day for five consecutive days. Throughout each session subjects stood wearing a lower limb exoskeleton while their EEG signals were recorded, as shown in Figure 3. One session was composed of the initial stimulation, followed by 80 MI trials. Each trial lasted around 35 seconds and was comprised of: an initial relax period where they had to clear their mind as much as possible; then, a beep auditory signal which indicated the subject to start the gait (walking) imagination until they heard a double beep auditory signal; after this, they had to relax again until the experiment finished. Therefore, there were two *Relax* periods which lasted 8 seconds each, separated by a longer *Imagine* period that lasted 16 seconds. A couple of seconds were needed to establish the connection between the BMI and the exoskeleton. Figure 4 represents the temporal sequence of this experiment.

In this experiment, the first 40 trials were used to train the BMI and the rest to test it. During the training, the exoskeleton moved by itself during the gait imagery period in order to provide the subjects with a more realistic feeling. Then, during the remaining 40 trials, the exoskeleton was turned off during the *Relax* periods and was activated according to the subject's EEG signals (i.e. using the BMI output) during the *Imagine* periods. The subjects were supposed to imagine the motor task instead of trying to execute it. More details on the BMI can be found in Section 2.5.

2.3 Supply of tDCS

As previously mentioned, the idea was to excite simultaneously the right cerebrocerebellum and the motor cortex because both areas are involved in motor imagery. To do that, one anode was located over the right cerebrocrebellum (two centimeters right and one centimeter down of the inion) and the other one over Cz on M1. The cathode was placed over FC2 (right hemisphere). Figure 5 shows a scheme of the position and placement of the electrodes. The cathode produces neural inhibition, meaning that the left hemisphere is being favored. This is because, in the future, the idea is to focus on patients that have suffered a CVA over the left hemisphere, which in turn affects their right lower limb.

The intensity was established to 0.2 mA and 0.3 mA for the cerebrocerebellum and Cz anodes respectively. These intensities were chosen because anodal tDCS over the right cerebrocerebellum produces inhibition over the brain motor area (Angulo-Sherman et al., 2017), so to counteract this effect and excite the motor area, the second anode was placed over Cz with a slightly higher current. Using this configuration resulted in a cathode current density of 0.16 mA/cm^2, which is higher than that used in most studies (about 0.06 mA/cm^2). Having said that, this current density is well within the range of neurological safety that avoids brain damage (Bikson et al., 2016).

In order to corroborate that the areas of interest in the brain (motor area, right cerebrocerebellum, thalamus, contralateral hemisphere, red nucleus) were involved during the stimulation, an electric field simulation was carried out first. SimNIBS free platform (Thielscher et al., 2015) was used for the simulation. The parameters of the electrodes were set according to the materials employed in the experiments. All the electrodes were 1 cm of radius (surface area of π cm^2), 3 mm of thickness and with 4 mm of space for the conductive gel. Figure 6 shows the magnitude of the electric field generated by the two anodes and one cathode in axial, coronal and sagittal views. The electric field produced was analyzed and it was confirmed that the sign of the electric field was negative over the cathode (showing directionality). Furthermore, the most affected area (red) is close to the thalamus and the red nucleus. Both areas belong to the cerebellum ascending output pathways to M1 and PM (Llinas and Negrello, 2015).

At the beginning of each experimental session, the StarStim R32 (Neuroelectrics, Barcelona, Spain) supplied direct current stimulation to the subject's brain. The duration was taken to be 15 minutes (each of the five days of the experiment), since various studies which treat different diseases obtained satisfactory

results applying tDCS for that duration during 5 consecutive days (Bolognini et al., 2015; Ferrucci et al., 2016; Marangolo et al., 2011). Subjects in the active tDCS group were subjected to 15 minutes of such stimulation, while those in the sham group received a fake stimulation to create a placebo effect. This consisted of a 3 seconds ramp up followed by a 3 seconds ramp down to zero; then, 15 minutes of zero current; and lastly, another repetition of 3 seconds ramp up and ramp down.

2.4 EEG Acquisition

The StarStim R32 (Neuroelectrics, Barcelona, Spain) was also used to acquire 30 EEG signals based on the International 10-10 system (P7, P4, CZ, PZ, P3, P8, O1, O2, C2, C4, F4, FP2, FZ, C3, F3, FP1, C1, OZ, PO4, FC6, FC2, AF4, CP6, CP2, CP1, CP5, FC1, FC5, AF3, PO3) with two reference electrodes (CMS and DRL) at a frequency of 500 Hz. The device was connected to the computer through a USB isolator.

2.5 Brain-machine Interface (BMI)

Custom software in MATLAB (MathWorks Inc., Massachusetts, United States) was utilized for all data analysis. The first four trials of E1 and the first 40 trials of E2 were used to train a support vector machine (SVM) classifier with a radial basis function as kernel. This classifier was chosen because it was effective in previous studies and is one of the most robust classifiers (Rodríguez-Ugarte et al., 2017). The SVM was in charge of categorizing data and determining if it belonged to relax or gait MI tasks. The remaining trials, six of E1 and 40 of E2, were utilized to test the BMI by measuring the detection accuracy, which was defined as the percentage of total correct classifications divided by the total number of classifications in each run.

Both training and test data in the two experiments were processed in very similar ways. The first two seconds of each task were discarded to assure the total concentration of the subject in the task and to get rid of the cue (visual or auditory) artifacts on the EEG. Data was processed in 1 second epochs each 0.2 seconds. For each epoch, the following process was carried out:

- a 4th order Butterworth high-pass filter with a cut-off frequency of 0.05 Hz was applied to remove the direct current;
- a Notch filter was used to eliminate the power line interference at 50 Hz;
- a 4th order Butterworth low-pass filter with cut-off frequency of 45 Hz was utilized;
- a Laplacian spacial filter was employed as in (McFarland et al., 1997) to eliminate the influence of the other electrodes by means of weighting by their distance;
- nine electrodes from the M1, SMA and PM were selected: Cz, CP1, CP2, C1, C2, C3, C4, FC1 and FC2.

In both experiments, the training data was further analyzed. For each electrode, the power at each integer frequency from 6 to 35 Hz was calculated. This data was separated into relax and imagine groups for each frequency, and the frequency that attained the maximum power difference between relax and imagine was designated as the optimum frequency of that electrode. Finally, the power at the optimum frequency for each electrode was computed. Therefore, each epoch was associated with nine features (one for each electrode). Using the features, the SVM classifier was trained.

For the actual testing of the real-time BMI, the nine features of each epoch were computed using the power at the precomputed optimum frequencies from the training phase. Then the data was classified using the SVM classifier into relax or gait MI. As visual feedback, in E1 every correct classification resulted in

the increase in size of a green bar shown in the screen. Meanwhile, in E2 the exoskeleton moved one step forward whenever three consecutive gait MI classifications were detected.

2.6 Exoskeleton

The lower limb robotic exoskeleton used was the H2 (Technaid, Madrid, Spain) designed by Bortole et al. (2015). The H2 has six degrees of freedom where hip, knee and ankle of each leg are powered joints. It was constructed for adults of heights between 1.5 m and 1.95 m and a maximum weight of 100 kg. The H2 has a lithium polymer battery of 22.5 VDC voltage and 12 Ah of capacity. It also has direct current (DC) motors to activate the joints actuators and sensors: potentiometers, Hall effect sensors, strain gauges and foot switches to determine the joint angles and human-orthosis interaction torques on the links.

The communication between the BMI and the H2 was through a bluetooth port. The connection was established in an Intel Core i7 laptop using MATLAB (MathWorks Inc., Massachusetts, United States) software. Each 0.5 seconds and during gait imagination periods, the BMI sent the user's output from the classifier to the exoskeleton.

2.7 Post-processing

2.7.1 Statistical Analysis

For the E1 experiment, data was analyzed via the Statistical Package Social Science (SPSS), version 22.0 (IBM Corporation, Armonk, NY, United States). The dependent variable was the classification accuracy and the independent variables were the group (sham or active tDCS) and the day of the experiment (from day 1 to day 5). Therefore, there were two types of studies: the difference between groups and the evolution of the performance of the subjects (here called plasticity) within groups. Hence, the appropriate statistical test to make was a mixed factorial ANOVA, but before doing so, the Kolmogorov-Smirnov (K-S) normality test was computed to check the existence of outliers. Then, for the study within groups, Mauchly's sphericity test was carried out to check the equality of the variances (Field, 2013). Lastly, the mixed factorial ANOVA analysis was completed. Furthermore, Bonferroni adjustments were applied for multiple pairwise comparisons between groups and within groups. A value of $p < 0.05$ was considered statistically significant.

For the E2 pilot experiment, the sample sizes were too small (two users per group) to rigorously justify the statistical analysis mentioned above. Therefore, the average accuracies were used directly to make the appropriate and relevant comparisons. Having said that, these results and their implications should come with a warning that this is only a preliminary study, and the sample sizes are small, so larger samples are needed to increase the accuracy of predictions.

2.7.2 Analysis of Optimal Frequencies

As mentioned in Section 2.5, based on the training data, an optimal frequency (where the greatest differences between relax and gait imagery was observed) was assigned to each electrode of each subject on any given day. These frequencies form a fundamental part of the model used to construct the BMI. Having said that, analyzing these frequencies independently provides more useful information. Indeed, after removing any outliers, it is possible to make a histogram of the optimal frequencies associated to each group on each day (each relevant subject in the group will have 9 optimal frequencies, one for each electrode, on any given day) that discriminates between three distinct frequency bands: high theta and mu rhythm (6-12 Hz), low and mid-range beta rhythm (13-20 Hz) and high beta rhythm (21-30Hz). With

this histogram, one can then determine the preferred frequency bands for each group and their evolution throughout the experiment.

2.7.3 ERD/ERS Analysis

Event-related desynchronization and synchronization (ERD/ERS) are EEG fluctuations during cognitive or motor processes. They are highly frequency-band specific and while ERD represents an increase of excitability, ERS represents the opposite (Pfurtscheller, 2001). For an electrode e, and for a fixed frequency f, let

$$ERD_e(f) = \Big(\frac{G(f) - R(f)}{R(f)}\Big), \tag{1}$$

where $G(f)$ is the average of the power at the frequency f over all gait-imagery-epochs, and $R(f)$ is the same but averaged over all relax-imagery-epochs. Low values of G, resulting in negative values of ERD_e, represent ERD, while higher values of G, resulting in positive values of ERD_e, represent ERS. To obtain an average value of ERD_e over a frequency band, simply average over all integer frequencies, f, of interest (e.g. in the 6-12 Hz band, it would be the average of $ERD_e(f)$ for $f = 6, 7, 8, 9, 10, 11, 12$). A frequency-band ERD_e can be calculated for each electrode on each day of the experiment for each subject. This allows to produce a topographic map of the variable in the scalp, which one can then analyze to determine patterns of activation across the different areas of the brain.

3 RESULTS

3.1 E1 Experiment

The normality test indicated that there was an outlier within the sham group. This subject was removed from the data.

3.1.1 Effects of tDCS in MI

This section studies if there exist any effects of tDCS on the subjects. Results from the mixed factorial ANOVA showed that subjects were significantly affected by the group they belonged, $F(1, 9) = 9.47$, $p < 0.05$. Figure 7 shows the mean accuracy achieved by each group, with the tDCS and sham groups getting 65% and 52.4% of detection accuracy respectively.

Moreover, the comparison was broken down on a day by day basis, by making pairwise comparisons. Table 1 shows the p-values of those comparisons and Figure 8 illustrates the mean accuracy achieved by each group on each day. The results show that there were significant differences ($p < 0.05$) between the sham and tDCS groups from the second day onwards.

3.1.2 MI plasticity

This section analyzes the interaction effects between the days within groups. The results of Mauchly's test of sphericity show that the condition of sphericity was met, $\chi^2(9) = 17.52$, $p > 0.05$, so it was not necessary to apply a correction factor.

The mixed factorial ANOVA showed no significant interaction between the days and the group, $F(4, 36) = 0.27$, $r = 0.1$, $p > 0.05$, meaning that there does not seem to be any major plasticity development throughout the five days of the experiment.

3.1.3 Optimal Frequencies and ERD/ERS Results

A histogram showing the percentage of electrode optimal frequencies lying in the relevant frequency bands (high theta and mu rhythm, low and mid-range beta rhythm, and high beta rhythm) for each group and day of the E1 experiment is shown in Table 2. Clearly, the preferred frequency band is the high theta and mu rhythm (6-12 Hz).

Since the high theta and mu rhythm (6-12 Hz) was the preferred frequency band, on each day of the E1 experiment and for each electrode, e, the variable ERD_e was averaged over all subjects common to a group (excluding outliers) and over the relevant frequency band (6-12 Hz). The resulting topographic map for the active tDCS and the sham groups is shown in Figure 11 (top).

3.2 E2 Experiment

3.2.1 Effects of tDCS in MI

Figure 9 shows the mean accuracy achieved by each group, with the tDCS and sham groups getting 81.6% and 73.4% of detection accuracy respectively. Furthermore, Figure 10 illustrates the mean accuracy achieved by each group on each day, and there does not seem to be any significant changes in the accuracy as the days progress for either group (i.e. no plasticity is evident). Having said this, due to the preliminary nature of the E2 pilot study, these results have limitations as they involve very small sample sizes (two subjects per group), and larger data sets are necessary to be able to produce more robust results from the statistical standpoint.

3.2.2 Optimal Frequencies and ERD/ERS Results

As in Section 3.1.3, the associated histogram for E2 is shown in Table 3. The preferred frequency band was once again the high theta and mu rhythm (6-12 Hz).

Meanwhile, the analogous topographic map for E2 for the preferred frequency band (6-12 Hz) is shown in Figure 11 (bottom).

4 DISCUSSION

The results of E1 and the preliminary results of the pilot test in E2, seem to support the hypothesis that this novel tDCS montage improves the real-time classification of lower limb MI tasks. Before discussing the specific results further, a deeper neurological explanation for why the tDCS montage seems to have successfully worked is merited. The aim of the setup was to enhance the brain's learning abilities while stimulating the motor cortex which is responsible for lower limb movement (and imagination). With this in mind, an anode was placed over the cerebellum, since this improves the brain's learning abilities according to several studies (Mandolesi et al., 2003; Ferrucci et al., 2013; Hardwick and Celnik, 2014b; Shah et al., 2013). However, placing this anode over the cerebellum also has other consequences. Namely, it produces the activation of Purkinje cells which inhibit the dentate nucleus and provoke disfacilitation of the motor cortex (Grimaldi et al., 2014; Lefaucheur et al., 2017; Cengiz and Boran, 2016), which is the opposite of what is desired regarding the activation of the motor cortex. For this reason, to counteract the effect of the first anode and excite the neural activity of the motor cortex, a second anode was placed directly in Cz over the motor cortex, and with a slightly higher current. Indeed, the currents used were 0.2 mA for the first anode and 0.3 mA for the second anode. The tDCS electrodes were not in direct contact with the skin, but rather with the hair. This reduced the probability of skin burns (Wang et al., 2015), which were not

observed during the experiments (participants were encouraged to report any discomfort, but none was reported in association with the tDCS).

The active tDCS group achieved average detection accuracies of 65% and 81.6% for E1 and E2 respectively. When compared to the sham group, the active tDCS group obtained 12.6% and 8.2% higher accuracy performance in E1 and E2 respectively (Figure 7 and Figure 9). In addition, the active tDCS group of E1 was at least 10% better than the sham group at each given day (see Figure 8), while in E2, it was at least 4% better on each day (see Figure 10). Lastly, this data and the p-values from Table 1 indicate that from the second day onwards, the active tDCS group obtained significantly different and better results than the sham group in E1.

These conclusions are further supported with the results of analyzing the optimal frequencies and the ERD/ERS patterns in the brain. Regarding the optimal frequencies, Table 2 and the preliminary results of Table 3 show the stability of the frequency band trained, which in both cases corresponded to the high theta and mu rhythms (6-12 Hz). In E1 (Table 2) the preferred frequency band for the active tDCS group represented at least 78% of the optimal frequencies on any given day, while for the sham group it varied between 57% and 76%. The results of E2 show an even starker difference, with at least 94% of optimal frequencies lying in the the preferred frequency band for the active tDCS group, while they ranged between 50% and 66% for the sham group. This seems to indicate that the tDCS favors a specific frequency band to train the new task.

Moreover, the ERD/ERS analysis shows that overall for both E1 and E2, there seems to be more desynchronization (ERD) on the mu rhythms of the tDCS group than in the sham group (see Figure 11). Furthermore, this mu wave desynchronization is occurring mostly in the sensorimotor area, as is reported widely in the literature when there is either motor execution or motor imagery (Matsumoto et al., 2010; Pfurtscheller and Da Silva, 1999). This desynchronization seems to be more evident in the preliminary study E2 than in E1, but in both cases it is observed. Thus, the active tDCS group for both experiments appears to enhance the modulation of the mu rhythm and the BMI control.

As observed from Figure 8 and Figure 10, for both experiments, the changes in accuracy for each group as the days progressed seems to have been minimal. Thus, one can say that there was little plasticity developed in the brain during the five days of the experiment. This is probably due to the simplicity of the task and the fact that the brain could have quickly adapted to this task early on in the training phase of the experiment of the first day.

Comparing the differences between E1 and E2 is very interesting but one must be careful in rushing to any conclusions, as the experimental protocols were different, and more importantly, the results of E2 are only preliminary at the time. Overall, E2 produced better accuracy results than E1: the active tDCS and sham groups of E2 were 16.7% and 21.2% more accurate than the respective groups of E1. Some differences in the protocol that could have led to these results, are that the duration of *Relax* and *Imagine* periods between the two experiments was different; and more notably, that the nature of the cues and feedback was different as well. Indeed, it should be mentioned that all subjects in E1 reported frustration about the visual feedback (a green bar that increased with each real-time correct detection), saying that they became anxious when the green bar did not move. Naturally, this could have affected the results. Meanwhile, in E2 the feedback was much more natural as it involved movement of the body. In fact, no such frustration was reported by the users in E2.

Comparing the results of E1 and the preliminary results of E2 through the ERD/ERS analysis is also of interest (see Figure 11). Indeed, the desynchronization is observed to be stronger and more consistent in E2

than in E1. This seems to be consistent with some results in the literature involving upper limb exoskeletons (Gomez-Rodriguez et al., 2011), which found the discriminative power of the sensorimotor area to be higher when using an exoskeleton, thus providing a benefit in terms of the resulting BMI designed.

It should be noted that the pilot test E2 was a challenging experiment as it involved combining tDCS with a real-time BMI connected to an exoskeleton. Exoskeletons are often simply pre-programmed or controlled directly through third party interfaces (joysticks, cellphone applications, etc.), but only until relatively recently have they begun to be controlled via BMIs. Designing a real-time BMI is also not trivial in itself (it is sometimes preceded by the design of offline BMIs). Thus, the study of real-time BMI control of exoskeletons is only starting and has many potential clinical applications, especially in the rehabilitation of patients. Thus, combining this concept with tDCS, which is aimed to improve and accelerate cognitive ability, enriches and increases those applications even more. Indeed, the intention is to use this setup in the future to enhance the recovery of CVA patients with an affected lower right limb. Having said that, the study carried out here was only a preliminary pilot study involving only a few subjects. To confirm the results, a larger sample of subjects or even patients is necessary, but the limited results obtained for now look promising.

Some final comments are warranted regarding the real-time functioning of the exoskeleton in E2. To have a realistic usability of the BMI with the exoskeleton, the analysis of the false detections during relax periods is important, and reducing it is an essential objective. The rate of such detections is referred to as the false positive rate, or FPR (which is the complement of the accuracy when restricted to only relax periods). When averaging both groups in E2, the FPR was 11.7% (equivalently, an accuracy of 88.3% during relax), with an FPR of 11.3% for the tDCS group and of 12.1% for the sham group. The values for both groups were very similar, which shows that the overall increase in accuracy resulting from the stimulation of the tDCS group, was due to an increase in accuracy during the imagination periods (indeed, the accuracy on those periods was 92.7% for the tDCS group and of 80.4% for the sham group). In any case, overall, these values of FPR seem reasonable for this preliminary experiment, but reducing them further should be a future design goal.

5 CONCLUSION

A novel tDCS configuration was successfully designed to improve the detection of two MI tasks (relax and gait MI) using a real-time BMI. Two anodes and one cathode were used: one anode was located over the right cerebrocerebellum and supplied 0.2 mA, the other anode was over Cz and supplied 0.3 mA, and the cathode was located over FC2. Two single-blind experiments, E1 and E2, were carried out, where subjects were randomly separated into two groups of the same size: sham and active tDCS. The sham group received a fake stimulation while the active tDCS group was truly stimulated. E1 involved twelve healthy subjects in total who received visual instructions and real-time feedback through a screen. Meanwhile, E2 was a pilot study involving only four healthy subjects who received auditory cues and wore a lower limb exoskeleton as feedback. E2 has potentially many clinical applications in the future. In particular, it can be used in the rehabilitation of patients that have suffered a cerebrovascular accident (CVA) affecting their right lower limb. The analysis indicated differences between the active tDCS and sham group in both experiments. The active tDCS group achieved 12.6% and 8.2% higher detection accuracy than the sham group in E1 and E2 respectively, reaching 65% and 81.6% mean accuracy in each experiment. Furthermore, the preliminary results indicate that the exoskeleton (in E2) enhanced the detection of the MI tasks with respect to the visual feedback (in E1), increasing the accuracy obtained in 16.7% and 21.2% for the active

tDCS and sham groups respectively. Having said that, more studies with larger samples of actual patients are needed to validate this observation.

CONFLICT OF INTEREST STATEMENT

The authors declare that the research was conducted in the absence of any commercial or financial relationships that could be construed as a potential conflict of interest.

AUTHOR CONTRIBUTIONS

M. Rodríguez-Ugarte is responsible for the design, implementation, acquisition and data analysis. In addition, E. Iáñez and M. Ortíz supervised the work and contributed with the revision process. J.M. Azorín actively contributed as director of the work.

FUNDING

This research was carried out in the framework of the project Associate titled: Decoding and stimulation of motor and sensory brain activity to support long term potentiation through Hebbian and paired associative stimulation during rehabilitation of gait (DPI2014-58431-C4-2-R), which is funded by the Spanish Ministry of Economy and Competitiveness and by the European Union through the European Regional Development Fund (ERDF), "A way to build Europe".

NON-STANDARD ABBREVIATIONS

tDCS: transcranial direct current stimulation
MI: motor imagery
ME: motor execution
BMI: brain-machine interface
EEG: electroencephalographic
fMRI: functional magnetic resonance imaging
M1: primary motor cortex
SMA: supplementary motor area
PM: premotor area
CVA: cerebrovascular accident
SVM: support vector machine

ACKNOWLEDGMENTS

M. Rodríguez-Ugarte wishes to thank Federico Fuentes for useful discussions and the revision of the manuscript. Furthermore, Brain-Machine Interface Systems Lab wishes to thank the R & D Unit in Biomechanics and Technical Aid of the National Paraplegic Centre at Toledo for providing users and lending the exoskeleton.

REFERENCES

Allali, G., Van Der Meulen, M., Beauchet, O., Rieger, S. W., Vuilleumier, P., and Assal, F. (2013). The neural basis of age-related changes in motor imagery of gait: an fMRI study. *Journals of Gerontology Series A: Biomedical Sciences and Medical Sciences* 69, 1389–1398

Angulo-Sherman, I. N., Rodríguez-Ugarte, M., Sciacca, N., Iáñez, E., and Azorín, J. M. (2017). Effect of tdcs stimulation of motor cortex and cerebellum on eeg classification of motor imagery and sensorimotor band power. *Journal of neuroengineering and rehabilitation* 14, 31

Barrios, L. J., Hornero, R., Perez-Turiel, J., Pons, J. L., Vidal, J., and Azorin, J. M. (2017). State of the art in neurotechnologies for assistance and rehabilitation in spain: fundamental technologies. *REVISTA IBEROAMERICANA DE AUTOMATICA E INFORMATICA INDUSTRIAL* 14, 346–354

Bikson, M., Grossman, P., Thomas, C., Zannou, A. L., Jiang, J., Adnan, T., et al. (2016). Safety of transcranial direct current stimulation: evidence based update 2016. *Brain Stimulation: Basic, Translational, and Clinical Research in Neuromodulation* 9, 641–661

Boehringer, A., Macher, K., Dukart, J., Villringer, A., and Pleger, B. (2013). Cerebellar transcranial direct current stimulation modulates verbal working memory. *Brain stimulation* 6, 649–653

Bolognini, N., Spandri, V., Ferraro, F., Salmaggi, A., Molinari, A. C., Fregni, F., et al. (2015). Immediate and sustained effects of 5-day transcranial direct current stimulation of the motor cortex in phantom limb pain. *The Journal of Pain* 16, 657–665

Bortole, M., Venkatakrishnan, A., Zhu, F., Moreno, J. C., Francisco, G. E., Pons, J. L., et al. (2015). The H2 robotic exoskeleton for gait rehabilitation after stroke: early findings from a clinical study. *Journal of neuroengineering and rehabilitation* 12, 54

Bradnam, L. V., Graetz, L. J., McDonnell, M. N., and Ridding, M. C. (2015). Anodal transcranial direct current stimulation to the cerebellum improves handwriting and cyclic drawing kinematics in focal hand dystonia. *Frontiers in human neuroscience* 9, 286

Cengiz, B. and Boran, H. E. (2016). The role of the cerebellum in motor imagery. *Neuroscience letters* 617, 156–159

Clancy, J. A., Johnson, R., Raw, R., Deuchars, S. A., and Deuchars, J. (2014). Anodal transcranial direct current stimulation (tDCS) over the motor cortex increases sympathetic nerve activity. *Brain stimulation* 7, 97–104

Coffman, B. A., Clark, V. P., and Parasuraman, R. (2014). Battery powered thought: enhancement of attention, learning, and memory in healthy adults using transcranial direct current stimulation. *Neuroimage* 85, 895–908

Ferrucci, R., Brunoni, A. R., Parazzini, M., Vergari, M., Rossi, E., Fumagalli, M., et al. (2013). Modulating human procedural learning by cerebellar transcranial direct current stimulation. *The Cerebellum* 12, 485–492

Ferrucci, R., Mameli, F., Ruggiero, F., and Priori, A. (2016). Transcranial direct current stimulation as treatment for Parkinson's disease and other movement disorders. *Basal Ganglia* 6, 53–61

Ferrucci, R. and Priori, A. (2014). Transcranial cerebellar direct current stimulation (tcDCS): motor control, cognition, learning and emotions. *Neuroimage* 85, 918–923

Field, A. (2013). *Discovering statistics using IBM SPSS statistics* (Sage)

Filmer, H. L., Dux, P. E., and Mattingley, J. B. (2014). Applications of transcranial direct current stimulation for understanding brain function. *Trends in neurosciences* 37, 742–753

Foerster, Á., Melo, L., Mello, M., Castro, R., Shirahige, L., Rocha, S., et al. (2017). Cerebellar transcranial direct current stimulation (ctdcs) impairs balance control in healthy individuals. *The Cerebellum* , 1–4

Galea, J. M., Jayaram, G., Ajagbe, L., and Celnik, P. (2009). Modulation of cerebellar excitability by polarity-specific noninvasive direct current stimulation. *Journal of Neuroscience* 29, 9115–9122

Gomez-Rodriguez, M., Peters, J., Hill, J., Schölkopf, B., Gharabaghi, A., and Grosse-Wentrup, M. (2011). Closing the sensorimotor loop: haptic feedback facilitates decoding of motor imagery. *Journal of neural engineering* 8, 036005

Grimaldi, G., Argyropoulos, G., Boehringer, A., Celnik, P., Edwards, M., Ferrucci, R., et al. (2014). Non-invasive cerebellar stimulation—a consensus paper. *The Cerebellum* 13, 121–138

Grimaldi, G., Argyropoulos, G. P., Bastian, A., Cortes, M., Davis, N. J., Edwards, D. J., et al. (2016). Cerebellar transcranial direct current stimulation (ctDCS) a novel approach to understanding cerebellar function in health and disease. *The Neuroscientist* 22, 83–97

Hardwick, R. M. and Celnik, P. A. (2014a). Cerebellar direct current stimulation enhances motor learning in older adults. *Neurobiology of aging* 35, 2217–2221

Hardwick, R. M. and Celnik, P. A. (2014b). Cerebellar direct current stimulation enhances motor learning in older adults. *Neurobiology of aging* 35, 2217–2221

Hétu, S., Grégoire, M., Saimpont, A., Coll, M.-P., Eugène, F., Michon, P.-E., et al. (2013). The neural network of motor imagery: an ALE meta-analysis. *Neuroscience & Biobehavioral Reviews* 37, 930–949

Hortal, E., Planelles, D., Resquin, F., Climent, J. M., Azorín, J. M., and Pons, J. L. (2015). Using a brain-machine interface to control a hybrid upper limb exoskeleton during rehabilitation of patients with neurological conditions. *Journal of neuroengineering and rehabilitation* 12, 92

Lefaucheur, J.-P., Antal, A., Ayache, S. S., Benninger, D. H., Brunelin, J., Cogiamanian, F., et al. (2017). Evidence-based guidelines on the therapeutic use of transcranial direct current stimulation (tDCS). *Clinical Neurophysiology* 128, 56–92

Llinas, R. and Negrello, M. N. (2015). Cerebellum. *Scholarpedia* 10, 4606

Mandolesi, L., Leggio, M., Spirito, F., and Petrosini, L. (2003). Cerebellar contribution to spatial event processing. *European Journal of Neuroscience* 18, 2618–2626

Marangolo, P., Marinelli, C., Bonifazi, S., Fiori, V., Ceravolo, M., Provinciali, L., et al. (2011). Electrical stimulation over the left inferior frontal gyrus (IFG) determines long-term effects in the recovery of speech apraxia in three chronic aphasics. *Behavioural brain research* 225, 498–504

Marquez, C. M. S., Zhang, X., Swinnen, S. P., Meesen, R., and Wenderoth, N. (2013). Task-specific effect of transcranial direct current stimulation on motor learning. *Frontiers in human neuroscience* 7

Matsumoto, J., Fujiwara, T., Takahashi, O., Liu, M., Kimura, A., and Ushiba, J. (2010). Modulation of mu rhythm desynchronization during motor imagery by transcranial direct current stimulation. *Journal of neuroengineering and rehabilitation* 7, 27

McFarland, D. J., McCane, L. M., David, S. V., and Wolpaw, J. R. (1997). Spatial filter selection for EEG-based communication. *Electroencephalography and clinical Neurophysiology* 103, 386–394

Monti, A., Ferrucci, R., Fumagalli, M., Mameli, F., Cogiamanian, F., Ardolino, G., et al. (2013). Transcranial direct current stimulation (tdcs) and language. *J Neurol Neurosurg Psychiatry* 84, 832–842

Nelson, J. T., McKinley, R. A., Golob, E. J., Warm, J. S., and Parasuraman, R. (2014). Enhancing vigilance in operators with prefrontal cortex transcranial direct current stimulation (tDCS). *Neuroimage* 85, 909–917

Park, C., Looney, D., ur Rehman, N., Ahrabian, A., and Mandic, D. P. (2013). Classification of motor imagery BCI using multivariate empirical mode decomposition. *IEEE Transactions on neural systems and rehabilitation engineering* 21, 10–22

Pfurtscheller, G. and Da Silva, F. L. (1999). Event-related eeg/meg synchronization and desynchronization: basic principles. *Clinical neurophysiology* 110, 1842–1857

Reynolds, C., Osuagwu, B. A., and Vuckovic, A. (2015). Influence of motor imagination on cortical activation during functional electrical stimulation. *Clinical Neurophysiology* 126, 1360–1369

Rodríguez-Ugarte, M., Costa, Á., Iáñez, E., Úbeda, A., and Azorín, J. (2017). Pseudo-online detection of intention of pedaling start cycle through EEG signals. In *Converging Clinical and Engineering Research on Neurorehabilitation II* (Springer). 1103–1107

Rodrıguez-Ugarte, M., Sciacca, N., Iánez, E., and Azorın, J. M. (2016). Transcranial direct current stimulation (tDCS) and transcranial current alternating stimulation (tACS) review. *XXXVII Jornadas de Automática*

Sehm, B., Kipping, J., Schäfer, A., Villringer, A., and Ragert, P. (2013). A comparison between uni-and bilateral tDCS effects on functional connectivity of the human motor cortex. *Frontiers in human neuroscience* 7

Shah, B., Nguyen, T. T., and Madhavan, S. (2013). Polarity independent effects of cerebellar tDCS on short term ankle visuomotor learning. *Brain stimulation* 6, 966–968

Sharma, N. and Baron, J.-C. (2013). Does motor imagery share neural networks with executed movement: a multivariate fMRI analysis. *Frontiers in human neuroscience* 7

Thielscher, A., Antunes, A., and Saturnino, G. B. (2015). Field modeling for transcranial magnetic stimulation: A useful tool to understand the physiological effects of TMS? In *Engineering in Medicine and Biology Society (EMBC), 2015 37th Annual International Conference of the IEEE* (IEEE), 222–225

Wang, J., Wei, Y., Wen, J., and Li, X. (2015). Skin burn after single session of transcranial direct current stimulation (tdcs). *Brain Stimulation: Basic, Translational, and Clinical Research in Neuromodulation* 8, 165–166

Wiethoff, S., Hamada, M., and Rothwell, J. C. (2014). Variability in response to transcranial direct current stimulation of the motor cortex. *Brain stimulation* 7, 468–475

Zapparoli, L., Invernizzi, P., Gandola, M., Verardi, M., Berlingeri, M., Sberna, M., et al. (2013). Mental images across the adult lifespan: a behavioural and fMRI investigation of motor execution and motor imagery. *Experimental brain research* 224, 519–540

FIGURE CAPTIONS

5.1 Tables

Table 1. Pairwise comparison of detection accuracy for each day between the tDCS and sham groups (E1).

day	p**-value**
1	0.06
2	0.04*
3	0.04*
4	0*
5	0.02*

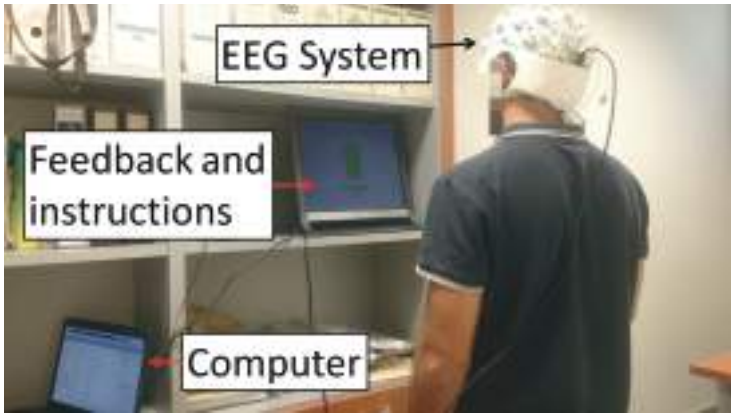

Figure 1. E1 experimental setup. Subjects stood in front of a screen that supplied instructions while their EEG signals were recorded. The instructions given were: *Relax*, *Imagine* and + (transition). During *Relax*, subjects had to clear their mind as much as possible. During *Imagine*, they had to visualize they were walking. Tasks appeared at random but two tasks of the same type never appeared more than twice in a row. The + (transition) period represented a transition to separate the *Relax* and *Imagine* tasks. Written informed consent was given by the subject to publish the photo.

Figure 2. E1 temporal sequence on each day. Subjects were randomly separated into two groups: sham or active tDCS. During 15 minutes participants received the corresponding stimulation according to their group. After that, subjects performed 10 trials of motor imagery (MI) tasks. The tasks were composed of *Relax* and *Imagine* tasks separated by transition periods represented by + displayed on the screen. One trial consisted of 10 *Relax* and 10 *Imagine* tasks.

Figure 3. E2 experimental setup. Subjects stood wearing an exoskeleton while their EEG signals were recorded. Once the experiment started, subjects had to relax, clearing their mind as much as possible. Then, a beep auditory signal indicated to the subject to start gait imagery until they heard a double beep auditory signal. After this second beep, subjects had to relax again until the experimental trial finished.Written informed consent was given by the subject to publish the photo.

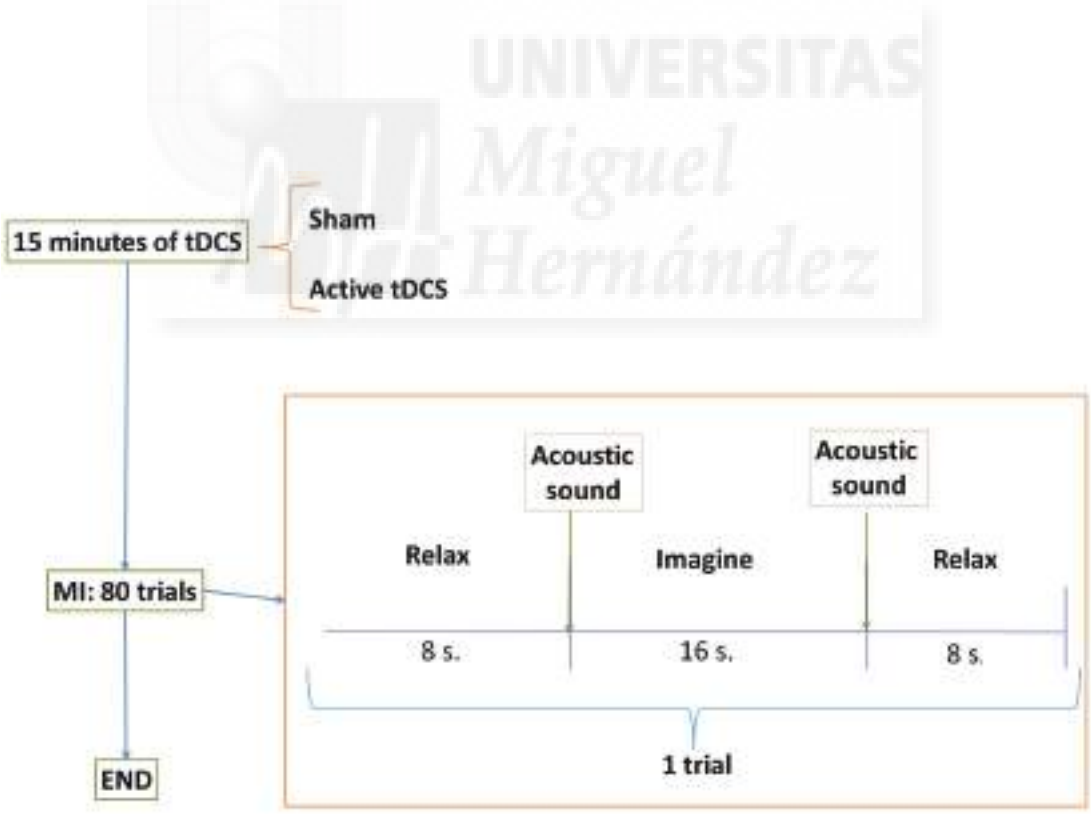

Figure 4. E2 temporal sequence on each day. Subjects were randomly separated into two groups: sham or active tDCS. During 15 minutes participants received the corresponding stimulation according to their group. After that, subjects performed 80 trials of motor imagery (MI) tasks. The trial was composed of two relax periods separated by one task of gait imagination.

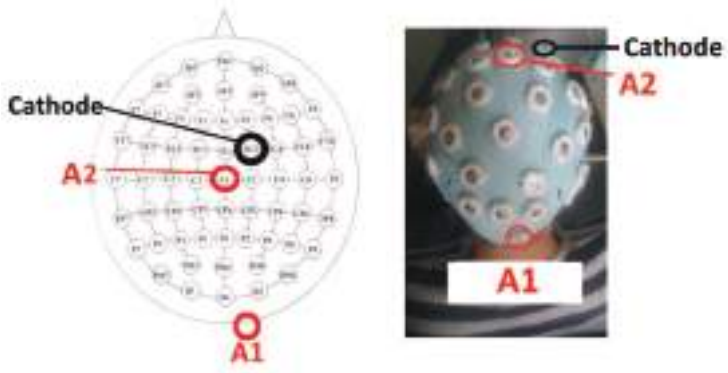

Figure 5. The tDCS montage. Placement of tDCS electrodes as a scheme (left) and experimentally (right). The first anode (A1) is over the right cerebrocerebellum (two centimeters right and one centimeter down of the inion), the second anode (A2) is over Cz, and the cathode is over FC2.

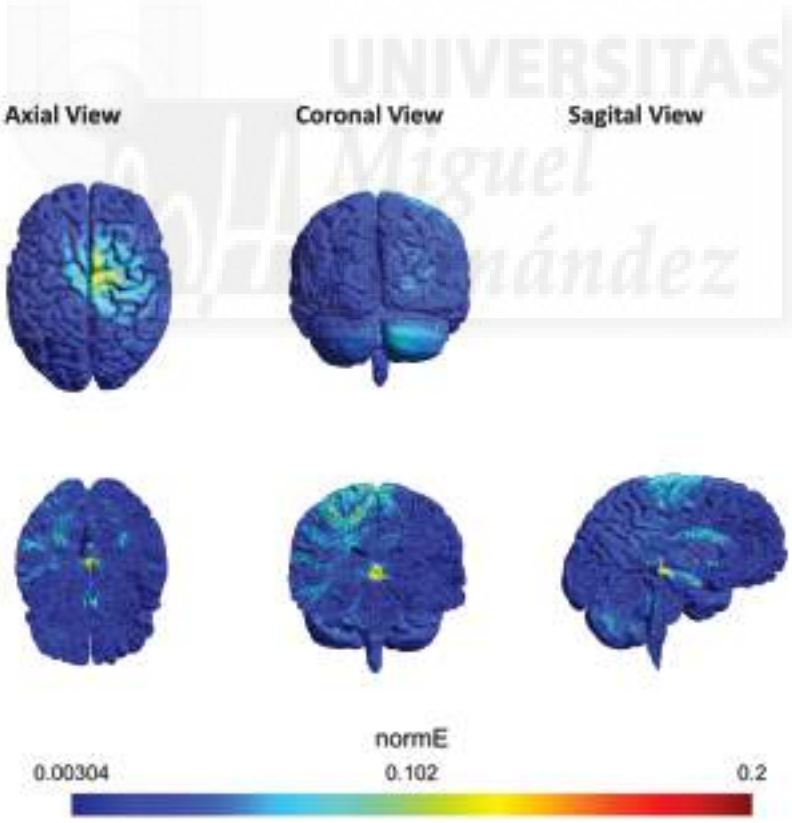

Figure 6. Axial, coronal and sagittal view of the tDCS simulation using SimNIBS. The scale represents the magnitude of the electric field (V/m) induced by the anodes A1 and A2. A1 was located over the right cerebrocerebellum and A2 over Cz. The cathode was located over FC2. A1 supplied 0.2 mA and A2 0.3 mA. The most affected area (red) is close to the red nucleus.

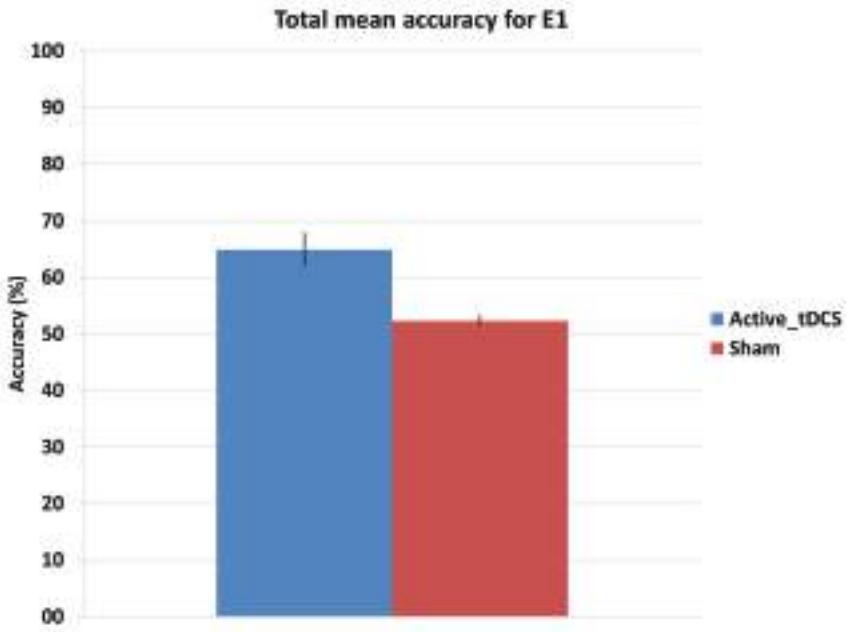

Figure 7. Mean accuracy for each group in the E1 experiment. The error bars indicate a standard deviation from the mean.

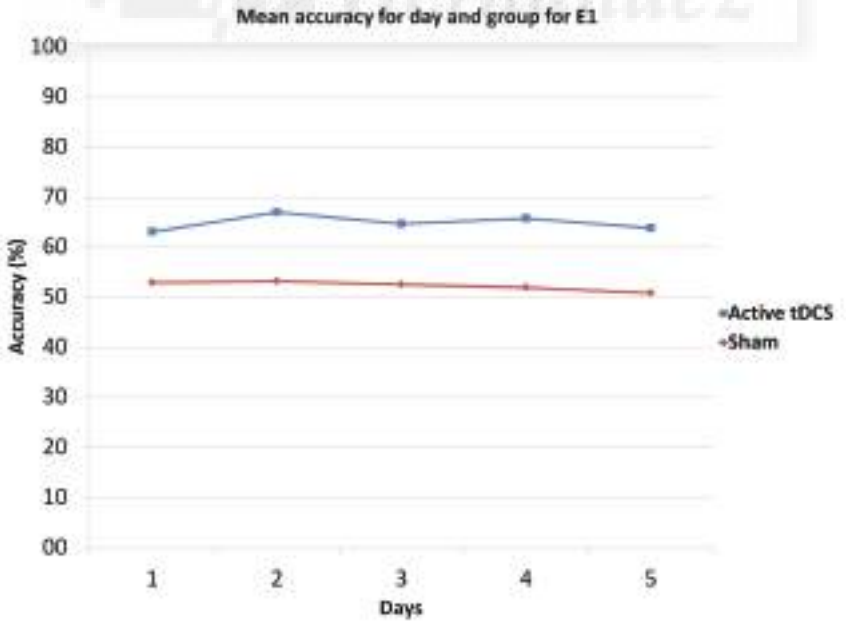

Figure 8. Mean accuracy for each day and group in E1.

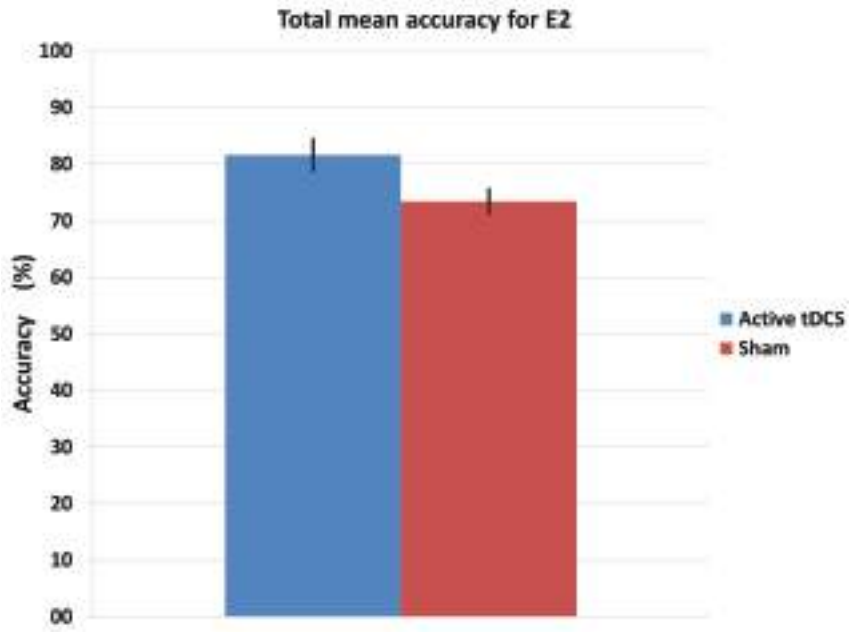

Figure 9. Mean accuracy for each group in the E2 experiment. The error bars indicate a standard deviation from the mean.

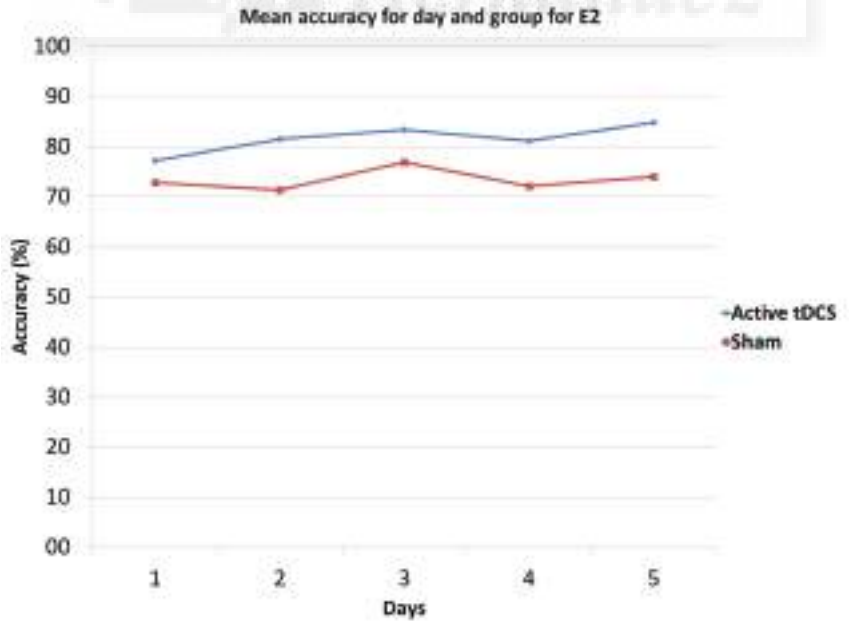

Figure 10. Mean accuracy for each day and group in E2.

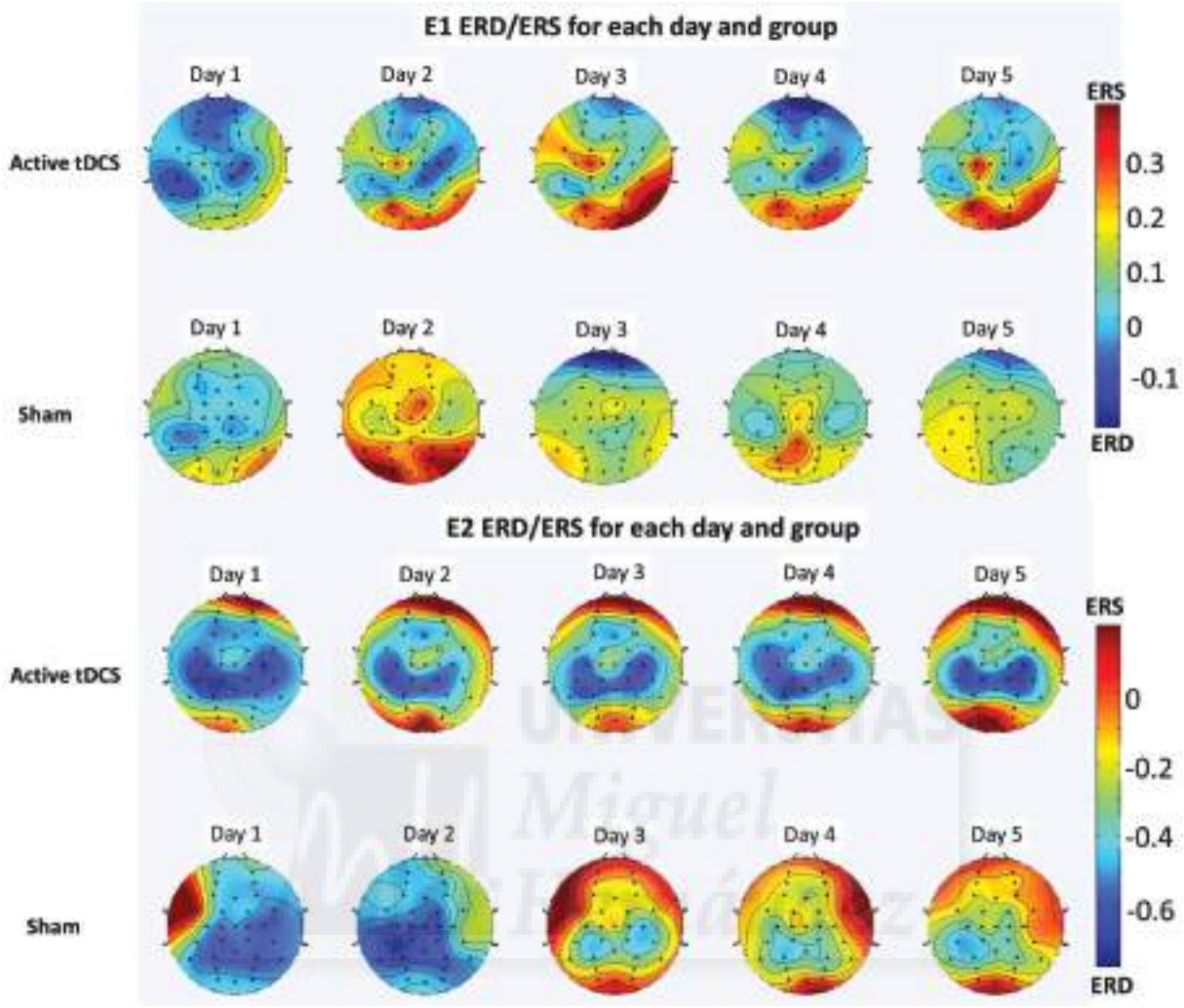

Figure 11. Topographic maps showing ERS (red) and ERD (blue) for the 6-12 Hz frequency band averaged over all participants for each day and group of each experiment. The results of E1 are shown in the top and those of E2 are shown in the bottom.

Table 2. E1 histogram of optimal frequencies for each day and group.

Group	Frequency range	Day 1 (%)	Day 2 (%)	Day 3 (%)	Day 4 (%)	Day 5 (%)
active tDCS	(6 - 12) Hz	81.5	77.8	81.5	85.2	79.6
	(13 - 20) Hz	11.1	13.0	11.1	7.4	16.7
	(21 - 30) Hz	7.4	9.3	7.4	7.4	3.7
sham	(6 - 12) Hz	75.6	57.8	68.9	64.4	64.4
	(13 - 20) Hz	4.4	17.8	4.4	28.9	20.0
	(21 - 30) Hz	20.0	24.4	26.7	6.7	17.8

Table 3. E2 histogram of optimal frequencies histogram for each day and group.

Group	Frequency range	Day 1 (%)	Day 2 (%)	Day 3 (%)	Day 4 (%)	Day 5 (%)
active tDCS	(6 - 12) Hz	100.0	100.0	100.0	100.0	94.4
	(13 - 20) Hz	0.0	0.0	0.0	0.0	0.0
	(21 - 30) Hz	0.0	0.0	0.0	0.0	5.6
sham	(6 - 12) Hz	66.7	66.7	50.0	50.0	50.0
	(13 - 20) Hz	0.0	0.0	0.0	0.0	0.0
	(21 - 30) Hz	33.3	33.3	50.0	50.0	50.0

UNIVERSITAS
Miguel
Hernández

Bibliografía

[1] M. Rodríguez-Ugarte, E. Iáñez, M. Ortíz, y J. M. Azorín, "Personalized offline and pseudo-online BCI models to detect pedaling intent," *Frontiers in Neuroinformatics*, vol. 11, p. 45, 2017.

[2] M. Rodríguez-Ugarte, E. Iáñez, M. Ortiz García, y J. Azorín, "Effects of tDCS on real-time BCI detection of pedaling motor imagery," *Sensors*, vol. 18, no. 4, p. 1136, 2018.

[3] M. Rodríguez Ugarte, E. Iáñez, M. Ortiz, y J. M. Azorin, "Improving real-time lower limb motor imagery detection using tdcs and an exoskeleton," *Frontiers in Neuroscience*, vol. 12, p. 757, 2018.

[4] T. Shakespeare y A. Officer, "World report on disability," *Disabil Rehabil*, vol. 33, no. 17-18, p. 1491, 2011.

[5] B. Ovbiagele y M. N. Nguyen-Huynh, "Stroke epidemiology: advancing our understanding of disease mechanism and therapy," *Neurotherapeutics*, vol. 8, no. 3, p. 319, 2011.

[6] W. H. Organization, *World health statistics 2015*. World Health Organization, 2015.

[7] S. E. de Neurología, G. de Estudio de las Enfermedades Vasculares Cerebrales *et al.*, "Guía para el diagnóstico y tratamiento del ictus," *Barcelona: Prous Science. ISBN*, pp. 84–8124, 2006.

[8] A. Louveau, I. Smirnov, T. J. Keyes, J. D. Eccles, S. J. Rouhani, J. D. Peske, N. C. Derecki, D. Castle, J. W. Mandell, K. S. Lee *et al.*, "Structural and fun-

ctional features of central nervous system lymphatic vessels," *Nature*, vol. 523, no. 7560, p. 337, 2015.

[9] N. Tsukahara y M. Kawato, "Dynamic and plastic properties of the brain stem neuronal networks as the possible neuronal basis of learning and memory," en *Competition and cooperation in neural nets*. Springer, 1982, pp. 430–441.

[10] S. J. Harkema, "Neural plasticity after human spinal cord injury: application of locomotor training to the rehabilitation of walking," *The Neuroscientist*, vol. 7, no. 5, pp. 455–468, 2001.

[11] J. D. Schaechter, "Motor rehabilitation and brain plasticity after hemiparetic stroke," *Progress in Neurobiology*, vol. 73, no. 1, pp. 61–72, 2004.

[12] M. Severens, M. Perusquia-Hernandez, B. Nienhuis, J. Farquhar, y J. Duysens, "Using actual and imagined walking related desynchronization features in a BCI," *IEEE Transactions on Neural Systems and Rehabilitation Engineering*, vol. 23, no. 5, pp. 877–886, 2015.

[13] S. J. Lee y M. H. Chun, "Combination transcranial direct current stimulation and virtual reality therapy for upper extremity training in patients with subacute stroke," *Archives of Physical Medicine and Rehabilitation*, vol. 95, no. 3, pp. 431–438, 2014.

[14] E. Achilles, P. Weiss-Blankenhorn, K. Moos, M. Hesse, R. Sparing, y G. Fink, "P649: Transcranial direct current stimulation (tDCS) of left parietal cortex facilitates gesture processing in healthy subjects," *Clinical Neurophysiology*, vol. 125, pp. S226–S227, 2014.

[15] P. Wei, W. He, Y. Zhou, y L. Wang, "Performance of motor imagery brain-computer interface based on anodal transcranial direct current stimulation modulation," *IEEE Transactions on Neural Systems and Rehabilitation Engineering*, vol. 21, no. 3, pp. 404–415, 2013.

[16] F. Pichiorri, G. Morone, M. Petti, J. Toppi, I. Pisotta, M. Molinari, S. Paolucci, M. Inghilleri, L. Astolfi, F. Cincotti *et al.*, "Brain–computer interface

boosts motor imagery practice during stroke recovery," *Annals of Neurology*, vol. 77, no. 5, pp. 851–865, 2015.

[17] J. O'Shea, M.-H. Boudrias, C. J. Stagg, V. Bachtiar, U. Kischka, J. U. Blicher, y H. Johansen-Berg, "Predicting behavioural response to tDCS in chronic motor stroke," *Neuroimage*, vol. 85, pp. 924–933, 2014.

[18] H. Markus, "Stroke: causes and clinical features," *Medicine*, vol. 40, no. 9, pp. 484–489, 2012.

[19] V. Gil Chang, "Fundamentos de medicina de rehabilitación," *Costa Rica: Editorial EUCR*, 2006.

[20] B. Furie y B. C. Furie, "Mechanisms of thrombus formation," *New England Journal of Medicine*, vol. 359, no. 9, pp. 938–949, 2008.

[21] V. Kumar, A. K. Abbas, N. Fausto, y J. C. Aster, *Robbins and Cotran pathologic basis of disease, professional edition e-book*. elsevier health sciences, 2014.

[22] C. S. Kase y L. R. Caplan, *Intracerebral Hemorrhage*. Butterworth-Heinemann, 1994.

[23] J. B. Bederson, *Subarachnoid hemorrhage: Pathophysiology and management*. Amer Assn of Neurological Surgeons, 1997, vol. 27.

[24] W. H. Organization, I. S. of Hypertension Writing Group *et al.*, "2003 world health organization (WHO)/international society of hypertension (ISH) statement on management of hypertension," *Journal of Hypertension*, vol. 21, no. 11, pp. 1983–1992, 2003.

[25] D. Combs, "Dorland's illustrated medical dictionary," *Journal of Family Practice*, vol. 40, no. 2, pp. 191–192, 1995.

[26] C. A. Schinstock, R. C. Albright, A. W. Williams, J. J. Dillon, E. J. Bergstralh, B. M. Jenson, J. T. McCarthy, y K. A. Nath, "Outcomes of arteriovenous fistula creation after the fistula first initiative," *Clinical Journal of the American Society of Nephrology*, vol. 6, no. 8, pp. 1996–2002, 2011.

[27] S. L. Tokgözoglu, M. K. Batur, M. A. Topçuoglu, O. Saribas, S. Kes, y A. Oto, "Effects of stroke localization on cardiac autonomic balance and sudden death," *Stroke*, vol. 30, no. 7, pp. 1307–1311, 1999.

[28] P. Plummer, A. L. Behrman, P. W. Duncan, P. Spigel, D. Saracino, J. Martin, E. Fox, M. Thigpen, y S. A. Kautz, "Effects of stroke severity and training duration on locomotor recovery after stroke: a pilot study," *Neurorehabilitation and Neural Repair*, vol. 21, no. 2, pp. 137–151, 2007.

[29] R. P. Pallejà y F. J. G. Gisbert, "Esperanza de vida en España a lo largo del siglo xx: las tablas de mortalidad del Instituto Nacional de Estadística," *Documentos de trabajo (Fundación BBVA)*, no. 11, p. 1, 2006.

[30] P. Langhorne, J. Bernhardt, y G. Kwakkel, "Stroke rehabilitation," *The Lancet*, vol. 377, no. 9778, pp. 1693–1702, 2011.

[31] J. B. Green, "Brain reorganization after stroke," *Topics in Stroke Rehabilitation*, vol. 10, no. 3, pp. 1–20, 2003.

[32] J. Liepert, H. Bauder, W. H. Miltner, E. Taub, y C. Weiller, "Treatment-induced cortical reorganization after stroke in humans," *Stroke*, vol. 31, no. 6, pp. 1210–1216, 2000.

[33] R. Carter, *The brain book*. Dorling Kindersley Ltd, 2014.

[34] H. Gray y C. M. Goss, "Anatomy of the human body." *American Journal of Physical Medicine & Rehabilitation*, vol. 53, no. 6, p. 293, 1974.

[35] G. D. Schott, "Penfield's homunculus: a note on cerebral cartography." *Journal of Neurology, Neurosurgery, and Psychiatry*, vol. 56, no. 4, p. 329, 1993.

[36] "Penfield hommunculus," https://commons.wikimedia.org/wiki/File:Homunculus-de.svg, accessed: 2018-03-11.

[37] C.-B. Rivara, C. C. Sherwood, C. Bouras, y P. R. Hof, "Stereologic characterization and spatial distribution patterns of betz cells in the human primary motor cortex," *The Anatomical Record*, vol. 270, no. 2, pp. 137–151, 2003.

[38] A. Potgieser, B. De Jong, M. Wagemakers, E. Hoving, y R. Groen, "Insights from the supplementary motor area syndrome in balancing movement initiation and inhibition," *Frontiers in Human Neuroscience*, vol. 8, p. 960, 2014.

[39] "Brain," https://www.flickr.com/photos/flamephoenix1991/8376271918, accessed: 2018-03-11.

[40] N. Li, K. Daie, K. Svoboda, y S. Druckmann, "Robust neuronal dynamics in premotor cortex during motor planning," *Nature*, vol. 532, no. 7600, p. 459, 2016.

[41] S. Uithol, M. Franca, K. Heimann, D. Marzoli, P. Capotosto, L. Tommasi, y V. Gallese, "Single-pulse transcranial magnetic stimulation reveals contribution of premotor cortex to object shape recognition," *Brain Stimulation: Basic, Translational, and Clinical Research in Neuromodulation*, vol. 8, no. 5, pp. 953–956, 2015.

[42] E. DAngelo y S. Casali, "Seeking a unified framework for cerebellar function and dysfunction: from circuit operations to cognition," *Frontiers in Neural Circuits*, vol. 6, p. 116, 2013.

[43] D. Purves, R. Cabeza, S. A. Huettel, K. S. LaBar, M. L. Platt, M. G. Woldorff, y E. M. Brannon, *Cognitive Neuroscience*. Sunderland: Sinauer Associates, Inc, 2008.

[44] J. Dobbing y J. Sands, "Quantitative growth and development of human brain," *Archives of Disease in Childhood*, vol. 48, no. 10, pp. 757–767, 1973.

[45] J. E. LeDoux, *Synaptic self: How our brains become who we are*. Penguin, 2003.

[46] R. B. Livingston, "Brain mechanisms in conditioning and learning," en *Neurosciences research symposium summaries*, vol. 2. MIT Press Cambridge, MA, 1967, p. 91.

[47] P. D. Marasco y T. A. Kuiken, "Amputation with median nerve redirection (targeted reinnervation) reactivates forepaw barrel subfield in rats," *Journal of Neuroscience*, vol. 30, no. 47, pp. 16 008–16 014, 2010.

[48] M. Rijntjes y C. Weiller, "Recovery of motor and language abilities after stroke: the contribution of functional imaging," *Progress in Neurobiology*, vol. 66, no. 2, pp. 109–122, 2002.

[49] K. Herholz y W.-D. Heiss, "Functional imaging correlates of recovery after stroke in humans," *Journal of Cerebral Blood Flow & Metabolism*, vol. 20, no. 12, pp. 1619–1631, 2000.

[50] H. Janssen, L. Ada, J. Bernhardt, P. McElduff, M. Pollack, M. Nilsson, y N. Spratt, "Physical, cognitive and social activity levels of stroke patients undergoing rehabilitation within a mixed rehabilitation unit," *Clinical Rehabilitation*, vol. 28, no. 1, pp. 91–101, 2014.

[51] L. D. Jong, F. Wijck, R. E. Stewart, A. C. Geurts, y P. U. Dijkstra, "Content of conventional therapy for the severely affected arm during subacute rehabilitation after stroke: An analysis of physiotherapy and occupational therapy practice," *Physiotherapy Research International*, vol. 23, no. 1, 2018.

[52] T. Ros, M. A. Munneke, D. Ruge, J. H. Gruzelier, y J. C. Rothwell, "Endogenous control of waking brain rhythms induces neuroplasticity in humans," *European Journal of Neuroscience*, vol. 31, no. 4, pp. 770–778, 2010.

[53] M. L. Blefari, J. Sulzer, M.-C. Hepp-Reymond, S. Kollias, y R. Gassert, "Improvement in precision grip force control with self-modulation of primary motor cortex during motor imagery," *Frontiers in Behavioral Neuroscience*, vol. 9, p. 18, 2015.

[54] M. Witkowski, M. Cortese, M. Cempini, J. Mellinger, N. Vitiello, y S. R. Soekadar, "Enhancing brain-machine interface (BMI) control of a hand exoskeleton using electrooculography (EOG)," *Journal of Neuroengineering and Rehabilitation*, vol. 11, no. 1, p. 165, 2014.

[55] M. A. Dimyan y L. G. Cohen, "Neuroplasticity in the context of motor rehabilitation after stroke," *Nature Reviews Neurology*, vol. 7, no. 2, p. 76, 2011.

[56] E. C. Leuthardt, G. Schalk, J. R. Wolpaw, J. G. Ojemann, y D. W. Moran, "A brain–computer interface using electrocorticographic signals in humans," *Journal of Neural Engineering*, vol. 1, no. 2, p. 63, 2004.

[57] J. O'Keefe y A. Speakman, "Single unit activity in the rat hippocampus during a spatial memory task," *Experimental Brain Research*, vol. 68, no. 1, pp. 1–27, 1987.

[58] D. H. Hubel, "Single unit activity in lateral geniculate body and optic tract of unrestrained cats," *The Journal of Physiology*, vol. 150, no. 1, pp. 91–104, 1960.

[59] E. Bizzi y P. H. Schiller, "Single unit activity in the frontal eye fields of unanesthetized monkeys during eye and head movement," *Experimental Brain Research*, vol. 10, no. 2, pp. 151–158, 1970.

[60] K. Mihr, "Notas de clase de brain machine interface," Marzo 2012.

[61] "Ecog," https://openi.nlm.nih.gov/detailedresult.php?img=PMC2778557_pone.0008081.g002&req=4, accessed: 2018-03-11.

[62] Y. Okada, "Neurogenesis of evoked magnetic fields," *Biomagnetism, an Interdisciplinary Approach*, 1983.

[63] "National institute of mental health," http:/https://images.nimh.nih.gov/public_il/image_details.cfm?id=80, accessed: 2018-03-11.

[64] P. Olejniczak, "Neurophysiologic basis of EEG," *Journal of Clinical Neurophysiology*, vol. 23, no. 3, pp. 186–189, 2006.

[65] V. Jurcak, D. Tsuzuki, y I. Dan, "10/20, 10/10, and 10/5 systems revisited: their validity as relative head-surface-based positioning systems," *Neuroimage*, vol. 34, no. 4, pp. 1600–1611, 2007.

[66] "Sistema internacional 10-10," https://commons.wikimedia.org/wiki/File:21_electrodes_of_International_10-20_system_for_EEG.svg, accessed: 2018-04-11.

[67] C. Michel, D. Lehmann, B. Henggeler, y D. Brandeis, "Localization of the sources of EEG delta, theta, alpha and beta frequency bands using the FFT dipole approximation," *Electroencephalography and Clinical Neurophysiology*, vol. 82, no. 1, pp. 38–44, 1992.

[68] D. Creel, "Visually evoked potentials," *University of Utah Health Sciences Center*, 2012.

[69] N. Kraus y T. Nicol, "Auditory evoked potentials," en *Encyclopedia of neuroscience*. Springer, 2008, pp. 214–218.

[70] S. Punch, B. Van Dun, A. King, L. Carter, y W. Pearce, "Clinical experience of using cortical auditory evoked potentials in the treatment of infant hearing loss in australia," en *Seminars in hearing*, vol. 37, no. 1. Thieme Medical Publishers, 2016, p. 36.

[71] M. Scherg y D. Von Cramon, "Evoked dipole source potentials of the human auditory cortex," *Electroencephalography and Clinical Neurophysiology/Evoked Potentials Section*, vol. 65, no. 5, pp. 344–360, 1986.

[72] D. S. Goodin, K. C. Squires, y A. Starr, "Long latency event-related components of the auditory evoked potential in dementia," *SAGE, Lighting research and Technology*, 1978.

[73] S. Fukuda, "Somatosensory evoked potential," *Masui. The Japanese Journal of Anesthesiology*, vol. 55, no. 3, pp. 280–293, 2006.

[74] G. L. Engler, N. Spielholz, W. Bernhard, F. Danziger, H. Merkin, y T. Wolff, "Somatosensory evoked potentials during harrington instrumentation for scoliosis," *J Bone Joint Surg Am*, vol. 60, no. 4, pp. 528–532, 1978.

[75] J. J. Cunningham, J. Laschinger, y F. Spencer, "Monitoring of somatosensory evoked potentials during surgical procedures on the thoracoabdominal aorta. IV. clinical observations and results." *The Journal of Thoracic and Cardiovascular Surgery*, vol. 94, no. 2, pp. 275–285, 1987.

[76] A. S. Hilibrand, D. M. Schwartz, V. Sethuraman, A. R. Vaccaro, y T. J. Albert, "Comparison of transcranial electric motor and somatosensory evoked potential monitoring during cervical spine surgery," *JBJS*, vol. 86, no. 6, pp. 1248–1253, 2004.

[77] S. J. Luck, *An introduction to the event-related potential technique*. MIT press, 2014.

[78] N. Sharma y J.-C. Baron, "Does motor imagery share neural networks with executed movement: a multivariate fMRI analysis," *Frontiers in Human Neuroscience*, vol. 7, p. 564, 2013.

[79] G. Pfurtscheller y A. Aranibar, "Evaluation of event-related desynchronization (ERD) preceding and following voluntary self-paced movement," *Clinical Neurophysiology*, vol. 46, no. 2, pp. 138–146, 1979.

[80] R. Salazar-Varas, Á. Costa, E. Iáñez, A. Úbeda, E. Hortal, y J. Azorín, "Analyzing EEG signals to detect unexpected obstacles during walking," *Journal of Neuroengineering and Rehabilitation*, vol. 12, no. 1, p. 101, 2015.

[81] U. Strehl, U. Leins, G. Goth, C. Klinger, T. Hinterberger, y N. Birbaumer, "Self-regulation of slow cortical potentials: a new treatment for children with attention-deficit/hyperactivity disorder," *Pediatrics*, vol. 118, no. 5, pp. e1530–e1540, 2006.

[82] A. L. Benabid, "Deep brain stimulation for Parkinsons disease," *Current Opinion in Neurobiology*, vol. 13, no. 6, pp. 696–706, 2003.

[83] M. L. Kringelbach, N. Jenkinson, S. L. Owen, y T. Z. Aziz, "Translational principles of deep brain stimulation," *Nature Reviews Neuroscience*, vol. 8, no. 8, p. 623, 2007.

[84] "Deep brain stimulation," http://kids.frontiersin.org/article/10.3389/frym.2014.00012, accessed: 2018-04-11.

[85] R. K. Wangsness, "Electromagnetic fields," *Electromagnetic Fields, 2nd Edition, by Roald K. Wangsness, pp. 608. ISBN 0-471-81186-6. Wiley-VCH, July 1986.*, p. 608, 1986.

[86] M. Hallett y S. Chokroverty, *Magnetic stimulation in clinical neurophysiology*. Elsevier Health Sciences, 2005.

[87] E. M. Wassermann, "Risk and safety of repetitive transcranial magnetic stimulation: report and suggested guidelines from the international workshop on the safety of repetitive transcranial magnetic stimulation, june 5–7, 1996," *Electroencephalography and Clinical Neurophysiology/Evoked Potentials Section*, vol. 108, no. 1, pp. 1–16, 1998.

[88] M. S. George, Z. Nahas, M. Molloy, A. M. Speer, N. C. Oliver, X.-B. Li, G. W. Arana, S. C. Risch, y J. C. Ballenger, "A controlled trial of daily left prefrontal cortex TMS for treating depression," *Biological Psychiatry*, vol. 48, no. 10, pp. 962–970, 2000.

[89] S. Aurora, B. Ahmad, K. Welch, P. Bhardhwaj, y N. Ramadan, "Transcranial magnetic stimulation confirms hyperexcitability of occipital cortex in migraine," *Neurology*, vol. 50, no. 4, pp. 1111–1114, 1998.

[90] "Transcranial magnetic stimulation," https://commons.wikimedia.org/wiki/File:Transcranial_magnetic_stimulation.jpg, accessed: 2018-03-11.

[91] H. Kumru, N. Murillo, J. Benito-Penalva, J. M. Tormos, y J. Vidal, "Transcranial direct current stimulation is not effective in the motor strength and gait recovery following motor incomplete spinal cord injury during lokomat® gait training," *Neuroscience Letters*, vol. 620, pp. 143–147, 2016.

[92] M. Rodrıguez-Ugarte, N. Sciacca, E. Iánez, y J. M. Azorın, "Transcranial direct current stimulation (tDCS) and transcranial current alternating stimulation (tACS) review," *Actas de las XXXVII Jornadas de Automática (7, 8 y 9 de septiembre de 2016, Madrid)*, pp. 137–143, 2016.

[93] G. Batsikadze, V. Moliadze, W. Paulus, M.-F. Kuo, y M. Nitsche, "Partially non-linear stimulation intensity-dependent effects of direct current stimulation on motor cortex excitability in humans," *The Journal of Physiology*, vol. 591, no. 7, pp. 1987–2000, 2013.

[94] S. Bai, S. Dokos, K.-A. Ho, y C. Loo, "A computational modelling study of transcranial direct current stimulation montages used in depression," *Neuroimage*, vol. 87, pp. 332–344, 2014.

[95] B. A. Coffman, V. P. Clark, y R. Parasuraman, "Battery powered thought: enhancement of attention, learning, and memory in healthy adults using transcranial direct current stimulation," *Neuroimage*, vol. 85, pp. 895–908, 2014.

[96] S. Wiethoff, M. Hamada, y J. C. Rothwell, "Variability in response to transcranial direct current stimulation of the motor cortex," *BRAIN STIMULATION: Basic, Translational, and Clinical Research in Neuromodulation*, vol. 7, no. 3, pp. 468–475, 2014.

[97] H. L. Filmer, P. E. Dux, y J. B. Mattingley, "Applications of transcranial direct current stimulation for understanding brain function," *Trends in Neurosciences*, vol. 37, no. 12, pp. 742–753, 2014.

[98] A. Monti, R. Ferrucci, M. Fumagalli, F. Mameli, F. Cogiamanian, G. Ardolino, y A. Priori, "Transcranial direct current stimulation (tDCS) and language," *J Neurol Neurosurg Psychiatry*, vol. 84, no. 8, pp. 832–842, 2013.

[99] Á. Foerster, L. Melo, M. Mello, R. Castro, L. Shirahige, S. Rocha, y K. Monte-Silva, "Cerebellar transcranial direct current stimulation (ctDCS) impairs balance control in healthy individuals," *The Cerebellum*, vol. 16, no. 4, pp. 872–875, 2017.

[100] A. Antal, I. Alekseichuk, M. Bikson, J. Brockmöller, A. Brunoni, R. Chen, L. Cohen, G. Dowthwaite, J. Ellrich, A. Flöel *et al.*, "Low intensity transcranial electric stimulation: Safety, ethical, legal regulatory and application guidelines," *Clinical Neurophysiology*, vol. 128, no. 9, pp. 1774–1809, 2017.

[101] T. G. Hornby, D. D. Campbell, J. H. Kahn, T. Demott, J. L. Moore, y H. R. Roth, "Enhanced gait-related improvements after therapist-versus robotic-assisted locomotor training in subjects with chronic stroke: a randomized controlled study," *Stroke*, vol. 39, no. 6, pp. 1786–1792, 2008.

[102] H. A. Abdullah, C. Tarry, C. Lambert, S. Barreca, y B. O. Allen, "Results of clinicians using a therapeutic robotic system in an inpatient stroke rehabilitation unit," *Journal of Neuroengineering and Rehabilitation*, vol. 8, no. 1, p. 50, 2011.

[103] N. A. Bhagat, A. Venkatakrishnan, B. Abibullaev, E. J. Artz, N. Yozbatiran, A. A. Blank, J. French, C. Karmonik, R. G. Grossman, M. K. O'Malley *et al.*, "Design and optimization of an EEG-based brain machine interface (BMI) to an upper-limb exoskeleton for stroke survivors," *Frontiers in Neuroscience*, vol. 10, p. 122, 2016.

[104] E. A. Corbett, N. A. Sachs, K. P. Körding, y E. J. Perreault, "Multimodal decoding and congruent sensory information enhance reaching performance in subjects with cervical spinal cord injury," *Frontiers in Neuroscience*, vol. 8, p. 123, 2014.

[105] A. M. Dollar y H. Herr, "Lower extremity exoskeletons and active orthoses: challenges and state-of-the-art," *IEEE Transactions on Robotics*, vol. 24, no. 1, pp. 144–158, 2008.

[106] "exoskeleton H2," http://www.elcorreo.com/vizcaya/multimedia/fotos/innova/20131211/exoesqueletos-rehabilitacion-307435962823-mm.html, accessed: 2018-04-11.

[107] R. Holland y J. Crinion, "Can tDCS enhance treatment of aphasia after stroke?" *Aphasiology*, vol. 26, no. 9, pp. 1169–1191, 2012.

[108] J. Reis, E. Robertson, J. W. Krakauer, J. Rothwell, L. Marshall, C. Gerloff, E. Wassermann, A. Pascual-Leone, F. Hummel, P. A. Celnik *et al.*, "Consensus:can tDCS and TMS enhance motor learning and memory formation?," *Brain Stimulation*, vol. 1, no. 4, p. 363, 2008.

[109] D. M. Martin, R. Liu, A. Alonzo, M. Green, y C. K. Loo, "Use of transcranial direct current stimulation (tDCS) to enhance cognitive training: effect of timing of stimulation," *Experimental Brain Research*, vol. 232, no. 10, pp. 3345–3351, 2014.

[110] F. Fregni, P. S. Boggio, M. Nitsche, F. Bermpohl, A. Antal, E. Feredoes, M. A. Marcolin, S. P. Rigonatti, M. T. Silva, W. Paulus *et al.*, "Anodal transcranial direct current stimulation of prefrontal cortex enhances working memory," *Experimental Brain Research*, vol. 166, no. 1, pp. 23–30, 2005.

[111] R. Ferrucci, A. R. Brunoni, M. Parazzini, M. Vergari, E. Rossi, M. Fumagalli, F. Mameli, M. Rosa, G. Giannicola, S. Zago *et al.*, "Modulating human procedural learning by cerebellar transcranial direct current stimulation," *The Cerebellum*, vol. 12, no. 4, pp. 485–492, 2013.

[112] A. Rogalewski, C. Breitenstein, M. A. Nitsche, W. Paulus, y S. Knecht, "Transcranial direct current stimulation disrupts tactile perception," *European Journal of Neuroscience*, vol. 20, no. 1, pp. 313–316, 2004.

[113] L. Randazzo, I. Iturrate, R. Chavarriaga, R. Leeb, y J. d. R. Millán, "Detecting intention to grasp during reaching movements from EEG," en *Engineering in Medicine and Biology Society (EMBC), 2015 37th Annual International Conference of the IEEE*. IEEE, 2015, pp. 1115–1118.

[114] E. Lew, R. Chavarriaga, S. Silvoni, y J. d. R. Millán, "Detection of self-paced reaching movement intention from EEG signals," *Front. Neuroeng*, vol. 5, no. 13, 2012.

[115] P. Toffanin, A. Johnson, R. De Jong, y S. Martens, "Rethinking neural efficiency: effects of controlling for strategy use." *Behavioral Neuroscience*, vol. 121, no. 5, p. 854, 2007.

[116] C. S. Nam, Y. Jeon, Y.-J. Kim, I. Lee, y K. Park, "Movement imagery-related lateralization of event-related (de) synchronization (ERD/ERS): motor-imagery duration effects," *Clinical Neurophysiology*, vol. 122, no. 3, pp. 567–577, 2011.

[117] D. J. McFarland, L. M. McCane, S. V. David, y J. R. Wolpaw, "Spatial filter selection for eeg-based communication," *Electroencephalography and clinical Neurophysiology*, vol. 103, no. 3, pp. 386–394, 1997.

[118] O. Bai, V. Rathi, P. Lin, D. Huang, H. Battapady, D.-Y. Fei, L. Schneider, E. Houdayer, X. Chen, y M. Hallett, "Prediction of human voluntary movement before it occurs," *Clinical Neurophysiology*, vol. 122, no. 2, pp. 364–372, 2011.

[119] O. Bai, P. Lin, S. Vorbach, J. Li, S. Furlani, y M. Hallett, "Exploration of computational methods for classification of movement intention during human voluntary movement from single trial EEG," *Clinical Neurophysiology*, vol. 118, no. 12, pp. 2637–2655, 2007.

[120] A. I. Sburlea, L. Montesano, R. C. de la Cuerda, I. M. A. Diego, J. C. Miangolarra-Page, y J. Minguez, "Detecting intention to walk in stroke patients from pre-movement EEG correlates," *Journal of Neuroengineering and Rehabilitation*, vol. 12, no. 1, p. 1, 2015.

[121] T. C. Bulea, S. Prasad, A. Kilicarslan, y J. L. Contreras-Vidal, "Sitting and standing intention can be decoded from scalp EEG recorded prior to movement execution," *Frontiers in Neuroscience*, vol. 8, p. 376, 2014.

[122] N. Jiang, L. Gizzi, N. Mrachacz-Kersting, K. Dremstrup, y D. Farina, "A brain–computer interface for single-trial detection of gait initiation from movement related cortical potentials," *Clinical Neurophysiology*, vol. 126, no. 1, pp. 154–159, 2015.

[123] J. Ibáñez, J. Serrano, M. Del Castillo, y L. Barrios, "An asynchronous BMI system for online single-trial detection of movement intention," en *2010 Annual International Conference of the IEEE Engineering in Medicine and Biology*. Buenos Aires: IEEE, 2010, pp. 4562–4565.

[124] G. Pfurtscheller y C. Neuper, "Motor imagery and direct brain-computer communication," *Proceedings of the IEEE*, vol. 89, no. 7, pp. 1123–1134, 2001.

[125] D. Liu, W. Chen, K. Lee, Z. Pei, y J. d. R. Millán, "An EEG-based brain-computer interface for gait training," en *Control And Decision Conference (CCDC), 2017 29th Chinese*. IEEE, 2017, pp. 6755–6760.

[126] C. Zich, S. Debener, C. Kranczioch, M. G. Bleichner, I. Gutberlet, y M. De Vos, "Real-time EEG feedback during simultaneous EEG–fMRI identifies the cortical signature of motor imagery," *Neuroimage*, vol. 114, pp. 438–447, 2015.

[127] C. Guger, H. Ramoser, y G. Pfurtscheller, "Real-time EEG analysis with subject-specific spatial patterns for a brain-computer interface (BCI)," *IEEE Transactions on Rehabilitation Engineering*, vol. 8, no. 4, pp. 447–456, 2000.

[128] G. Prasad, P. Herman, D. Coyle, S. McDonough, y J. Crosbie, "Applying a brain-computer interface to support motor imagery practice in people with stroke for upper limb recovery: a feasibility study," *Journal of Neuroengineering and Rehabilitation*, vol. 7, no. 1, p. 60, 2010.

[129] T. Yu, J. Xiao, F. Wang, R. Zhang, Z. Gu, A. Cichocki, y Y. Li, "Enhanced motor imagery training using a hybrid BCI with feedback," *IEEE Transactions on Biomedical Engineering*, vol. 62, no. 7, pp. 1706–1717, 2015.

[130] P. Horki, T. Solis-Escalante, C. Neuper, y G. Müller-Putz, "Combined motor imagery and SSVEP based BCI control of a 2 dof artificial upper limb," *Medical & Biological Engineering & Computing*, vol. 49, no. 5, pp. 567–577, 2011.

[131] L. Mandolesi, M. Leggio, F. Spirito, y L. Petrosini, "Cerebellar contribution to spatial event processing," *European Journal of Neuroscience*, vol. 18, no. 9, pp. 2618–2626, 2003.

[132] R. M. Hardwick y P. A. Celnik, "Cerebellar direct current stimulation enhances motor learning in older adults," *Neurobiology of aging*, vol. 35, no. 10, pp. 2217–2221, 2014.

[133] B. Shah, T. T. Nguyen, y S. Madhavan, "Polarity independent effects of cerebellar tDCS on short term ankle visuomotor learning," *Brain stimulation*, vol. 6, no. 6, pp. 966–968, 2013.

[134] G. Grimaldi, G. Argyropoulos, A. Boehringer, P. Celnik, M. Edwards, R. Ferrucci, J. M. Galea, S. J. Groiss, K. Hiraoka, P. Kassavetis *et al.*, "Non-

invasive cerebellar stimulationa consensus paper," *The Cerebellum*, vol. 13, no. 1, pp. 121–138, 2014.

[135] J.-P. Lefaucheur, A. Antal, S. S. Ayache, D. H. Benninger, J. Brunelin, F. Cogiamanian, M. Cotelli, D. De Ridder, R. Ferrucci, B. Langguth *et al.*, "Evidence-based guidelines on the therapeutic use of transcranial direct current stimulation (tDCS)," *Clinical Neurophysiology*, vol. 128, no. 1, pp. 56–92, 2017.

[136] B. Cengiz y H. E. Boran, "The role of the cerebellum in motor imagery," *Neuroscience letters*, vol. 617, pp. 156–159, 2016.

[137] J. Matsumoto, T. Fujiwara, O. Takahashi, M. Liu, A. Kimura, y J. Ushiba, "Modulation of mu rhythm desynchronization during motor imagery by transcranial direct current stimulation," *Journal of neuroengineering and rehabilitation*, vol. 7, no. 1, p. 27, 2010.

[138] G. Pfurtscheller y F. L. Da Silva, "Event-related EEG/MEG synchronization and desynchronization: basic principles," *Clinical neurophysiology*, vol. 110, no. 11, pp. 1842–1857, 1999.

[139] M. Gomez-Rodriguez, J. Peters, J. Hill, B. Schölkopf, A. Gharabaghi, y M. Grosse-Wentrup, "Closing the sensorimotor loop: haptic feedback facilitates decoding of motor imagery," *Journal of neural engineering*, vol. 8, no. 3, p. 036005, 2011.